B Factories

Boštjan Golob

January 2, 2019

Contents

About the Author

Boštjan Golob is a professor of physics at the University of Ljubljana, Slovenia. His research field is experimental particle physics, which he has pursued for more than 20 years, at the European Organization for Nuclear Research, CERN, Geneva, Swiss, and lately at the High Energy Accelerator Research Organization, KEK, Tsukuba, Japan. Specifically, he investigates breaking of the *CP* symmetry, a phenomena responsible for the Universe to be composed of matter and not anti-matter. As a member of international collaborations Belle and Belle II he takes part in taking, analysing and interpreting data recorded in electron positron collisions at the KEKB and recently at the SuperKEKB collider. In the international collaborations he assumed various responsibilities, from leading the study group of charmed hadrons within the Belle collaboration to coordination of the Belle II experiment physics program.

He is also a co-editor of ”The Physics of the B Factories” book, summarizing a decade long work of physicists at electron positron colliders in measuring the asymmetry between particles and anti-particles.

Abstract

B Factories are particle colliders at which specific subatomic particles - *B* mesons - are being abundantly produced. The purpose is to study the properties of their decays in great details in order to shed light on a mystery of eminently larger scale: why do we live in a Universe composed of matter and no anti-matter? In expert language the asymmetry between matter and anti-matter is called the *CP* asymmetry. It represents a necessary condition for our Universe to evolve in the way it has, with its visible part being composed almost completely of particles and no anti-particles. There is an unanswered puzzle, though: the amount of the asymmetry as measured at the subatomic level is much too small to successfully explain the matter asymmetry of the Universe.

The *B* Factories book is an introductory text to physics laws of the *CP* asymmetry, touching experimental requirements needed to perform such measurements at the subatomic level, and illustrating the main findings of the contemporary *B* factories. Deviations between the experimental results and predictions based on the current theoretical knowledge are exposed and discussed in terms of the near future frontier particle physics experimental endeavours.

Chapter 1

Into the *B* World

1.1 Heavy Particles

1.1.1 Concept of elementary particles

In terms of understanding the basic constituents of matter we have - through the history of scientific endeavour - come a long way from, for example, the teachings of Empedocles, in the 5th century BC. He believed that the world is made of four basic elements: air, fire, water and earth (see Fig. 1.1).

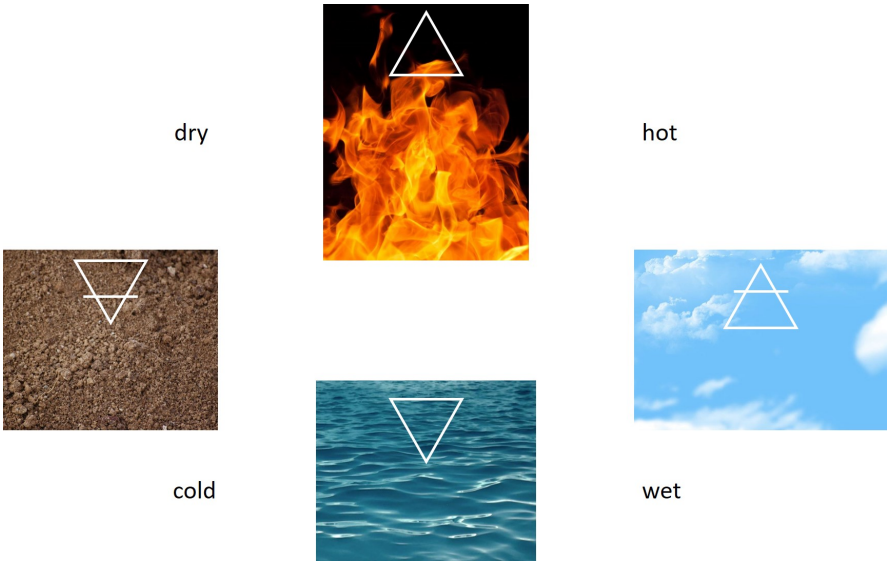

Figure 1.1: Simplified basic constituents of matter according to teachings of Empedocles. Also shown are alchemical symbols of individual elements.

Nowadays the picture of elementary particles, the smallest indivisible parts of matter, is significantly refined. We have developed sophisticated theoretical models based on and confirmed by accurate measurements, which prove that atoms of various chemical elements consist of a tiny atomic nucleus, carrying the positive electrical charge, and negatively charged

electrons scattered around a relatively large space enclosing the nucleus. While a typical dimension of an atom is 10^{-10} meters, the size of the nucleus is of the order of a femtometer, 10^{-15} m.

A nucleus is further composed of nucleons - a common name for positively charged protons and electrically neutral neutrons. Nucleons are composed of quarks. Quarks come in various flavours. These flavours are, unfortunately perhaps, nothing else but a quantum number, a property of an individual quark, like the electrical charge, spin and similar. The basic constituents of matter are sketched in Fig1.2.

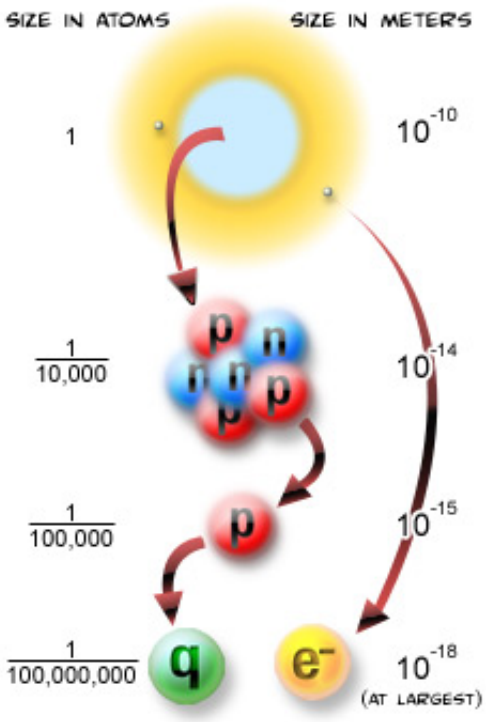

Figure 1.2: Basic constituents of matter as revealed by contemporary scientific methods [1].

The dimension of quarks is less than approximately 10^{-18} m. Why less than? Because with the contemporary experimental methods one can only probe the structure of matter down to scales of around 10^{-18} m. In order to do so, waves with a wavelength of the order of less than 10^{-18} m, let's say 10^{-19} m are needed. According to the de Broglie relation such a wavelength corresponds to a momentum of

$$cp = \frac{ch}{\lambda_B} \sim \frac{197 \text{ MeV fm}}{10^{-19} \text{ m}} \sim 2 \times 10^{12} \text{ eV} \ , \tag{1.1}$$

where h is the Planck constant, c is the speed of electromagnetic waves in vacuum, and λ_B denotes the de Broglie wavelength. Accelerated particles with momentum of 2 Tera[1] electronvolts$/c$ thus represent waves by which the smallest details of matter are revealed.

[1] Tera = 10^{12}.

Such a value of cp is the capability of the highest energy particle accelerator in the world, the Large Hadron Collider - LHC[2].

The concept of elementary particles is thus a subject of the experimental methods available for investigations of matter. With the most powerful contemporary microscopes, particle accelerators, one is able to study details in the structure of matter down to around 10^{-18} m. At this point of human scientific ingenuity we believe that the basic constituents of matter are quarks, like the ones building up nucleons, and leptons such as electrons in the atoms.

Note: Particles that with the contemporary scientific exploration methods appear indivisible and are thus regarded as elementary particles are quarks (like the ones making up protons and neutrons in the atomic nucleus) and leptons (like electrons in the atoms).

1.1.2 Quark World

We mentioned that quarks arise in different flavours. Out of 6 different flavours of quarks one can combine a rich palette of hadrons - heavy particles, like protons and neutrons, composed of quarks. We will consider two well investigated types of hadrons, baryons and mesons. In a simplified quark model the former are composed of three quarks, and the latter from one quark and one anti-quark[3]. In this simplified hadron-building exercise a proton is represented as a $|u\ u\ d\rangle$ state, i.e. composed of two u and a d quark. u and d stands for up and down quarks, respectively, two distinct quark flavours. The lightest charged meson, a positive pion π^+, is represented by $|u\ \bar{d}\rangle$. Knowing that each proton carries one positive elementary charge, $e_0 = 1.6 \times 10^{-19}$ As[4] , and the same holds for a positive pion, it is clear that quarks must carry a non-integer elementary charge. Indeed, u quarks belong to a family of up-like quarks with charge $+(2/3)e_0$, and d quarks to a family of down-like quarks with charge $-(1/3)e_0$. Of course anti-quarks have all the quantum numbers of the corresponding quark reversed, including its electrical charge: $\bar{u}$ charge is $-(2/3)e_0$ and for $\bar{d}$ it is $+(1/3)e_0$. It is not difficult to envisage the neutron quark composition, $|u\ d\ d\rangle$, and a neutral pion one, $|u\ \bar{u}\rangle$ or $|d\ \bar{d}\rangle$[5].

By extending the set of available quark flavours in composing various hadrons the number of hadron species increases dramatically.... Well, actually, as a power law; when composing baryons from two quark flavours the number of possible combinations is 2^3, with three quarks flavours it is 3^3, etc. Inclusion of strange quarks (s) enriches the hadron ZOO with kaons (for example a charged kaon, $|K^+\rangle = |u\ \bar{s}\rangle$), Sigma baryons (for example $|\Sigma^+\rangle = |u\ u\ s\rangle$), and several other species. One should also keep in mind that mesons with a

[2]The highest achieved energy of the accelerated proton beams in the LHC at CERN, Geneva, is 7 TeV. However, in collisions of protons at these energies, interactions are taking place among the constituent quarks. Each of the quarks only carries a fraction - around one third - of the total proton energy.

[3]The theory describing strong nuclear interaction among the quarks, which binds them into the hadrons - Quantum Chromodynamics (QCD) - in principle does not preclude heavy particles composed from quarks in a different manner than baryons and mesons. Indeed such bound states of quarks have been experimentally observed, perhaps the most well known is $X(3872)$, presumably composed of four quarks.

[4]In particle physics units for electric charge are not often used, typically charges are expressed simply in units of the elementary charge e_0. We use here Ampere seconds (As), instead of Coulomb (C); the two units are identical, C=As.

[5]In the quark model of hadrons, the neutral pion is a linear combination $(1/\sqrt{2})[|u\ \bar{u}\rangle + |d\ \bar{d}\rangle]$.

given quark composition in addition appear as spin 0 or spin 1 particles (summing spins of two quarks - $1/2$ - according to the angular momentum summation rules yields the total spin 0 or 1). Note that by the abbreviation spin we refer to the spin quantum number, s, which is related to the magnitude of the intrinsic angular momentum through $\hat{s^2}|\psi\rangle = s(s+1)\hbar^2|\psi\rangle$ with $\hat{s^2}$ representing the operator of the square of the intrinsic angular momentum operator. Similar to mesons, baryons may carry spin 1/2 or 3/2. Adding charm quarks (c) brings us to the ground states[6] of mesons and baryons shown in Fig.1.3. Axes denoted by I_3, S and C[7] reflect the number of up and down, strange, and charm quark constituents, respectively.

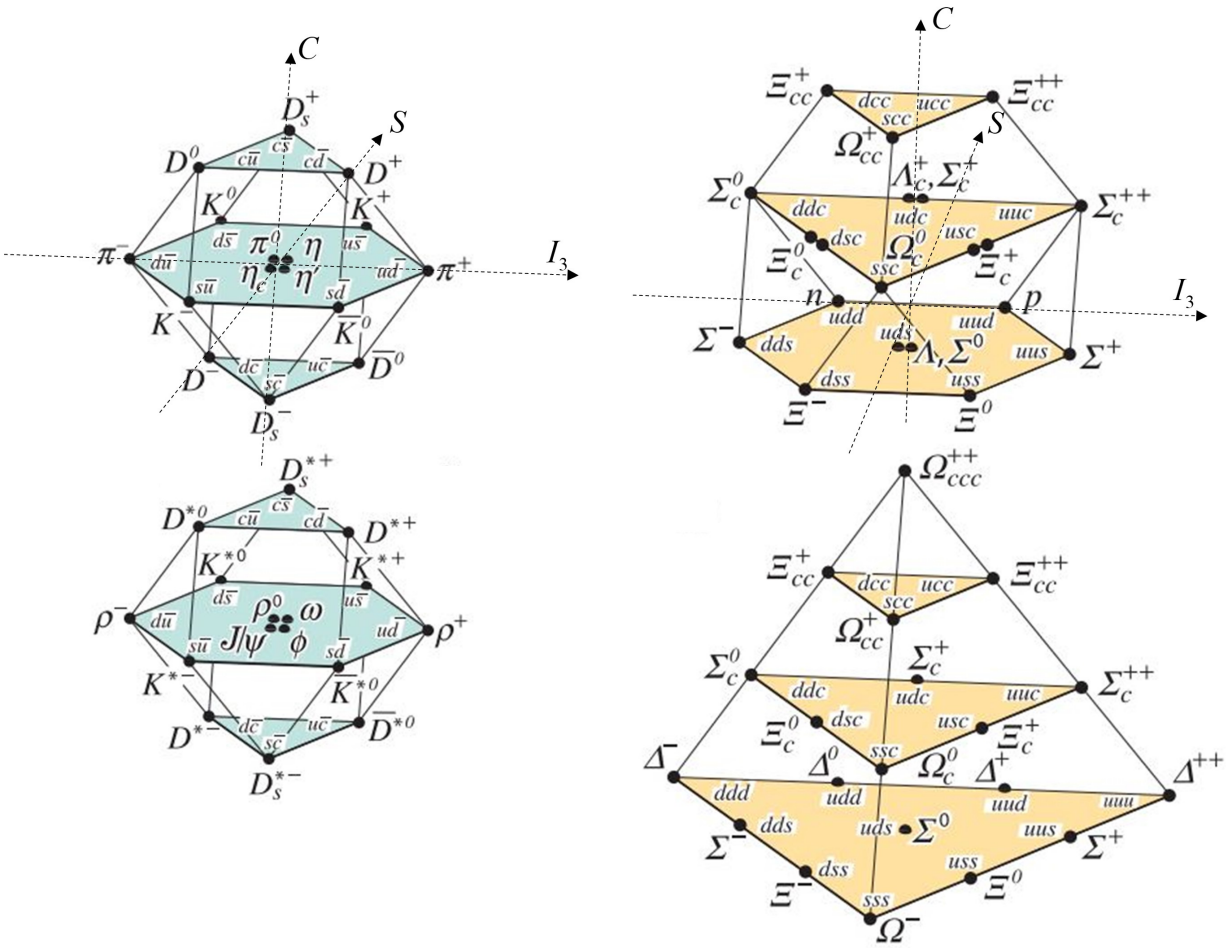

Figure 1.3: Ground states of mesons (left) with spin 0 (top) and spin 1 (bottom) and baryons (right) with spin 1/2 (top) and spin 3/2 (bottom), composed of up, down, strange and charm quarks. Adopted from [2].

It should be noted at this point that the main aim of the contemporary particle physics

[6]Ground state implies that the orbital angular momentum of constituent quarks is 0. In excited hadron states the orbital angular momentum of quarks is non-zero (i.e. 1, 2,...).

[7]These quantum numbers are called the third component of isospin, strangeness and charm, respectively.

is not of a book-keeping nature, that is to classify all different hadrons (and perhaps adding some leptons), but rather to understand the basic interactions among elementary particles, properties of these interactions and understanding of how these properties influence the evolution and the current shape of the universe of our existence. The basic interactions in Nature are the gravitational interaction, electromagnetic interaction, strong nuclear, and weak nuclear interaction. All but the first can be and are studied in the world of subatomic particles. Properties of the three types of interactions relevant for subatomic particles are also described and predicted in the theory called the Standard Model (SM). It is nowadays one of best experimentally verified theories, nevertheless there are several phenomena that the SM is unable to fully explain. One of those is the matter / anti-matter asymmetry of the Universe, discussed in more details in Chapter 2. For this reason for more than a decade both experimental and theoretical effort in particle physics has been focused on finding and eventually explaining phenomena and so far unknown particles beyond the framework of the SM. These processes and particles are commonly addressed as the New Physics (NP).

Note: Quarks appear as six different species, called flavours. Three of them have negative ($-1/3\ e_0$) and three of them positive ($+2/3\ e_0$) electric charge. They compose heavy particles - hadrons.

1.1.3 B Mesons

Adding beauty quarks[8] (b) to the scheme of hadrons, described in the previous section, appears to be impossible graphically since the fourth dimension to the existing scheme should be added (counting the number of b quarks inside a hadron). In the absence of a graphical representation analogous to the one shown in Fig.1.3, let us focus on the hadron species most central to further discussion: B mesons. They are composed of a $\bar{b}$ antiquark and another quark. The rule of calling a B meson the one carrying a $\bar{b}$ antiquark, and a $\bar{B}$ antimeson the one with a b quark is a matter of convention, not really important from the physics point of view, nevertheless to be remembered for the latter treatment.

For a more rigorous mathematical description various flavours of quarks are described by appropriate quantum numbers. While the light quarks u and d carry a quantum number isospin, strange quarks s posses strangeness $S = -1$, charm quarks are attributed charm $C = +1$, and beauty quarks carry beauty $B = -1$.

While the notation B meson stands for any meson carrying a $\bar{b}$ quark, specific notations are used to emphasize the other quark in the meson:

$$\begin{aligned} B_d^0 &: |\bar{b}\, d\rangle \\ B_s^0 &: |\bar{b}\, s\rangle \\ B^+ &: |\bar{b}\, u\rangle \\ B_c^+ &: |\bar{b}\, c\rangle \end{aligned}$$

The existence of the b quarks was predicted in 1973 by Makoto Kobayashi and Toshihide Maskawa. They realized that in order to theoretically accommodate the violation of the CP

[8] In the literature the name of b quark often oscillates between "bottom" and "beauty".

1st generation	2nd generation	3rd generation	
e^- electron	μ^- muon	τ^- tau lepton	charged leptons charge $-e_0$
ν_e electron neutrino	ν_μ muon neutrino	ν_τ tau neutrino	neutral leptons charge 0
u up	c charm	t top	up-like quarks charge $+2/3e_0$
d down	s strange	b beauty	down-like quarks charge $-1/3e_0$

Table 1.1: Three generations of elementary fermions - leptons and quarks.

symmetry, which we describe in Chapter 2, three (instead of just two, as known at the time) generations of quarks must exist. Known quarks and leptons (all fermions[9]) are organized into three generations according to their appearance in interactions and mathematical equations describing those. Concerning the physical properties, individual generations differ in the mass of their members. Quark and lepton generations are shown in Table 1.1.

B mesons possess several properties that make this hadron species unique in testing some predictions of the Standard Model. The constituent bottom quark b is heavy and hence the mass of B mesons is large, around 5.5 GeV. As a matter of fact, the b quark is the heaviest quark that can be bound in a hadron. Top quarks are heavier, but do not form any hadron[10]. A reader may wonder why the mass of an object is stated in units of energy, electronvolts. It is common, and quite practical one should say, to use the "natural" system of units by putting $\hbar = c = 1$. By doing that, quantities E (energy), cp (momentum multiplied by the speed of light) and mc^2 (rest energy) are all expressed in units of eV. Also, equations, specifically those of special relativity, become easier to write. For example the expression for the energy,

$$E = \sqrt{(mc^2)^2 + (cp)^2} \ , \tag{1.2}$$

becomes simply

$$E = \sqrt{m^2 + p^2} \ . \tag{1.3}$$

When a need for the SI system units occurs, one merely introduces $c = 3 \cdot 10^8$ m/s and $\hbar c = 197$ MeV fm (or powers of those) to regain the "proper" units.

So the B mesons have roughly a mass of 5-6 protons, or somewhere between a Helium and a Lithium atom, and are significantly heavier than mesons, composed of charm quarks c, named D mesons. The latter have around twice lower mass. In decay of a B meson the constituent b quark must change into another quark which, as we will see in Sect. 1.2.3, is predominantly a c quark. The only interaction capable of changing the quark flavor (at the lowest order of a process) is the weak interaction. As the name suggests, processes

[9] All quarks and leptons have a spin of 1/2. Fermion is a common name for all particles with a half-integer spin, and which as a consequence follow the Fermi-Dirac statistics.

[10] Because the t quark is heavier than the charged weak boson W^+, the quark decays into a W^+ boson and a b quark before being able to form a hadron.

mediated by the weak interaction occur with a lower probability than processes which occur as a consequence of the strong and electromagnetic interactions. A decay of a b quark into a c quark and two leptons is depicted in Fig. 1.4. In the figure, powers of the weak coupling

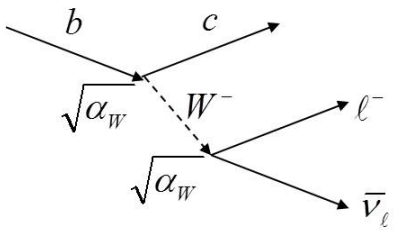

Figure 1.4: Feynman diagram of a b quark decay. Weak interaction is the only interaction that can - at the lowest order of a process - change the flavor of a quark. Denoted are the powers of the weak coupling constant α_W entering the amplitude for the process in each vertex.

constant α_W entering the amplitude $\mathscr{M}$ for the process are shown. Each vertex ($b-c$ and $\ell^- - \bar{\nu}_\ell$) contributes $\sqrt{\alpha_W}$ to the amplitude and hence $\mathscr{M} \propto \alpha_w$. Probability for the process is thus $w \propto |\mathscr{M}|^2 \propto \alpha_w^2$. Higher order processes include higher powers of α_W. Due to the small value of $\alpha_W \sim 0.03$ such higher order process are less probable[11]. The fact that B meson decays are governed by the weak interaction reflects in their lifetime τ_B. Compared to decays of hadrons mediated by the strong or electromagnetic interaction, decays of B mesons proceed at a lower rate, and hence they have a longer lifetime. The average lifetime of various B mesons listed above is around 1.5 ps ($1.5{\cdot}10^{-12}$ s, compared to, for example, a J/ψ meson that decays through the strong and electromagnetic interaction and has a lifetime of the order of 10^{-20} s). It should be noted that the mentioned lifetime is a proper lifetime, i.e. the lifetime of a particle in its rest frame. When a particle is moving, the Lorentz transformation from its rest frame into the moving frame causes time dilation. The lifetime in a moving frame is $\gamma\tau$, with γ the appropriate Lorentz factor[12].

To summarize, B mesons appear in few variations, with several common properties: being composed of a heavy quark b they all have large mass, decay through a weak interaction process, and possess - for particles at the subatomic level - a relatively long lifetime.

Note: B mesons are hadrons composed of a $\bar{b}$ anti-quark and another quark. They poses a large mass and relatively long lifetime.

[11] The weak coupling constant α_W is actually larger than the coupling constant of the electromagnetic interaction, $\alpha = 1/137$. However, mediators of the weak interaction posses a large mass M, contrary to massless photons mediating the electromagnetic interaction. Probability of a process proceeding through the weak interaction is proportional to α_W^2/M^2 which causes weak interaction processes to be less probable than the electromagnetic processes.

[12] $\gamma = 1/\sqrt{1-v^2/c^2}$, where v is the velocity of the moving frame and c the speed of light in vacuum.

1.2 Weak liaison

1.2.1 Weak Interaction

As mentioned in the previous section the basic interactions influencing the world of elementary particles are strong, electromagnetic, and weak interaction. The latter exhibits some specific properties which - at the time they were experimentally revealed - caused a significant amount of bewilderment and required much consideration in order to be explained. As we will also see, nowadays there are experimental facts (indeed perhaps not related exclusively to weak interaction) that the current theoretical knowledge is unable to explain.

Weak interaction is responsible for specific (β) decays of some of the nuclei. An example of such a decay is ${}^{10}C \rightarrow {}^{10}B\, e^+ \nu_e$ [13], in which a proton inside the initial nuclei decays into a neutron, positron and a neutrino. In early 1930s Enrico Fermi made a theoretical description of such β decays in analogy with the already known electromagnetic interaction. He merely substituted the coupling constant of the electromagnetic interaction (also known as the fine structure constant, $\alpha \sim 1/137$) by a different one, known today as the Fermi coupling constant G_F. The description was successful in explaining most of the properties of β decays, assuming of course that the process is mediated by a so far unknown interaction (i.e. an interaction with a different coupling constant[14]). Evidence for another type of interaction becomes perhaps most obvious when comparing lifetimes of charged and neutral pions (mesons composed of u and d quarks):

$$\begin{aligned} \tau_{\pi^\pm} &= 2.6 \cdot 10^{-8}\ \mathrm{s} \\ \tau_{\pi^0} &= 8.5 \cdot 10^{-17}\ \mathrm{s}\ . \end{aligned}$$

Why do the lifetimes of the two mesons of similar quark composition differ by 9 orders of magnitude? Pions are the lightest hadrons and hence can not decay through the strong interaction into lighter hadrons. The neutral pion can, however, decay through an electromagnetic process, $\pi^0 \rightarrow \gamma\gamma$. On the other hand, electromagnetic decays with photons in the final state are not possible for the charged pion. The decay $\pi^+ \rightarrow e^+\gamma$, for example, is forbidden by the lepton number conservation [15]. A possible decay mode of charged pion is $\pi^+ \rightarrow e^+\nu_e$, proceeding through the weak interaction (actually, by far the most abundant decay mode of charged pions is an analogous decay mode $\pi^+ \rightarrow \mu^+\nu_\mu$). Hence the reason for the above lifetime difference is the fact that neutral pions decay through the electromagnetic interaction, while charged pion decays are governed by the weak interaction. By inspection of Fig. 1.5 one can convince herself that β decays and charged pion decays indeed proceed through the same weak interaction mediated by charged weak bosons $W^\pm$.

It should be noted that the term weak interaction encompasses not only the interaction described, the charged weak interaction propagated by the charged weak bosons $W^\pm$, but

[13] Notation ${}^AX$ represents an isotope of the element X with A nucleons. Decays in which positrons are produced are denoted as β^+, and those with electrons in the final state as β^-.

[14] The Fermi coupling constant is related to the "genuine" weak coupling constant of Fig. 1.4 through $G_F = \sqrt{2}\alpha_W^2/8M_W^2$, where M_W is the mass of the charged weak boson $W^\pm$.

[15] Lepton number is defined as a difference between the number of leptons and the number of anti-leptons. The lepton number is conserved in all known processes.

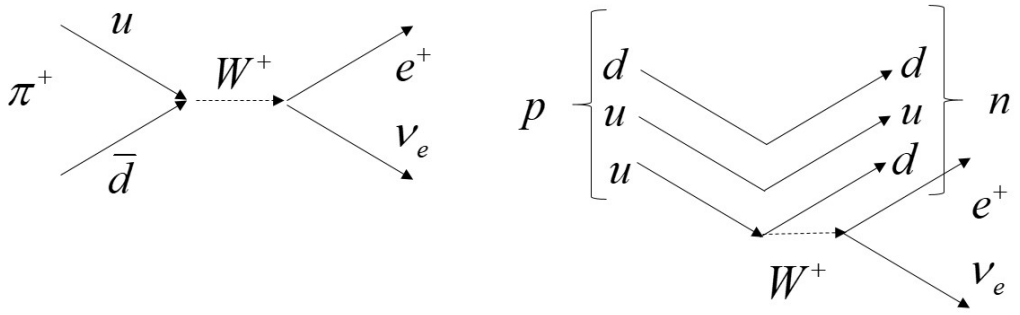

Figure 1.5: Feynman diagram of a charged pion (left) and β^+ (right) decay.

also neutral weak interaction, propagated by neutral weak bosons[16] Z^0. While the former is of special interest for measurements at the B Factories and as such in the focus of interest within this book, the latter played an utmost important role in establishing what is nowadays known as the Standard Model of particle interactions. Properties of Z^0 bosons were studied in great detail at the Large Electron Positron Collider (LEP), the predecessor of the Large Hadron Collider (LHC) at CERN.

Note: Beside the gravitational, strong, and electromagnetic interaction, also the weak interaction exists, and is mediated by charged ($W^{\pm}$) or neutral (Z^0) weak bosons. Processes governed by this interaction occur at a lower rate than processes governed by other interactions.

1.2.2 Parity

Following the postulation of weak interaction, the so called $\theta - \tau$ puzzle was one of the important unanswered questions of particle physics in the 1950s. The puzzle consisted of decays of what was originally believed to be two different particles, θ^+ and τ^+ (note that τ^+ has nothing to do with the contemporary τ lepton). While the former was decaying into two pion final state, the latter exhibited decays into three pions in the final state. At that time experimental evidence for the two particles being actually the same had been building up. If indeed the same particle exhibited decays into the mentioned two distinct final states it would represent a violation of the parity conservation, as we will elaborate on further in Chapter 2.

Conservation of parity assumes that the process under question proceeds exactly in the same manner when observed in a mirror, i.e. when all quantities are reflected over the coordinate system origin. Various physics observables behave differently under such a transformation. Examples for a few classical variables are shown in Fig. 1.6. Velocity ($\vec{v}$) and momentum ($\vec{p}$), vector variables, change sign in such inversion. Angular momentum ($\vec{L}$), on the other hand, is an axial vector and remains unchanged under the parity transformation[17].

[16] At high energies - close to $M_Z = 91.2$ GeV - the Z^0 exchange represents the main contribution to, for example, b quark pair production $e^+e^- \to b\bar{b}$.

[17] Not surprisingly, one should say, since $\vec{L} = \vec{r} \times \vec{p}$. While both, coordinate vector $\vec{r}$ and momentum vector

Although an intrinsic angular momentum - spin - of a particle ($\vec{s}$) doesn't have any classical analogy, under parity transformation it behaves in the same manner as the classical angular momentum, i.e. as an axial vector.

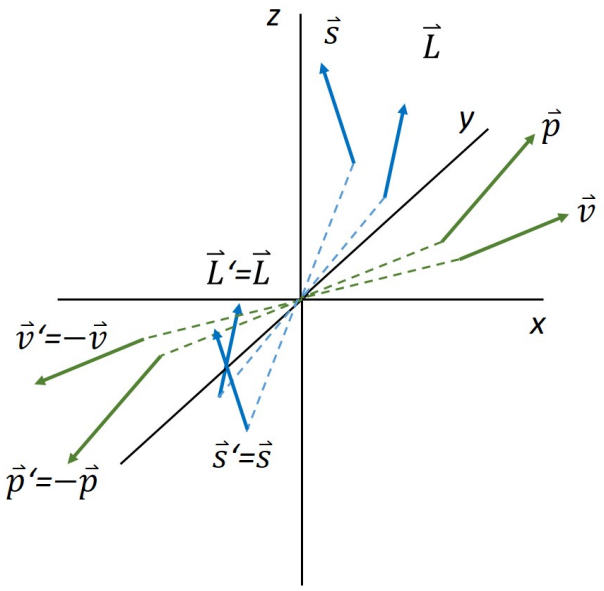

Figure 1.6: Behaviour of some of the physics variables under the parity transformation. Symbols marked by prime denote the quantities after the transformation.

In 1956 Tsung Duo Lee and Chen-Ning Yang examined the available experimental data and suggested that the $\theta - \tau$ puzzle and some similar decays can be interpreted by the weak interaction that violates parity conservation - the process caused by the weak interaction does not proceed exactly the same when observed in a mirror. They proposed an experiment carried out by Chien Siung Wu, the famous Cobalt-60 experiment. It involved a ^{60}Co isotope, decaying through β decay to ^{60}Ni: $^{60}Co \rightarrow ^{60}Ni\, e^- \bar{\nu}_e$. The idea of the experiment is sketched in Fig 1.7. A ^{60}Co nucleus carries the spin quantum number $s = 5$. The Co sample was put in a strong external magnetic field ($\vec{B}$) and cooled to a low temperature. At low temperatures almost all nuclei spins align in parallel to the external field. Spin of the final state nucleus (^{60}Ni) is 4. Hence the electron and the antineutrino in the decay carry away one unit of spin. In the experiment, the rate of electrons emerging under a given direction with respect to the direction of the magnetic field has been recorded. In two extreme cases - electrons flying parallel or anti-parallel to spins of initial nuclei - the projections of the spins onto the $\vec{B}$ axis are shown in the figure. The measurement results were asymmetric: While most of the electrons flew in the direction anti-parallel to the Co spin, no electrons were found emitted in the direction of the Co spin. In case we would be observing the process in a mirror, electrons would be preferentially emitted in the direction of Co spin (note that the direction of the spin would not be reversed in the mirror). This represents a violation of the parity symmetry. The weak interaction responsible for β decays does not preserve this symmetry.

$\vec{p}$, change the sign, the angular momentum remains unaffected.

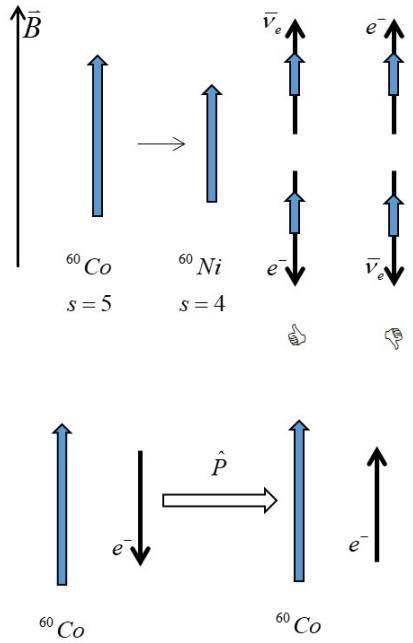

Figure 1.7: Schematics of the Cobalt-60 experiment. Top: Two extremes in the decay $^{60}Co \rightarrow ^{60} Ni\ e^-\ \bar{\nu}_e$ are shown, electrons flying parallel or anti-parallel to the direction of the external magnetic field $\vec{B}$ (direction of electron and anti-neutrino momentum is denoted by thin black arrows). Conservation of the angular momentum requires the spin projections as denoted by thick blue arrows (note that spin quantum number s is 5 for ^{60}Co, 4 for ^{60}Ni, and 1/2 for e^- and $\bar{\nu}_e$). In the measurement electrons were emitted preferentially in the direction opposite to $\vec{B}$, while no electrons were found to fly in the direction of $\vec{B}$. Bottom: Parity transformation $\hat{P}$ reverses the direction of an electron momentum and leaves spin of a Co nucleus unaltered. While the situation on the left is observed in the experiment, the one on the right is not. Hence the process - β decay proceeding through the weak interaction - does not conserve parity.

T.D. Lee and C.N. Yang shared the Nobel prize in physics in 1957 for the discovery of parity violation. T.D. Lee was at the age of 30 the third youngest Nobel prize laureate (after W.L. Bragg, who was 25 in 1915, and W. Heisenberg, aged 30 in 1932).

Note: Weak interaction has several peculiar properties. One of those is the violation of parity: processes proceeding through the weak interaction do not occur in the same manner when looked at in the mirror.

1.2.3 Cabibbo-Kabayahi-Maskawa

Nature seems to be playful when determining the properties of charged weak interaction. Another puzzle that needed to be cracked back in the 1960s was the difference of probabilities for decays that at first sight seemed almost analogous. If one peeks at two decay modes of a τ lepton, $\tau^+ \rightarrow \pi^+ \nu_\tau$ and $\tau^+ \rightarrow K^+ \nu_\tau$, sketched in Fig. 1.8, at first sight they

seem very similar[18]. The only difference appears in the quark content of a pion and a kaon (c.f. Fig. 1.3), and in the mass difference between the two (which is small, however, compared to the mass of the τ lepton; $M_\tau = 1.78$ GeV, $M_\pi = 0.14$ GeV, $M_K = 0.49$ GeV). The

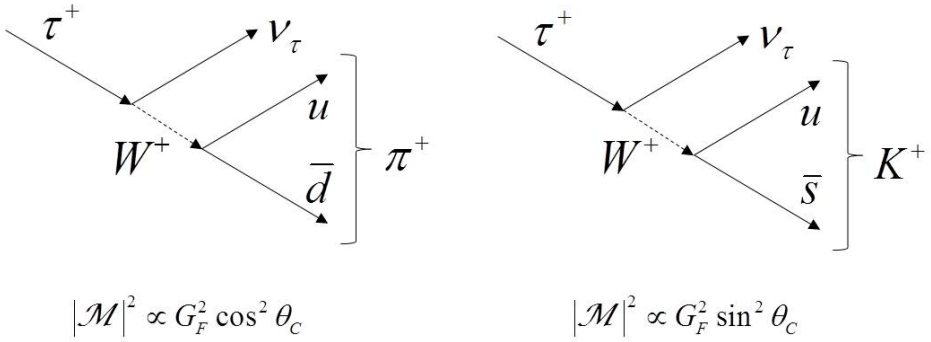

Figure 1.8: Semileptonic decays of a τ lepton with a pion (left) and a kaon (right) in the final state. The expected rate proportionality taking into account the Cabibbo angle is shown below the diagrams.

decay branching fractions, defined as the probability for a specific decay among all possible decays of a particle, expose a significant difference, though: $Br(\tau^+ \to \pi^+\nu_\tau) = 0.11$ and $Br(\tau^+ \to K^+\nu_\tau) = 7 \cdot 10^{-3}$. Difference in rates of such decays proceeding through the weak interaction required an explanation. In 1963 Nicola Cabibbo introduced an addition to the weak coupling constant explaining the observed difference. Nowadays Cabibbo's explanation is interpreted as follows: quark states involved in the charged weak interaction are a linear combination of those involved in the strong (or, for that matter, electromagnetic) interaction. The W boson couples to e.g. ud' or us' quarks, where

$$\begin{bmatrix} d' \\ s' \end{bmatrix} = \begin{bmatrix} \cos\theta_C & \sin\theta_C \\ -\sin\theta_C & \cos\theta_C \end{bmatrix} \begin{bmatrix} d \\ s \end{bmatrix} = \begin{bmatrix} \cos\theta_C\, d + \sin\theta_C\, s \\ -\sin\theta_C\, d + \cos\theta_C\, s \end{bmatrix} . \tag{1.4}$$

The rotation angle of down-like quarks involved in charged weak interaction, θ_C, is called the Cabibbo angle. Symbolically, in the weak interaction the following quark pairs take part:

$$[\bar{u},\ \bar{c}] \begin{bmatrix} d' \\ s' \end{bmatrix} = \bar{u}\, d\ \cos\theta_C + \bar{u}\, s\ \sin\theta_C - \bar{c}\, d\ \sin\theta_C + \bar{c}\, s\ \cos\theta_C\ . \tag{1.5}$$

When a $\bar{u}d$ pair couples to a W boson the Fermi coupling constant is multiplied by $\cos\theta_C$. The same is true in a $\bar{c}s$ weak interaction, while in the case of a $\bar{u}s$ and $\bar{c}d$ interaction the factor is $(-)\sin\theta_C$. Neglecting the small differences in masses of involved particles, the decay rates for $\tau^+ \to \pi^+\nu_\tau$ and $\tau^+ \to K^+\nu_\tau$ are proportional to factors shown in Fig. 1.8. The ratio of the branching fractions is thus $\cot^2\theta_C$ which using the experimentally determined value of θ_C ($\theta_C \approx 13^\circ$) amounts to $5 \cdot 10^{-2}$, in quite good agreement with the measured value of $6 \cdot 10^{-2}$.

[18] Actually, in the 1960s the two decay modes under consideration were $K^+ \to \mu^+\nu_\mu$ and $\pi^+ \to \mu^+\nu_\mu$. However, when comparing probabilities for these purely leptonic decays one has to take into account additional factors, not present in the τ semileptonic decays suggested as examples.

The introduction of the Cabibbo angle, or better to say the idea of linear combinations of down-like quarks entering the charged weak interaction, hence explained another puzzling behaviour of this type of interactions among the quarks.

In the 1960s, at the time N. Cabibbo offered the above explanation, only three flavours of quarks - u, d and s - were known to exist. In the following decade a series of experimental and theoretical breakthroughs, culminating in the 1974 discovery of a particle J/ψ, lead to evidence of a fourth - charm, c - quark existence. The J/ψ meson is a bound state of a $c\bar{c}$ quark anti-quark pair. It was discovered simultaneously and independently by the groups in Stanford Linear Accelerator Center and Brookhaven National Laboratory, lead by Burton Richter and Samuel C.C. Ting, respectively. The two heads of the groups shared the Nobel prize in 1976 for their discovery.

One year before the J/ψ discovery, in 1973, an article written by Japanese theorists Makoto Kobayashi and Toshihide Maskawa appeared in a scientific journal. For reasons to be explained in section 2.3.2 they expanded a set of quark flavours from four to six (i.e. they introduced what is nowadays known as beauty, b, and top, t, quarks). Following further experimental evidence on the properties of the charged weak interaction available at the time and with a deep and far-reaching insight they suggested a set of rotated down-like quarks involved in the charged weak interaction to be written as

$$\begin{bmatrix} d' \\ s' \\ b' \end{bmatrix} = V_{CKM} \begin{bmatrix} d \\ s \\ b \end{bmatrix} = \begin{bmatrix} V_{ud} & V_{us} & V_{ub} \\ V_{cd} & V_{cs} & V_{cb} \\ V_{td} & V_{ts} & V_{tb} \end{bmatrix} \begin{bmatrix} d \\ s \\ b \end{bmatrix} \quad . \tag{1.6}$$

The 3×3 matrix denoted by V_{CKM} is known today as the Cabibbo-Kobayashi-Maskawa (CKM) matrix . In general it has 9 complex elements, denoted by V_{ij} with $i = u,\ c,\ t$ and $j = d,\ s,\ b$. Squared magnitudes of the elements, $|V_{ij}|^2$, determine the relative rates of $W^+ \to \bar{q}_i q_j$ processes as sketched in Fig. 1.9.

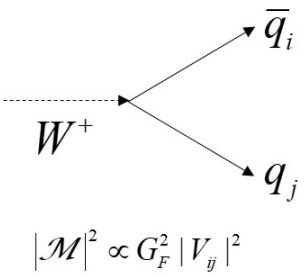

Figure 1.9: Process $W^+ \to \bar{q}_i q_j$ and the corresponding relative rate including the element of the CKM matrix V_{ij}.

The CKM matrix must be unitary. Mathematically,

$$V_{CKM}^{\dagger} V_{CKM} = I \ , \tag{1.7}$$

where I denotes an identity matrix, and $V_{CKM}^{\dagger}$ is a hermitian conjugate of V_{CKM}. The latter

means transpose and complex conjugate of the matrix, hence

$$V_{CKM}^{\dagger} = \begin{bmatrix} V_{ud}^* & V_{cd}^* & V_{td}^* \\ V_{us}^* & V_{cs}^* & V_{ts}^* \\ V_{ub}^* & V_{cb}^* & V_{tb}^* \end{bmatrix} \quad . \tag{1.8}$$

Among else, the unitarity of the CKM matrix describes an experimentally verified fact that in the nature processes in which the neutral weak interaction would couple two different flavours of down-type quarks, e.g. $Z^0 \to d\bar{s}$, do not exist. Schematically this is easy to see by writing the possible combinations of down-type quarks involved in the neutral weak interaction:

$$[\bar{d}',\, \bar{s}',\, \bar{b}'] \begin{bmatrix} d' \\ s' \\ b' \end{bmatrix} = \sum_{i=1}^{i=3} \bar{q}_i'\, q_j' = [\bar{d},\, \bar{s},\, \bar{b}]\, V_{CKM}^{\dagger}\, V_{CKM} \begin{bmatrix} d \\ s \\ b \end{bmatrix} = \sum_{i,j,k=1}^{i,j,k=3} \bar{q}_i\, V_{ij}^{\dagger}\, V_{jk}\, q_k \quad . \tag{1.9}$$

In the equation above we also used a notation explicitly exposing the summation involved in the multiplication of vectors and matrices. For a given value of i and k the sum entering the expression is

$$\bar{q}_i \sum_{j=1}^{j=3} [V_{ij}^{\dagger}\, V_{jk}] q_k \quad . \tag{1.10}$$

The sum in the brackets is nothing else but a product of the i-th row of $V_{CKM}^{\dagger}$ with the k-th column of V_{CKM}. According to Eq 1.7 this equals 0 for $i \neq k$ and 1 for $i = k$. The unitarity of the CKM matrix thus ensures

$$[\bar{d}',\, \bar{s}',\, \bar{b}'] \begin{bmatrix} d' \\ s' \\ b' \end{bmatrix} = [\bar{d},\, \bar{s},\, \bar{b}] \begin{bmatrix} d \\ s \\ b \end{bmatrix} = \bar{d}\, d + \bar{s}\, s + \bar{b}\, b \quad . \tag{1.11}$$

There are no neutral weak interaction processes coupling different flavours of quarks. The described theoretical mechanism is called Glashow-Iliopolous-Maiani (GIM) mechanism. Thus in the weak interaction the following pairs of quarks appear:

$$\underbrace{[\bar{d}',\, \bar{s}',\, \bar{b}'] \begin{bmatrix} d' \\ s' \\ b' \end{bmatrix} + [\bar{u},\, \bar{c},\, \bar{t}] \begin{bmatrix} u \\ c \\ t \end{bmatrix}}_{\text{neutral weak interaction}} + \underbrace{[\bar{d}',\, \bar{s}',\, \bar{b}'] \begin{bmatrix} u \\ d \\ s \end{bmatrix}}_{\text{charged weak interaction}} = \tag{1.12}$$

$$= \underbrace{\bar{d}\, d + \bar{s}\, s + \bar{b}\, b + \bar{u}\, u + \bar{c}\, c + \bar{t}\, t +}_{\text{neutral weak interaction}}$$

$$+ \underbrace{V_{ud}\, \bar{d}\, u + V_{us}\, \bar{s}\, u + V_{ub}\, \bar{b}\, u + V_{cd}\, \bar{d}\, c + V_{cs}\, \bar{s}\, c + V_{cb}\, \bar{b}\, c + V_{td}\, \bar{d}\, t + V_{ts}\, \bar{s}\, t + V_{tb}\, \bar{b}\, t}_{\text{charged weak interaction}} \quad .$$

Magnitudes of the CKM matrix elements determine the relative rate of charged $W^{\pm}$ bosons decays into specific quark anti-quark pairs. Elements of the CKM matrix are not known a priori, i.e. they are not predicted by the theory, they are free parameters. This means they have to be experimentally determined, measured. Measurements of B mesons decays,

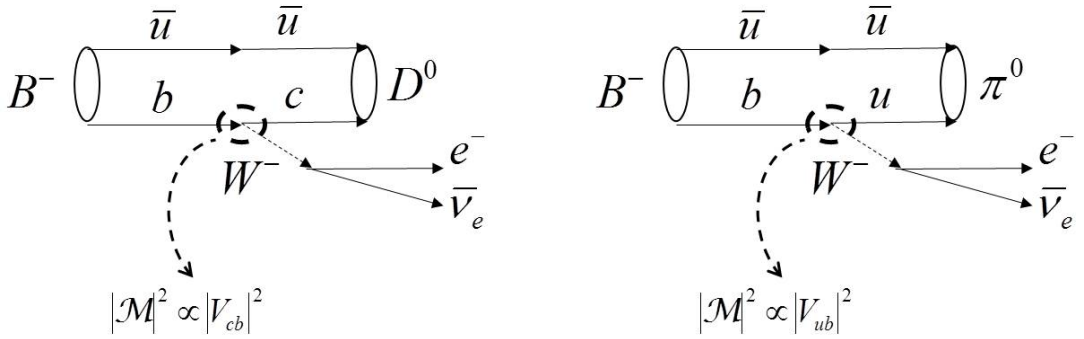

Figure 1.10: Examples of B meson decays with $b \to c$ and $b \to u$ quark sub-process. Measurements of rates of such decays enable determination of the corresponding CKM matrix element magnitude.

for example, like the ones depicted in Fig. 1.10, yield the value of the appropriate CKM element entering the process. Measurements of other hadron decays enable determination of magnitudes of individual CKM matrix elements.

A surprising feature of the CKM matrix is that the magnitudes of the diagonal elements of the matrix almost equal unity, next-to-diagonal elements are an order of magnitude smaller in magnitude, and the most off-diagonal elements have magnitudes of the order of $10^{-3} - 10^{-2}$. Numerically,

$$\begin{bmatrix} |V_{ud}| & |V_{us}| & |V_{ub}| \\ |V_{cd}| & |V_{cs}| & |V_{cb}| \\ |V_{td}| & |V_{ts}| & |V_{tb}| \end{bmatrix} = \begin{bmatrix} 0.974 & 0.225 & 0.004 \\ 0.224 & 0.974 & 0.042 \\ 0.009 & 0.041 & 0.999 \end{bmatrix} . \tag{1.13}$$

In other words, the charged weak interaction most often couples quarks of the same generation (see Table 1.1), and less likely quarks from different generations. The former processes are often addressed as Cabibbo allowed and the latter as Cabibbo suppressed[19]. Any underlying reasons for such an hierarchy are unknown.

The mentioned hierarchy of the CKM matrix elements reflects in decays of B mesons composed of b quarks. Out of elements related to b quarks - V_{tb}, V_{cb} and V_{ub} - the first one has the largest magnitude. Top (t) quarks are not produced at the energies involved at B Factories and hence direct quark decays $t \to b$ are not present there. This element does, however, importantly influence some of the processes with B mesons. Despite their (too) high mass t quarks appear in some higher order processes, in accordance with the Heisenberg uncertainty principle:

$$\Delta x \Delta p \geq \hbar/2 \ . \tag{1.14}$$

The principle relates indefiniteness of position and momentum determination in quantum mechanics. Once the position of any quantum system is determined to Δx, momentum is inherently undetermined to at least $\hbar/(2\Delta x)$, and vice versa. The principle is valid for any pair of complementary variables, also for energy and time. For the latter it is formulated as

[19]The Cabibbo suppressed decays are sometimes further divided into singly Cabibbo suppressed - those which include quarks of neighbouring generations, e.g. b and c - and doubly Cabibbo suppressed - those including quarks from non-neighbouring generations, e.g. b and u.

$\Delta E \Delta t \geq \hbar/2$. Let us interpret it using a specific example of a process shown in Fig. 1.11. This higher order weak interaction process ($\mathscr{M} \propto \alpha_W^4$) causes a B_d^0 meson in the course of

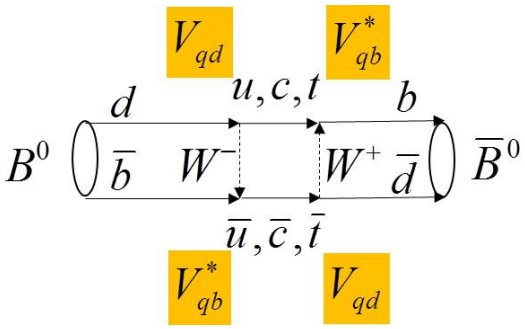

Figure 1.11: One of Feynman diagrams contributing to $B_d^0 \to \bar{B}_d^0$ transition, known as B_d^0 oscillations.

its lifetime to change into it's antiparticle and vice versa. The phenomena is called B meson mixing or oscillations. It appears not only in the system of neutral B mesons (for B_d^0 and B_s^0 mesons) but for all neutral mesons[20]. We will discuss the B meson oscillations further in Sect. 3.3. At this place we note the contribution of quarks with positive charge ($q = u,\ c,\ t$) in the process. Although the t quark is too heavy to appear as a decay product of any B meson, it can appear, for example, in the $d \to W^- t$ vertex as shown, in accordance with the uncertainty principle. Energy conservation in the vertex is violated by an amount ΔE (because the rest energy of W^- and t is much larger than that of a d quark). Nevertheless the process can proceed as long as the two heavy particles are reabsorbed within a time interval $\Delta t \sim \hbar/(2\Delta E)$. This is what indeed happens, t quark is immediately afterwards involved in a $tW^+ \to b$ vertex. Particles that appear in the process possible only within the realm of the uncertainty principle, and do not satisfy the usual relativistic relation $E = \sqrt{p^2 + m^2}$, are called virtual particles.

Coming back to the CKM matrix elements related to b quarks, from the remaining two elements the $|V_{cb}|$ is around ten times larger than $|V_{ub}|$, causing the quark transitions $b \to c$ around two orders of magnitude more frequent than $b \to u$. For example, $B_d^0 \to \bar{D}^0 e^+ \nu_e$ decay occurs in around 2% of all B_d^0 decays, while $B_d^0 \to \pi^0 e^+ \nu_e$ only once in around every 10^4 decays.

A careful reader may notice that so far we've only discussed the magnitudes of the CKM matrix elements despite the fact that in principle the elements are complex. As any complex number z they can be described by the magnitude and a phase, in a form $z = |z|e^{i\phi}$. The complex phase of the CKM matrix elements is indeed of utmost importance, closely related to the violation of CP symmetry, discussed further in Chapter 2.

Note: Quark states involved in the charged weak interaction are linear combinations of quarks involved in the strong interaction. These linear combinations, and consequently

[20] Also for K^0 and D^0 mesons. It doesn't exist for mesons composed of a $q\bar{q}$ (where q denotes quark and anti-quark of the same flavour), because such mesons (e.g. π^0 mesons, or quarkonium) are their own antiparticles (e.g. $\bar{\pi}^0 = \pi^0$).

rates of decays of $W^{\pm}$ bosons into different quark anti-quark pairs are governed by the Cabibbo-Kobayashi-Maskawa (CKM) matrix.

1.3 Frontiers

The mentioned hierarchy in the magnitudes of the CKM matrix elements, which is an experimental fact and no interpretation based on physical laws exists for it, is one of the reasons to believe that our current understanding of the basic interactions among the elementary particles (Standard Model) is not the ultimate one. There may exist some kind of underlying symmetry, so far unknown to us, that results in the observed CKM matrix elements hierarchy. There are several other shortcomings of the SM. The fact that roughly one quarter of the Universe is composed of a Dark Matter[21], the substance of which is still completely unknown, but cannot be of the SM particles, is clearly one of those. To continue, the SM does not explain the gravity, the fourth elementary interaction in Nature. And the coupling constants of the three types of interactions included in the SM, are - at least in processes taking place at the currently achievable energies - quite different. The question remains if at some high energy the strengths of interactions unify[22]. Unexplained but extremely pronounced hierarchies, like the ones in the CKM matrix, appear elsewhere. Masses of the elementary fermions (Tab. 1.1) span roughly a range from 0,5 MeV ($e^{\pm}$) to 170 GeV (t), interval of six orders of magnitude, not including the neutrinos[23]. What are deeper reasons for this? Already Richard Feynman, one of the fathers of quantum electrodynamics, considered this to be an important and interesting question. And, last but certainly not least, the observed dominance of matter over anti-matter in the observable Universe can not be explained by the current measurement results at the level of elementary particles and their theoretical description.

These and similar, within the SM unanswered questions have been a clear and present motivation for ongoing efforts of both, theoretical and experimental high energy physicists for over a decade. The efforts in searching for so far unknown processes and particles beyond the framework of the SM, the ones that constitute what is often addressed as "New Physics". Since the SM is clearly not the ultimate theory yielding answers to some basic questions but rather an - indeed extremely successful - effective theory describing majority of the so far observed phenomena in the world of subatomic particles, scientists are seeking for effects that would a) constitute an evidence of physics processes beyond the SM, and b) shed light on the "inner workings", i.e. help in understanding the basic physics laws of New Physics (NP).

Numerous experiments in the field of contemporary high energy physics can be grouped into several categories. The Energy Frontier experiments exploit highest achievable ener-

[21] The current cosmological knowledge tells that around 70% of the Universe is Dark Energy, 25% is Dark Matter, and only around 5% of the Universe is composed of the matter familiar to us.

[22] Coupling constants of individual interactions are not completely constant, they depend on the energy at which a certain process takes place. In theories that go beyond the SM (Grand Unified Theories) the coupling constants of strong, weak and electromagnetic interaction unify - they become equal - at an energy scale of around 10^{16} GeV. These interactions are assumed to further unify with the gravitational interaction at the so called Planck scale, 10^{19} GeV.

[23] Neutrinos are massless within the SM. Measurements of the neutrino oscillations phenomena have shown that they do have a small mass.

gies to search for heavy particles that can only be produced at such energies. The Intensity Frontier experiments, on the other hand, are performing measurements of unprecedented accuracy and comparison of results to the existing theories (most notably the SM), to search for possible deviations of the results from the predictions and by that identifying NP. The Cosmic Frontier experiments make use of measurements of phenomena in the Universe in trying to interpret those in terms of NP (e.g. Dark Matter). The three categories of scientific endeavour are not strictly divided and, more importantly, are complementary. Most probably it will not be possible to understand laws of NP without experimental results and theoretical interpretation of evidences from all three categories.

Note: The Standard Model (SM) of interactions among elementary particles has several serious shortcomings. Processes involving particles beyond those described within the SM must exists in Nature but have not been observed so far. Physicist are searching such New Physics processes at the Energy, Intensity and Cosmic Frontier.

Chapter 2

Into the Mirror

2.1 C & P

In Sec. 1.2.2 we discussed the operation of parity and non-conservation of parity in processes mediated by the weak interaction. The experiment with ^{60}Co established the parity violation in weak interaction processes. We can now formulate the parity operation, discussed so far in terms of observing a given process in the mirror, in a slightly more mathematical terms. The parity transformation reflects a chosen coordinate system through the origin. Denoting the parity operator by $\hat{P}$, the effect of the operation on a given function describing some quantum state (wave function) $|\psi(\vec{r})\rangle$ is

$$|\psi'(\vec{r})\rangle = \hat{P}|\psi(\vec{r})\rangle = e^{i\phi}|\psi(-\vec{r})\rangle \ . \tag{2.1}$$

$e^{i\phi}$ in the above equation must be added since the operator can - beside reversing all coordinates - also change the overall phase of a state. Applying operator $\hat{P}$ once again on the already transformed function $|\psi'(\vec{r})\rangle$ one obtains

$$\hat{P}|\psi'(\vec{r})\rangle = \hat{P}^2|\psi(\vec{r}\rangle = e^{2i\phi}|\psi(\vec{r})\rangle \ . \tag{2.2}$$

On the other hand, it's clear that reversing the coordinates twice does not have any effect and hence

$$\hat{P}^2|\psi(\vec{r}\rangle = |\psi(\vec{r})\rangle \ . \tag{2.3}$$

Comparing Eqs. 2.2 and 2.3 we find $e^{2i\phi} = 1$, hence $\phi = 0,\ \pi$ and

$$\hat{P}|\psi(\vec{r})\rangle = \pm|\psi(-\vec{r})\rangle \ . \tag{2.4}$$

The value of $e^{i0} = +1$ or $e^{i\pi} = -1$ is called an intrinsic parity of a particle. By convention we assign a positive parity to fermions (electrons, neutrinos, protons,....), while anti-fermions (positrons, anti-protons, anti-neutrinos,...) have negative parity[1]. Unlike fermions, bosons and corresponding anti-bosons have the same intrinsic parity.

Parity can be determined also for compound states, for example for a state of two particles, a and b, with a relative orbital angular momentum L. The spatial part of the wave

[1]The fact that a fermion and its anti-particle have opposite parities arises from the relativistic quantum mechanics, specifically from the Dirac equation.

function describing such a state is composed of spherical harmonics $Y_m^L(\theta,\phi)$, where θ and ϕ represent two of coordinates in a spherical coordinate system[2]. It can be shown that the parity transformation on a spherical harmonic results in

$$\hat{P}Y_m^L(\theta,\phi) = Y_m^L(\pi-\theta,\phi+\pi) = (-1)^L Y_m^L(\theta,\phi) \ . \tag{2.5}$$

Parity is a multiplicative quantum number and hence the total parity of such a system is $P_a P_b (-1)^L$, with $P_{a,b}$ denoting the intrinsic parities of involved particles.

Parities for some particles can be determined experimentally, using parity conserving processes - those mediated by strong or electromagnetic interactions. Parity of charged pions, for example, can be determined from the pion capture on deuteron resulting in a two neutrons final state, $\pi^- \, {}^2_1H \to n\,n$. Details of this measurement and of logic leading to the conclusions that the intrinsic parity of a pion is negative ($P_\pi = -1$) go beyond the scope of this book[3]. We will rather use the findings to explain the $\theta-\tau$ puzzle, mentioned in Sect.1.2.2.

The two decays in question were $\tau^+ \to \pi^+\pi^-\pi^0$ and $\theta^+ \to \pi^+\pi^0$. The two initial state particles, at that time called τ and θ, were both determined to have spin $s=0$ and consistent masses and lifetimes. Nevertheless, the former decays into a three pion final state, and the latter into a two pion final state. Pions in the final state have null orbital angular momentum (since the initial state particles as well as pions are spin zero particles) and hence the parity of the three pion state is $P_{3\pi} = P_\pi^3(-1)^0 = -1$ and that of the two pion state $P_{2\pi} = P_\pi^2(-1)^0 = +1$. If θ and τ are the same particle, there must be an interaction that does not conserve parity, a fact put forward and proved by T.D. Lee, C.N. Yang and C.S. Wu. Pions, as well as other mesons with null orbital angular momentum, depicted in Fig. 1.3(left), all have negative intrinsic parity. Specifically, this is true also for kaons, about which we shell discuss further in the next section.

In description of the Cobalt-60 experiment we were looking into the process through a space mirror. At this point we can imagine another mirror, a particle mirror - a mirror which changes all particles into their anti-particles and vice versa. The transformation replacing particles with anti-particles is called charge conjugation. Denoting the operator of charge conjugation by $\hat{C}$, the effect on a particle state $|\psi\rangle$ is

$$\hat{C}|\psi\rangle = e^{i\vartheta}|\bar{\psi}\rangle \ , \tag{2.6}$$

where $|\bar{\psi}\rangle$ denotes the state of an anti-particle. The operation of charge conjugation changes an electron into a positron, a proton into an anti-proton, etc. All additive quantum numbers, like electric charge, baryon number, lepton number, ... change sign under the transformation. The charge conjugation does not affect momentum and spin, though. Similarly as with the $\hat{P}$ operator, applying $\hat{C}$ twice to some state leads back to the original state. Hence $e^{2i\vartheta} = 1$ and $\vartheta = 0, \ \pi$.

There is an important distinction between the parity and the charge conjugation operators, $\hat{P}$ and $\hat{C}$: elementary fermions (quarks and leptons) are not eigenstates of the later. Hence the C-parity of fermions can't be determined, nor does their relative C-parity with respect

[2]Spherical harmonics are eigenfunctions of the orbital angular momentum operator $\hat{L}^2 Y_m^L(\theta,\phi) = L(L+1)Y_m^L(\theta,\phi)$

[3]The same is true for a parity of a neutral pion, which can be determined using rare decays $\pi^0 \to e^+e^-e^+e^-$ to be negative as well.

to their anti-particles follow from some underlying physics law as does for the P. Only neutral particles which are their own anti-particles are eigenstates of $\hat{C}$. Such a particle is a photon, for example. Properties of electromagnetic field reflect in its negative C-parity[4]. Also a neutral pion is self conjugated (a common term for particles that are eigenstates of the charge conjugation operator). Due to the electromagnetic $\pi^0 \to \gamma\gamma$ decay, the C-parity of a π^0 follows from $C_{\pi^0} = C_\gamma C_\gamma = +1$. Bound states of heavier same flavour quarks, $c\bar{c}$ and $b\bar{b}$, are also eigenstates of $\hat{C}$. Such states are commonly named quarkonium, with charmonium denoting the charm and bottomonium the beauty quarks bound states. C transformation of such a state switches the q and $\bar{q}$, and is thus effectively equal to the parity operation (see Fig. 2.1). Because of this the C eigenvalue receives a factor of $(-1)^L$. Furthermore, if the quark pair is in a spin $S = 1$ state the $q \leftrightarrow \bar{q}$ transformation has no effect, while it does make a change for the state with $S = 1$. This brings another factor of $(-1)^{S+1}$ to the C-parity. Finally, the transformed wave function receives additional factor of -1 due to the fermion anti-fermion exchange. Altogether the C parity of such a state is $(-1)^{L+S}$.

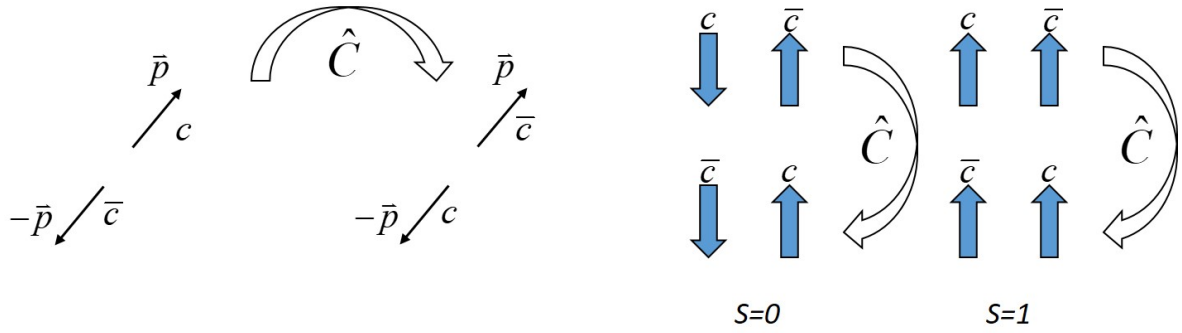

Figure 2.1: Left: The operator $\hat{C}$ effectively reverses the momenta in a bound state of quarkonium (shown here is an example for charmonium, $c\bar{c}$). Right: In case of a state with spin 1 the operator $\hat{C}$ has no effect on spin configuration, while in the case of spin 0 the quarks spin configuration is changed.

Although charged pions, for example, are not eigenstates of $\hat{C}$ operator, one can still determine a C eigenvalue of a composite system, like $\pi^+\pi^-$. The latter is composed of two bosons with spin 0, and hence the Bose-Einstein[5] statistics must apply to such a state. Treating the two charged pions as indistinguishable particles, i.e. taking their charges as one of components of their wave function, the latter must be symmetric under an interchange of the two particles. In the absence of spins the wave function consists of a spatial part and a charge part. An exchange of particles is just the inversion of spatial coordinates and of charge, in other words exactly what the $\hat{C}\hat{P}$ operator does. We can thus conclude that a CP eigenvalue of a $\pi^+\pi^-$ system is positive. Adding an additional neutral pion to the system changes the situation. If the relative angular momentum of a π^0 with respect to the charged pions is 0 (which is the most probable case if the three pions arise from a decay of a spinless

[4] Very generally one can say that the electromagnetic field is caused by (moving) charges which under the $\hat{C}$ transformation change sign, and hence $C(\gamma) = -1$.

[5] As opposed to fermion systems to which the Fermi-Dirac statistics apply.

particle, for example) we need to take into account C_{π^0} and P_{π^0}, adding $C_{\pi^0}P_{\pi^0} = 1 \cdot (-1) = -1$ to the CP value of the two pion system. Hence the CP value of $\pi^+\pi^-\pi^0$ system is negative.

We mentioned some quantum numbers, specifically the baryon (N_b) and lepton (N_l) number, which we will use in the later chapters and should look at them in some more details. Every baryon (like proton) is assigned a baryon number $N_b(B) = +1$. Every anti-baryon (like anti-proton), on the other hand, is assigned a negative baryon number, $N_b(\bar{B}) = -1$. Considering the quark model we can also assign a baryon number $N_b(q) = 1/3$ to every quark and $N_b(\bar{q}) = -1/3$ to every anti-quark. The total baryon number, the sum of baryon numbers of all particles in an initial state of a process, is conserved in all known processes among elementary particles. The baryon number conservation is a consequence of the fact that mediators of all interactions couple to $q\bar{q}$ pairs, and never to qq or $\bar{q}\bar{q}$ pairs. In weak interaction one always encounters $Z^0 \to q\bar{q}$ or $W^\pm \to q\bar{q}'$ processes, in strong interaction $g \to q\bar{q}$ and in electromagnetic interaction $\gamma \to q\bar{q}$. The baryon number conservation has some far reaching consequences, stability of protons, for example. Proton, as the lightest baryon, can not decay. Its decay would lead to a final state without baryons (since all of them are heavier than a proton) and would thus constitute a baryon number violating process.

In a similar manner as the baryon number one defines the lepton number: all leptons (like electron or electron neutrino) are are assigned $N_l(\ell) = +1$ and all anti-leptons (like positron or electron anti-neutrino) are assigned $N_l(\bar{\ell}) = -1$. Like the baryon number also the lepton number is conserved in all known processes.

The result of the Cobalt-60 experiment (sketched in Fig. 1.7) showed that there are no electrons flying in the direction of the magnetic field. Looking at the sketch of the two limiting situations one observes that this implies no anti-neutrino with the direction of its spin anti-parallel to the momentum direction being observed. The projection of particle's spin onto its momentum direction is called helicity. In the Cobalt-60 experiment only the positive helicity anti-neutrinos are observed, and no negative helicity ones. This fact establishes the violation of parity in the process, since as shown in the uppermost row of Fig. 2.2, the parity operator changes a positive helicity anti-neutrino into a negative helicity one. The opposite is true for neutrinos: while neutrinos with negative helicity exist, neutrinos with positive helicity are not observed (Fig. 2.2, second row). This implies that the weak interaction violates another symmetry: the symmetry under the charge conjugation $\hat{C}$. Namely, if one starts with a positive helicity anti-neutrino and performs the charge conjugation transformation (Fig. 2.2, third row) the result is a non-existing positive helicity neutrino. Analogously, starting with a negative helicity neutrino (Fig. 2.2, bottom row) one arrives to a non-existing negative helicity anti-neutrino[6].

The weak interaction thus violates both, the P as well as the C parity symmetry. In 1957 Lev Landau proposed that the true symmetry which is preserved (also) by the weak interaction is the symmetry under a combined CP transformation: first the parity operator $\hat{P}$ is applied to a state, followed by the operator $\hat{C}$. This is shown between the first two lines of Fig. 2.2. By this an initial positive helicity anti-neutrino is changed into a negative helicity

[6] Actually, the terminology here is not completely correct. What one observes is that in the charged weak interaction only negative helicity neutrinos and positive helicity anti-neutrinos are involved. Since the neutrinos interact only through the weak interaction one can do a slightly sloppy generalization about the existence of the two mentioned states and non-existence of the other two.

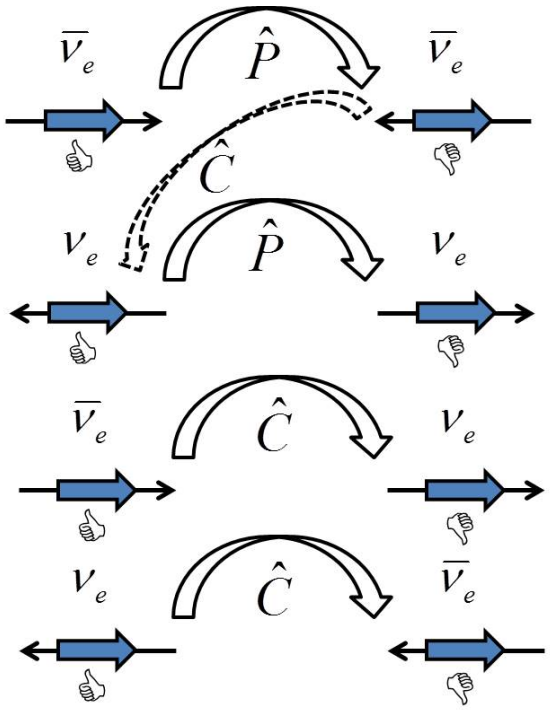

Figure 2.2: Effect of parity ($\hat{P}$) and charge conjugation ($\hat{C}$) operators on (anti-)neutrinos with negative and positive helicity. Thin black arrows denote the direction of momentum and thicker blue arrow the projection of a spin onto the momentum direction.

neutrino. The idea of *CP* conservation lasted for only seven years, as we shall explain in the next section[7].

Note: Weak interaction does not only violate parity, the processes governed by it also depend on particle / anti-particle nature of involved elementary constituents. In expert language the weak interaction violates also the *C* parity. For a brief time in history there was an idea, however, that it might preserve a combined *CP* symmetry.

2.2 Strange Particles

After establishing the parity violation in weak interaction in 1950's, surprises regarding the processes induced by this force have not diminished. In 1963 Val L. Fitch and James Cronin started a program of studies of neutral kaons in Brookhaven. Neutral kaons are composed of an $\bar{s}$ anti-quark and a d quark, $|K^0\rangle = |\bar{s}\, d\rangle$. Their anti-particles, anti-kaons, are composed as $|\bar{K}^0\rangle = |s\, \bar{d}\rangle$. These hadrons can be produced in strong interaction processes, for example in $\pi^- p \to \Lambda^0 K^0$ and $\pi^+ p \to K^+ \bar{K}^0 p$, depicted at the quark level in Fig. 2.3. Hadrons

[7] It should be mentioned that some physicist, Lev Okun, for example, already at that time argued that the *CP* conservation should be experimentally verified.

composed of strange s quark are always produced in pairs due to the fact that a gluon (g) can only produce quark anti-quark pairs of the same flavour ($u\bar{u}$, $d\bar{d}$, $s\bar{s}$, etc.). This fact can be formulated mathematically in the conservation of strangeness: assigning the quantum number strangeness (S) to strange quarks ($S=-1$ for s and $S=+1$ for $\bar{s}$ quark), this quantum number is conserved in all processes mediated by the strong interaction. The always-in-pair production is not the only reason why hadrons with s quarks are called strange; their decay properties, especially those of neutral kaons have been a serious puzzle in the second half of the 20th century.

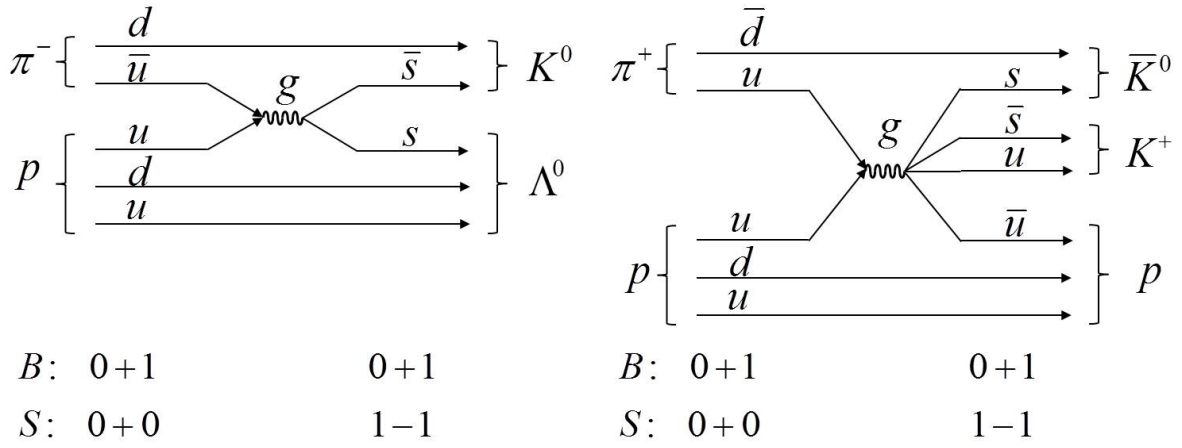

Figure 2.3: Examples of strong interaction processes in which neutral kaons are produced. Below the diagrams values of baryon number (B) and strangeness (S) are shown for the initial and final state.

Remembering the properties of $\hat{P}$ and $\hat{C}$ operators it is easy to establish for neutral kaons[8]

$$\begin{aligned} \hat{P}|K^0\rangle &= -|K^0\rangle,\ \hat{C}|K^0\rangle = |\bar{K}^0\rangle \Rightarrow \hat{C}\hat{P}|K^0\rangle = -|\bar{K}^0\rangle \\ \hat{P}|\bar{K}^0\rangle &= -|\bar{K}^0\rangle,\ \hat{C}|\bar{K}^0\rangle = |K^0\rangle \Rightarrow \hat{C}\hat{P}|\bar{K}^0\rangle = -|K^0\rangle\ . \end{aligned} \tag{2.7}$$

Hence neutral kaons are not eigenstates of the $\hat{C}\hat{P}$ operator. As such their CP eigenvalue is not determined. One can, however, construct a linear combination of $|K^0\rangle$ and $|\bar{K}^0\rangle$ which is an eigenstate of $\hat{C}\hat{P}$:

$$\begin{aligned} |K_1^0\rangle &= \frac{1}{\sqrt{2}}[|K^0\rangle - |\bar{K}^0\rangle] \\ |K_2^0\rangle &= \frac{1}{\sqrt{2}}[|K^0\rangle + |\bar{K}^0\rangle]\ . \end{aligned} \tag{2.8}$$

The two linear combinations denoted by $|K_1^0\rangle$ and $|K_2^0\rangle$ are eigenstates of the $\hat{C}\hat{P}$ operator with eigenvalues $+1$ and -1, respectively[9]. Neutral kaons decay into final state with pions

[8] Note that due to indefiniteness of C-parity for fermions we could also choose $\hat{C}\hat{P}|K^0\rangle(|\bar{K}^0\rangle) = +|\bar{K}^0\rangle(|K^0\rangle)$. However, the choice of this phase does not affect the physics observables. The phase convention is discussed further in Sect. 3.3.

[9] This is easily verifiable using the properties of $|K^0\rangle$ and $|\bar{K}^0\rangle$ under the $\hat{C}\hat{P}$ transformation from Eq. 2.7.

through the weak interaction (pions contain no strange quark, hence the quark flavours must be changed in the decay, and the only interaction capable of producing this is the charged weak interaction). If the *CP* symmetry is preserved in the weak interaction processes this implies that in such processes combinations $|K^0_{1,2}\rangle$ instead of states $|K^0\rangle$, $|\bar{K}^0\rangle$ take part. In such a case $|K^0_1\rangle$ decays into final states with *CP* quantum number $+1$, and $|K^0_2\rangle$ into states with $CP = -1$.

Nature has been kind in providing a possibility of disentangling the scenario in the neutral kaon system. The three pion final state possesses a negative *CP* value while the two pion state has a positive *CP* value, as explained in Sect. 2.1. Rest energy of three pions amounts to around 420 MeV, only slightly below the kaon mass of 498 MeV. Hence the decay of a neutral kaon into a three pion final state is significantly less probable than a decay into two pion final state, for which the available phase space is much larger ($m_{2\pi} \sim 280$ MeV $\ll$ $m_K \sim 498$ MeV). In the absence of other possible decays $|K^0_2\rangle$ thus decays into a 3π state (both with $CP = -1$) with relatively low probability and consequently a long lifetime, while $|K^0_1\rangle$ decays into 2π (both with $CP = +1$) with a relatively short lifetime.

To understand the principle of the measurement performed by the group led by Cronin and Fitch one has to dwell into some numeric values. The short-lived combination of neutral kaons ($|K^0_1\rangle$) has a mean decay distance, $c\tau_1$, of around 3 cm. On the other hand, the long-lived combination ($|K^0_2\rangle$) has $c\tau_2 \sim 15$ m. Neutral kaons, produced at $x = 0$ through the strong interaction as $|K^0\rangle$ and $|\bar{K}^0\rangle$, decay through the weak interaction process, exponentially as $|K^0_1\rangle$ and $|K^0_2\rangle$. The number of initially produced neutral kaons decreases exponentially with distance from the production point as $e^{-x/\gamma c\tau_{1,2}}$, where γ is the appropriate Lorentz factor, $\gamma = E_K/m_k$. Due to $\tau_1 \ll \tau_2$, after long enough decay distance ($x \gg c\tau_1$) one expects only $|K^0_2\rangle$ combination to survive resulting in decays to three pions only. The idea of the measurement is sketched in Fig. 2.4.

Cronin and Fitch performed the experiment in 1963 at the Alternating Gradient Synchrotron, a 30 GeV proton accelerator. The program of studies was by no means devoted to the study of *CP* symmetry alone. As Val Fitch said in his Nobel lecture:"Not many of our colleagues would have given us much credit for studying *CP* invariance, but we did anyway..." [14]. Protons were used to bombard a Be target to produce neutral kaons. These were in turn left to propagate through a $\sim$17 m decay tunnel, at the end of which detectors to reconstruct neutral kaons decays were installed. From experimental point of view an essential ingredient making the measurement possible was an optical spark chamber[10] enabling reconstruction of kaon decays in a rather high background environment. Taking into account the average Lorentz factor γ of kaons, the 17 m tunnel represented around 300 decay lengths $\gamma c\tau_1$ of the short-lived neutral kaon component [15]. At the end of the tunnel one thus has a ratio of the $|K^0_1\rangle$ to $|K^0_2\rangle$ of around $e^{-300}/e^{-300\ \tau_1/\tau_2} = e^{-300(1-\tau_1/\tau_2)} \sim e^{-300}$. If $|K^0_1\rangle$ only decays into 2π final state, and $|K^0_2\rangle$ only to 3π, the same ratio is of course expected for the numbers of detected two- and three-pion decays. Definitely a neglectably small number... The result of the experiment was shocking. Among around $23 \cdot 10^3$ 3π decays they found around 45 2π decays. A small ratio, indeed, but far from 10^{-300} (i.e. from zero)!

[10] Spark chamber is composed of a set of metal plates at high electric potential, with the intermediate space filled with gas. A traversing charged particle produces ionization of gas resulting in sparks between the plates. The sparks can be detected with an optical system.

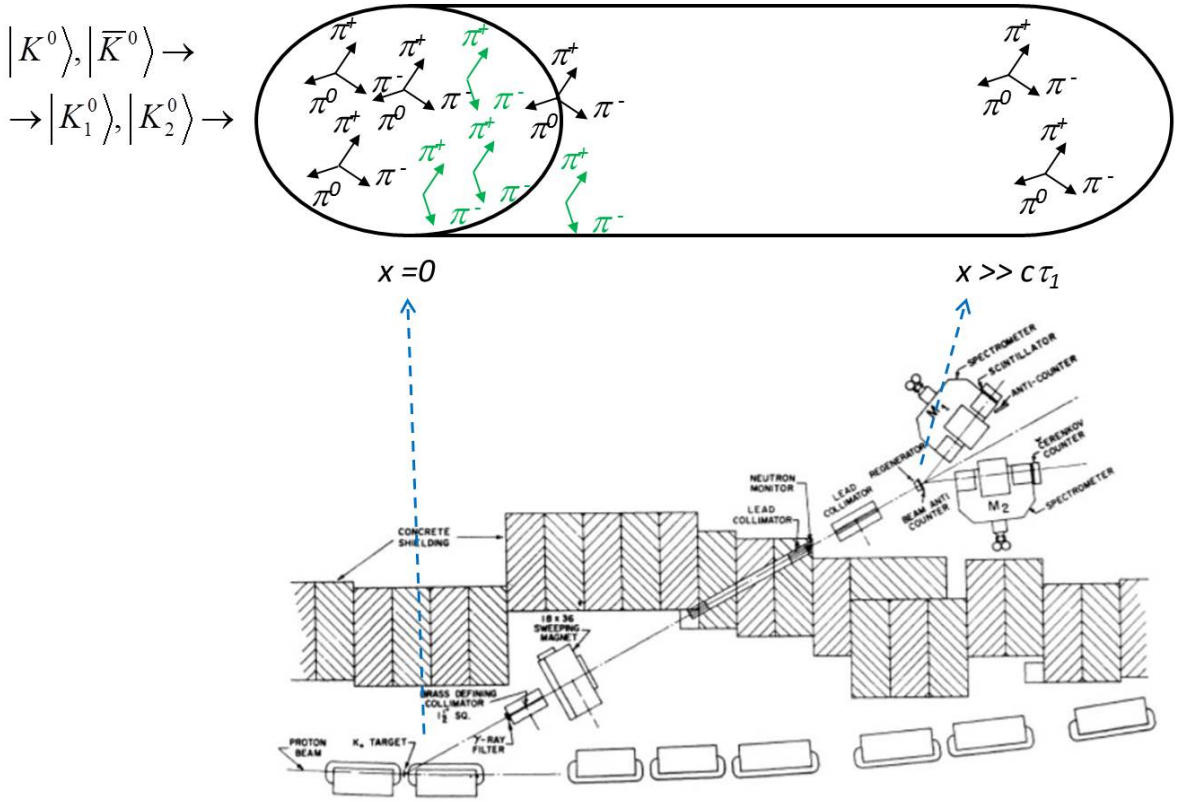

Figure 2.4: Experiment by Cronin and Fitch. Top: Produced neutral kaons decay into two- and three-pion final state. After long enough decay distance only the long-lived component of neutral kaons survive, which in case of *CP* conservation decays into the three-pion final state only. Bottom: The actual experiment schematics at the Brookhaven National Laboratory [13].

The result[11] [15] clearly showed that also the long-lived component of neutral kaons decays with a non-negligible probability[12] into a two-pion final state. In turn this means that an initial state with $CP = -1$ ($|K_2^0\rangle$) decays into a final state with either $CP = +1$ (two pions) or $CP = -1$ (three pions). The interaction responsible for the decay process, the weak interaction, does not conserve the *CP* symmetry. Assumption made by Lev Landau was thus shown to be wrong. But much more than that, the observed violation of the *CP* symmetry is linked in an essential way to the evolution of the Universe, as we will discuss in the next section. For their discovery Val Fitch and James Cronin received the Nobel prize in physics in 1980.

Nowadays, results of the Cronin-Fitch and follow-up experiments are incorporated in the

[11] The results of the experiment, performed in 1963, were published in 1964; the latter year is generally considered as the year of *CP* violation discovery.

[12] In the experiment, they determined the branching fraction for these decays of $2 \cdot 10^{-3}$, while a contemporary average of measurements yields a value of $(1.967 \pm 0.010) \cdot 10^{-3}$ [2].

following parametrization of the neutral kaons system:

$$\begin{aligned} |K_S^0\rangle &= \frac{1}{\sqrt{1+|\varepsilon|^2}}[|K_1^0\rangle + \varepsilon|K_2^0\rangle] = \\ &= \frac{1}{\sqrt{2(1+|\varepsilon|^2)}}[(1+\varepsilon)|K^0\rangle - (1-\varepsilon)|\bar{K}^0\rangle] \\ |K_L^0\rangle &= \frac{1}{\sqrt{1+|\varepsilon|^2}}[|K_2^0\rangle + \varepsilon|K_1^0\rangle] = \\ &= \frac{1}{\sqrt{2(1+|\varepsilon|^2)}}[(1+\varepsilon)|K^0\rangle + (1-\varepsilon)|\bar{K}^0\rangle] \ . \end{aligned} \tag{2.9}$$

In the above parametrization distinction is made between the short- and long-lived component of neutral kaons, $|K_S^0\rangle$ and $|K_L^0\rangle$ on one hand, and $\hat{C}\hat{P}$ eigenstates, $|K_1^0\rangle$ and $|K_2^0\rangle$ on the other. The parameter ε incorporates the experimentally determined violation of the *CP* symmetry in the neutral kaons system[13]. The magnitude of the parameter is small, $|\varepsilon| \sim 2.2 \cdot 10^{-3}$; $|K_L^0\rangle$ almost equals $|K_2^0\rangle$, and thus decays much more abundantly to three-pions than to two-pions final state.

Note: Experiments with neutral kaons, or better to say with the long- and short-lived component of K^0 and $\bar{K}^0$, proved that in the weak interaction processes also the combined *CP* symmetry is violated: a process in which all particles are replaced by corresponding anti-particles, and the process is observed in the mirror, does not proceed in exactly the same manner as the original process.

2.3 Humans, not Anti-humans

2.3.1 Sakharov Conditions

Nowadays the observable Universe - part of it which is accessible through the measurements using various contemporary experimental methods - is composed almost entirely of matter (particles) and no anti-matter (anti-particles). Evidently, our solar system is composed of particles, by which we mean mainly baryons as they build up the vast majority of mass we can observe in the Universe. If this would not be the case, any space mission coming into contact with bodies in our solar system would annihilate. Interacting particles and anti-particles annihilate into photons, as sketched in Fig. 2.5(left). Luckily this was not the case for the space missions. Furthermore, dedicated experiments in space have not detected any anti-nuclei. Specifically, the Alpha Magnetic Spectrometer (AMS) detector installed upon one of the space shuttle missions detected no anti-Helium nucleus and constrained the ratio of such nuclei to the Helium nuclei to less than one in a million, i.e. less than 10^{-6} [16]. Probes of possible anti-matter in other parts of our galaxy include studies of cosmic

[13] ε actually parametrizes only one of the *CP* violations forms. Various types of *CP* violation are discussed further in Sect. 3.3.2.

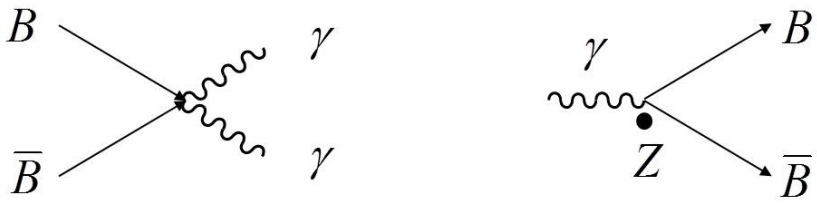

Figure 2.5: Left: Particles (B) and anti-particles ($\bar{B}$) annihilate into photons (γ). Right: Conversely, photons can create particle anti-particle pairs. The latter process can only take place in the presence of another (heavy) particle, denoted by Z, to conserve energy and momentum.

rays[14] in which fraction of positrons and anti-protons is found. While at the moment these are the only detected anti-particles not produced in the laboratories, their abundance can within the current measurement uncertainties be explained as a product of pair production (see Fig. 2.5(right)) in various astrophysics processes[15]. A possibility of the Universe being composed of large regions dominated by either matter or anti-matter, averaging the baryon number to zero, has been discussed. Remember that the total baryon number is the difference between the number of baryons ($n_{\rm bar}$) and the number of anti-baryons ($n_{\rm antibar}$),

$$N_b^{\rm tot} = n_{\rm bar} - n_{\rm antibar} = N_b(B) + N_b(\bar{B}) \ . \tag{2.10}$$

$N_b(B)$ and $N_b(\bar{B})$ denote the baryon number of baryons and anti-baryons, respectively, as defined in Sect. 2.1. It might be possible that in a given region of the Universe one encounters $n_{\rm bar} >> n_{\rm antibar}$ while in some other region $n_{\rm bar} << n_{\rm antibar}$, resulting in $N_b^{tot} = 0$ when averaged over all of the Universe. At the borders of such regions, however, particles and anti-particles would annihilate resulting in strong sources of gamma rays. These have not been observed. Studies of such scenarios conclude that if such regions indeed exist their dimensions should be comparable to the size of the known Universe [19]. All in all, ever since the discovery of positron by Carl D. Andersen in 1932, there is no experimental evidence that any anti-matter is present in the Universe that we observe, apart from the anti-particles produced in known processes (positrons that brought the 1936 Nobel prize in physics to Anderson were part of cosmic rays, and originated from pair creation process).

The Universe, according to the contemporary wisdom (and available experimental verifications[16]) originated in a Big Bang. Immediately after its creation it underwent a rapid expansion, known as the inflation. After the period of inflation the Universe was expanding

[14] Charged particles, mainly electrons and protons, originating from sources within as well as outside of our galaxy. Upon the impact on Earth's atmosphere they produce showers of particles from secondary interactions on the nuclei composing the atmosphere.

[15] A significant positron excess compared to theoretical expectations in the cosmic ray spectra has been observed by the Pamela experiment [17]. Current explanations include several possible sources (pulsars, dark-matter candidates,...). Also the upgrade of the AMS experiment, AMS02 installed on the International Space Station, observed some anti-Helium nuclei [18], the origin of which is unclear.

[16] It goes far beyond the scope of this book to discuss experimental evidence of what is nowadays called Inflationary Big Bang models. Nevertheless, one should mention that the smoking gun evidence for such models arises from the measurements of cosmic expansion and of the Cosmic Microwave Background.

at a much slower rate, and cooling down. The energy density was gradually decreasing. At that time, when the Universe was around 10^{-32} s "old", it was filled with a hot plasma of quarks, anti-quarks and gluons. Plasma means that the particles mentioned, due to much too high energies, did not form any bound states. Production and disappearance of quarks and anti-quarks through the processes of annihilation and pair creation were in equilibrium. Binding of quarks and anti-quarks into baryons and anti-baryons happened only much later, about 10^{-6} s after the Big Bang, when the Universe cooled down to around 10^{13} K[17]. It should be noted that the process of pair creation (Fig. 2.5(right)) requires a minimum energy of photons to create pairs. The energy should be larger than the rest energy of created particles, $E_\gamma > 2m_B$. As the Universe cooled down the energy became too low for pair creation of baryons. Only annihilation continued, until there were still pairs of baryons and anti-baryons that could annihilate.

Eventually, all baryon anti-baryon pairs annihilated into radiation (photons). Even today this radiation fills the Universe and is called the Cosmic Microwave Background (CMB). As the matter of fact, CMB is an extremely important tool for astrophysicists, offering an insight into conditions in the early Universe. Moreover, one can determine the density of these photons compared to the density of matter (baryons) in the current Universe:

$$\left.\frac{n_{\text{bar}}}{n_\gamma}\right|_{\text{now}} \approx 10^{-10} \quad . \tag{2.11}$$

Since there are no anti-baryons observed in the Universe today, one can write

$$\left.\frac{n_{\text{bar}} - n_{\text{antibar}}}{n_\gamma}\right|_{\text{now}} \approx 10^{-10} \quad , \tag{2.12}$$

where n_{antibar} denotes the density of anti-baryons.

As usually, the devil is in the detail... Note that we said that all baryon anti-baryon "pairs" in the early Universe annihilated. If there were isolate baryons in excess of anti-baryons they could not annihilate. It is those solitary baryons that make up all the matter in the Universe today. From the ratio 2.11 it is clear that a vast majority of pairs annihilated in the early stages. For each approximately 10^{10} pairs of baryons and anti-baryons there was a single baryon that did not have an anti-particle counterpart. Since almost all pairs in the early Universe annihilated into photons,

$$\left.\frac{n_{\text{bar}} - n_{\text{antibar}}}{n_\gamma}\right|_{\text{now}} = \left.\frac{n_{\text{bar}} - n_{\text{antibar}}}{n_{\text{bar}} + n_{\text{antibar}}}\right|_{\text{early}} \quad . \tag{2.13}$$

Hence the question arises what caused the tiny excess of baryons in the early Universe, which make all the greatness of the matter in today's Universe. Or, analogously, what caused the change of the total baryon number from $N_b^{\text{tot}} = 0$, in an early symmetric state of the Universe, to a positive N_b^{tot}.

In 1967 Andrei Sakharov[18] postulated three necessary conditions for the Universe to evolve into the matter / anti-matter asymmetric state which we observe nowadays. These

[17] Conversion into temperature is made from an average energy of particles present, using the Boltzman constant $k = 8.6 \cdot 10^{-5}$ eV K^{-1}, and corresponds to energies of around 100 MeV to 1 GeV.

[18] A. Sakharov, Russian nuclear physicist significantly participating in the building of the Soviet hydrogen bomb, was awarded the Nobel Peace Prize in 1975 for his work for human rights.

conditions are [20]

- non-conservation of the baryon number;
- violation of CP and C symmetry;
- period of departure from thermal equilibrium during the Universe evolution.

The first two necessities can be understood in terms of an (over)simplified model. Let's assume the existence of a particle P in the early Universe. For simplicity let it have only two decay modes: the first one into a final state f_1, that has a baryon number N_{b1}, and the second one into a final state f_2 with N_{b2}. Rates of probabilities for the two decays are denoted r and $1-r$, respectively. Particle P had its anti-particle $\bar{P}$, decaying into $\bar{f}_1$ with probability $\bar{r}$ and into $\bar{f}_2$ with probability $1-\bar{r}$. The two anti-particle final states posses baryon numbers $-N_{b1}$ and $-N_{b2}$. Can decays of these model particles P and $\bar{P}$ change the total baryon number?

$$\begin{aligned} \Delta N_b^{\text{tot}} &= r\,N_{b1} + (1-r)\,N_{b2} + \bar{r}\,(-N_{b1}) + (1-\bar{r})\,(-N_{b2}) \\ &= (r-\bar{r})\,(N_{b1}-N_{b2})\ . \end{aligned} \tag{2.14}$$

In the above equation we wrote the change of the baryon number, ΔN_b^{tot}, due to the assumed decays. It is evident that $\Delta N_b^{\text{tot}} \neq 0$ if $r \neq \bar{r}$ and $N_{b1} \neq N_{b2}$. The latter requirement states that the hypothetical particle P must decay into states with different baryon number (non-conservation of baryon number). The former requirement postulates C and CP violation as the necessary condition for the baryon number change. To see this explicitly we need to dig just a little bit deeper.

Imagine a specific decay of a hypothetical particle into a - for example - two quark final state, $P \to q_1\ q_2$. Probability for such a decay (branching fraction) is the ratio of the specific partial decay width, $\Gamma(P \to q_1\ q_2)$, and the total decay width, Γ_P. The latter is a sum of all of its partial decay widths, and is related to the lifetime of the particle through $\tau = 1/\Gamma$[19]. Hence

$$r = \frac{\Gamma(P \to q_1\ q_2)}{\Gamma_P}, \quad \bar{r} = \frac{\Gamma(\bar{P} \to \bar{q}_1\ \bar{q}_2)}{\Gamma_{\bar{P}}}\ . \tag{2.15}$$

Since particle and anti-particle lifetimes are equal we have $\Gamma_P = \Gamma_{\bar{P}}$[20]. The rate difference is thus

$$r - \bar{r} = \frac{\Gamma(P \to q_1\ q_2) - \Gamma(\bar{P} \to \bar{q}_1\ \bar{q}_2)}{\Gamma_P}\ . \tag{2.16}$$

Under the $\hat{C}$ transformation P, q_1, and q_2 transform into $\bar{P}$, $\bar{q}_1$, and $\bar{q}_2$, respectively, and $\Gamma(P \to q_1\ q_2) \to \Gamma(\bar{P} \to \bar{q}_1\ \bar{q}_2)$. Hence a conservation of the C symmetry would mean

[19] In accordance with the prescription mentioned in Sec. 1.1.3, the proper units of τ are obtained by multiplication with a conversion factor, $\hbar c = 197$ MeV fm, and division by $c = 3 \cdot 10^8$ m/s

[20] We dealt with this issue ignorantly. Actually, particle anti-particle lifetime equality, as well as the equality of their masses is a consequence of symmetry of physics laws under the $\hat{C}\hat{P}\hat{T}$ transformation. The latter is a combination of the already known $\hat{C}\hat{P}$, and of $\hat{T}$, the operator that reverses the arrow of time, $t \to -t$. The CPT conservation theorem is basis of all relativistic quantum field theories; if CPT symmetry is violated almost none of the contemporary theories is valid anymore. Needless to say that currently no experimental evidence of CPT violation exists.

$\Gamma(P \to q_1\ q_2) = \Gamma(\bar{P} \to \bar{q}_1\ \bar{q}_2)$. Therefore if there's no C violation then $r = \bar{r}$ and the baryon number is not changed.

In writing the partial decay width we can be more specific and separate quarks into those with negative ($q_{i,L}$) or positive ($q_{i,R}$) helicity (note that this is true only in the limit of ultrarelativistic quarks, i.e. when $E_q \gg m_q$; otherwise subscripts L and R denote left- and right-chirality of quarks[21]). The partial decay width can be decomposed as

$$\Gamma(P \to q_1\ q_2) = \Gamma(P \to q_{1,L}\ q_{2,L}) + \Gamma(P \to q_{1,R}\ q_{2,R}) + \Gamma(P \to q_{1,L}\ q_{2,R}) + \Gamma(P \to q_{1,R}\ q_{2,L})\ . \tag{2.17}$$

The rate difference can also be detailed into

$$r - \bar{r} = \frac{\Gamma(P \to q_{1,L}\ q_{2,L}) + \Gamma(P \to q_{1,R}\ q_{2,R}) + \Gamma(P \to q_{1,L}\ q_{2,R}) + \Gamma(P \to q_{1,R}\ q_{2,L})}{\Gamma_P} - \\ - \frac{\Gamma(\bar{P} \to \bar{q}_{1,L}\ \bar{q}_{2,L}) + \Gamma(\bar{P} \to \bar{q}_{1,R}\ \bar{q}_{2,R}) + \Gamma(\bar{P} \to \bar{q}_{1,L}\ \bar{q}_{2,R}) + \Gamma(\bar{P} \to \bar{q}_{1,R}\ \bar{q}_{2,L})}{\Gamma_P}\ . \tag{2.18}$$

The $\hat{C}\hat{P}$ operator changes $q_{i,(L,R)} \to \bar{q}_{i,(R,L)}$ (see Fig. 2.2 and description there), and hence $\Gamma(P \to q_{1,L}\ q_{2,L}) \to \Gamma(\bar{P} \to \bar{q}_{1,R}\ \bar{q}_{2,R})$, etc. In the case of the CP conservation one has $\Gamma(P \to q_{1,L}\ q_{2,L}) = \Gamma(\bar{P} \to \bar{q}_{1,R}\ \bar{q}_{2,R})$, etc. By inspection of the above equation we see that in this case individual partial decay widths in the numerator pairwise cancel. Like in the case of C violation we conclude that if there's no CP violation then $\Delta N_b^{\rm tot} = 0$. By this we demonstrated the first two of Sakharov's conditions.

What we also learn from the example is that in case the partial width of the original decay mode in any sense differs from the partial width of the CP conjugated decay mode, $\Gamma(P \to f) \neq \Gamma(\bar{P} \to \bar{f})$, this is a manifestation of both CP and C violation. Detailed studies of partial decay widths (i.e. of specific decay modes) hence offer a possibility of CP violation determination. This is also true for decay time dependence of the partial decay widths, i.e. for $d\Gamma(P \to f)/dt$.

The third Sakharov condition - departure from thermal equilibrium - may be understood naively from the fact that in a thermal equilibrium any potentially baryon number violating process would be in equilibrium with an opposite process; if the first one would change the baryon number by ΔN_b, the later would change it by $-\Delta N_b$. The two processes in equilibrium have the same rate and hence the net change in baryon number is zero. In other words, while the Universe is in thermal equilibrium, the baryon number can not change.

Violation of the CP symmetry is thus a necessary condition for the evolution of Universe into a state in which matter (particles) dominate over anti-matter (anti-particles). In a more poetic way one might say it's the reason why we are all humans and not anti-humans. In the next section we should make a connection between the CP violation in the subatomic world (described by the CKM matrix within the Standard Model) and the matter asymmetry of the Universe.

Note: Nowadays the matter in the observable Universe is composed almost entirely of particles and no anti-particles. One of the necessary conditions for the Universe to evolve into such a state is the violation of the CP symmetry.

[21] If $E \gg m_q$ does not hold, chirality does not equal helicity. The following argument about the CP violation still holds, nevertheless.

2.3.2 Small and Large

Let us return once again to the CKM matrix, introduced in Sect. 1.2.3. Specifically we need to talk about the so far forgotten complex phase of the CKM matrix elements. The CKM matrix is a unitary 3×3 complex matrix, describing the couplings of quark pairs to the charged $W^{\pm}$ bosons. In general, a complex square matrix of dimension 3 has 18 real parameters (9 complex elements, each described by the real and the imaginary component - $\mathrm{Re}(z) + i\,\mathrm{Im}(z)$, or, alternatively, by its magnitude and phase - $|z|e^{i\phi}$). Let's afford to be even a bit more general, and - not a subject to a lengthy debate, probably - conclude that a general square matrix of dimension n with complex elements is described by $2n^2$ real parameters (instead of only 3 generations of quarks we assumed n generations). The fact that the matrix is unitary (see Eq. (1.7)) leads to n^2 relations among these parameters (product of each row and complex conjugate column equals either 0 or 1). An example of such a relation[22] is:

$$V_{ud}V_{ub}^{*} + V_{cd}V_{cb}^{*} + V_{td}V_{tb}^{*} = 0 \tag{2.19}$$

With n^2 relations among $2n^2$ parameters we are left with $2n^2 - n^2 = n^2$ free parameters. Now we take into account that we are dealing with quarks, described by quantum mechanics, where only probability matters. Hence multiplication of any of the quark fields in Eq. (1.13) by an arbitrary phase $e^{i\phi_j}$, where j denotes the quark flavour, is unobservable. In other words, if we make substitutions $q_j \to q_j e^{i\phi_j}$ for $j = u,d,c,s,t,b$ in Eq. (1.13), the description of processes is not changed, for any value of individual ϕ_j[23]. The symbolic expression for the charged weak interaction (Eq. (1.13)) is then written as (taking into account $\bar{q}_j \to \bar{q}_j e^{-i\phi_j}$):

$$\begin{aligned} V_{ud}\,\bar{d}e^{-i\phi_d}\,ue^{i\phi_u} + V_{us}\,\bar{s}e^{-i\phi_s}\,ue^{i\phi_u} + V_{ub}\,\bar{b}e^{-i\phi_b}\,ue^{i\phi_u} + V_{cd}\,\bar{d}e^{-i\phi_d}\,ce^{i\phi_c} + \\ + V_{cs}\,\bar{s}e^{-i\phi_s}\,ce^{i\phi_c} + V_{cb}\,\bar{b}e^{-i\phi_b}\,ce^{i\phi_c} + V_{td}\,\bar{d}e^{-i\phi_d}\,te^{i\phi_t} + V_{ts}\,\bar{s}e^{-i\phi_s}\,te^{i\phi_t} + V_{tb}\,\bar{b}e^{-i\phi_b}\,te^{i\phi_t} \ . \end{aligned} \tag{2.20}$$

By inspection of the above expression one can see that multiplication of each of the quarks by an arbitrary phase effectively adds a difference of two complex phases to each of the CKM matrix elements: V_{ud} is multiplied by $e^{i(\phi_u - \phi_d)}$, etc. Since the phases ϕ_j are arbitrary, they may be chosen so that they cancel any potential complex phase that the CKM matrix element carries. Is by this possible to cancel all phases of the CKM matrix elements? Clearly not, we only have six quark flavours and hence six individual arbitrary phases. Moreover, there are only five independent phase differences. For example, $\phi_u - \phi_d$ ca be expressed as $\phi_u - \phi_s - (\phi_c - \phi_s) + \phi_c - \phi_d$. Three more phase differences (out of nine appearing in Eq. (2.21)) can be expressed in such a way. Altogether we have a freedom of cancelling $6 - 1 = 5$ potential CKM elements' complex phases. In generalization to n generations this means $2n - 1$ less free parameters (phases) to describe the $n \times n$ unitary matrix. We are down to $n^2 - (2n-1) = (n-1)^2$ free parameters. For $n = 3$ one is left with four parameters to describe the CKM matrix. Finally, the CKM matrix describes rotations among (down-like) quarks (see Eq. (1.6)). Rotations in n dimensions (remember, $n = 3$ in nature, as we understand it today) can be described using $1/2\ n\ (n-1)$ Euler angles (= 3 for $n = 3$). The

[22] Not randomly chosen; this specific relation is especially important for the processes in which B mesons are involved, as we shall see.

[23] A correct statement also from mathematical point of view is that the Standard Model Lagrangian remains invariant under such a transformation.

remaining parameters are complex phases, $(n-1)^2 - 1/2n(n-1) = 1/2(n-1)(n-2)$ in number. For $n = 3$ we need 3 angles and a single complex phase to parametrize the CKM matrix.

The CKM matrix parametrized in the above terms reads [21]

$$V_{CKM} = \begin{bmatrix} c_{12}c_{13} & s_{12}c_{13} & s_{13}e^{-i\phi} \\ -s_{12}c_{23} - c_{12}s_{23}s_{13}e^{i\phi} & c_{12}c_{23} - s_{12}s_{23}s_{13}e^{i\phi} & s_{23}c_{13} \\ s_{12}s_{23} - c_{12}c_{23}s_{13}e^{i\phi} & -c_{12}s_{23} - s_{12}c_{23}s_{13}e^{i\phi} & c_{23}c_{13} \end{bmatrix} . \tag{2.21}$$

In the above notation $s_{ij} = \sin\theta_{ij}$ and $c_{ij} = \cos\theta_{ij}$ for $ij = 12,\ 13,\ 23$, are the sine and cosine of the three angles, and ϕ is the complex phase. Such parametrization is not the only one possible. In Sect. 1.2.3 we mentioned a pronounced hierarchy in magnitudes of the CKM matrix elements (see Eq. (1.13)). A widely used parametrization, specifically exposing this hierarchy, is the Wolfenstein parametrization [22]. It is actually a Taylor expansion of the matrix elements in parameter $\lambda = |V_{us}| \sim 0.2$ up to the 3rd order:

$$V_{CKM} = \begin{bmatrix} 1-\lambda^2/2 & \lambda & A\lambda^3(\rho - i\eta) \\ -\lambda & 1-\lambda^2/2 & A\lambda^2 \\ A\lambda^3(1-\rho-i\eta) & -A\lambda^2 & 1 \end{bmatrix} + \mathcal{O}(\lambda^4) . \tag{2.22}$$

Instead of a complex phase ϕ one encounters here a real and an imaginary part of individual elements, ρ and η. Of course, also in this parametrization, together with A there are four parameters altogether. In this parametrization it is easy to spot diagonal elements with magnitude of the order of 1, first off-diagonal elements of the order of λ or λ^2, and second off-diagonal elements of the order of λ^3.

We started the section by mentioning the complex phase of the CKM matrix elements, the close relation of which to the violation of *CP* symmetry has also been mentioned before. Not only is the complex phase of the CKM matrix related to the *CP* violation; there would be no violation if the matrix was real. This is illustrated in Fig. 2.6. In a transition of a downlike

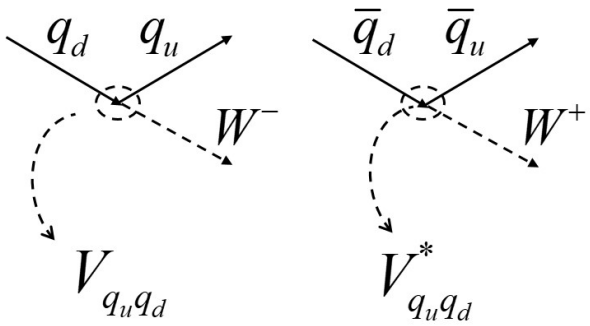

Figure 2.6: Transition of an uplike to a downlike quark and a transition of an uplike anti-quark to a downlike anti-quark. The CKM matrix elements appearing in the two processes are complex conjugates of one another.

quark (any quark with the charge $-1/3\ e_0$, q_d) to an uplike quark (any quark with the charge $+2/3\ e_0$, q_u) the $V_{q_u q_d}$ CKM matrix element is present in the amplitude. In the *CP* conjugated

transition $\bar{q}_d \to \bar{q}_u$ its complex conjugate, $V^*_{q_u q_d}$, appears. Hence if $V^*_{q_u q_d} = V_{q_u q_d}$, i.e. if the CKM matrix is real, the two processes will proceed in an exactly the same manner and no *CP* violation can occur. $V^*_{q_u q_d} \neq V_{q_u q_d}$ is within the Standard Model a necessary condition for *CP* violation.

Now one can understand better the decision of the Nobel Committee to award the Nobel prize to Kobayashi and Maskawa. With two generations of quarks, as suspected at the time of their postulation of the CKM matrix, the quark rotation matrix Eq. (1.4) has no complex phase. This can be easily verified employing the calculated number of angles and phases needed for parametrization of an $n \times n$ unitary matrix, given at the beginning of this section (number of complex phases is $1/2(n-1)(n-2)$, which for $n = 2$ vanishes). To describe the *CP* violation through a complex phase of the quark rotation matrix the number of generations must be at least three (resulting in a single complex phase). Realizing this, Kobayashi and Maskawa dared to predict the existence of further, experimentally yet to be observed quark flavours.

Let us now turn our attention to one of the unitarity relations for the CKM matrix elements, Eq. (2.19). Any complex number $z = \mathrm{Re}(z) + i\,\mathrm{Im}(z) = |z|e^{i\phi}$ can of course be presented as a vector in the complex plane, as illustrated in Fig. 2.7 (left). Unitarity relation

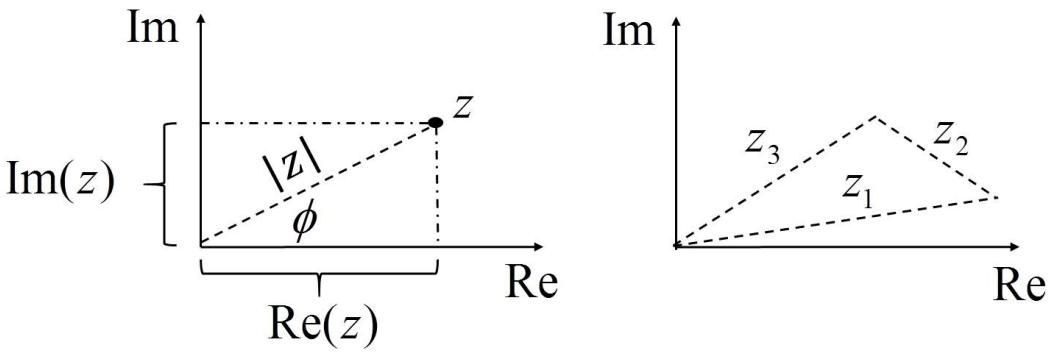

Figure 2.7: Left: Representation of a complex number in the complex plane. Right: Sum of three complex numbers with their sum equal to 0.

is a sum of three complex numbers, adding to zero. Hence in the complex plane they represent a triangle (Fig. 2.7 (right)). We can divide relation (2.19) by the middle term, $V_{cd}V^*_{cb}$. thus obtaining

$$\frac{V_{ud}V^*_{ub}}{V_{cd}V^*_{cb}} + 1 + \frac{V_{td}V^*_{tb}}{V_{cd}V^*_{cb}} = 0 \ . \tag{2.23}$$

The above is still a sum of three complex numbers (one of them real, actually, i.e. with the null imaginary component). They form a triangle in the complex plane, presented in Fig. 2.8 (left). In studies of B mesons this triangle is called the unitarity triangle. Elements of the CKM matrix entering the unitarity relation can be expressed in terms of the Wolfenstein parameters. It is easy to obtain Eq. (2.23) in these terms:

$$\rho + i\eta - 1 + (1 - \rho - i\eta) = 0 \ . \tag{2.24}$$

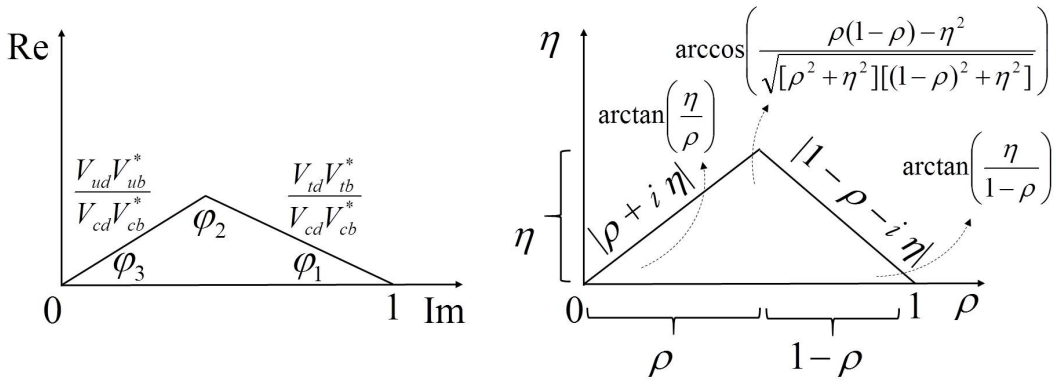

Figure 2.8: Left: The unitarity triangle. Right: The unitarity triangle expressed in Wolfenstein parametrization.

Ploting the sum of these three complex numbers ($\rho+i\eta$, -1 and $1-\rho-i\eta$, Fig. 2.8 (right)) in the complex plane one realizes that the uppex of the unitary triangle is positioned at (ρ,η)[24]. The axis of the coordinate system are thus annotated according to this. Angles of the triangle denoted by φ_1, φ_2 and φ_3[25] in the left plot, are just the complex phases of combinations of the CKM matrix elements:

$$\begin{aligned}\varphi_1 &= Arg\left[-\frac{V_{cd}V_{cb}^*}{V_{td}V_{tb}^*}\right]\\ \varphi_2 &= Arg\left[-\frac{V_{td}V_{tb}^*}{V_{ud}V_{ub}^*}\right]\\ \varphi_3 &= Arg\left[-\frac{V_{ud}V_{ub}^*}{V_{cd}V_{cb}^*}\right]\end{aligned} \quad . \tag{2.25}$$

These can be also expressed using the Wolfenstein parameters. The expressions are shown in the right plot of Fig. 2.8. If $\eta=0$, that is if the complex phase of the CKM matrix vanishes, angles φ_1 and φ_3 become zero, and $\varphi_2=\pi$. This means that in the case of no CP violation (i.e. if ϕ of (2.21) is 0) the area of the unitarity triangle is null.

It should be noted at this point that there are several other unitarity triangles. Every relation following from the unitarity of the CKM matrix (Eq. (2.5) can be represented in a form of the triangle in the complex plane. However, the one discussed here involves the CKM matrix elements appearing in various processes with B mesons. As we will see these elements can be determined through measurements of these processes. All possible unitarity triangles have the same area. With some algebra it can be shown that the area of any of the triangle is

$$S=\frac{1}{2}A^2\lambda^6\eta \tag{2.26}$$

No CP violation, or equivalently $\eta=0$, means $S=0$. S is in some sense a measure of CP violation. The elements of the CKM matrix must be experimentally determined. We have seen

[24]There is a subtlety to this: sometimes instead of ρ and η renormalized parameters $\bar{\rho}\approx\rho(1-\lambda^2)$ and $\bar{\eta}\approx\eta(1-\lambda^2)$ are used. By this the equations used are valid to a higher order in λ.

[25]In some literature on the subject the angles are commonly denoted by $\alpha=\varphi_2$, $\beta=\varphi_1$ and $\gamma=\varphi_3$.

that actually all elements can be expressed with four independent parameters. Measurements of individual CKM matrix elements hence yield values of these four parameters. Looking slightly ahead let us quote the value of S following from the measured values of A, λ and η: $S \approx 2 \cdot 10^{-5}$.

This appears to be a small value; however, to make such a claim we first need to know what to compare the value to. If one expresses S not in terms of the Wolfenstein parameters but rather using the parametrization (2.21), it reads $S = (1/2)c_{12}c_{23}c_{13}^2 s_{12}s_{23}s_{13}\sin\phi$[26]. The expression contains sines and cosines of angles; since these functions have a limited interval of values also the expression for S is limited. It turns out that the maximum value S can attain is $S_{max} = 1/(12\sqrt{3}) \sim 0.05$. The measured value is indeed more than three orders of magnitude smaller than the possible maximum value. Taking S as a general measure of *CP* violation we can now foresee that effects of *CP* violation are indeed small.

We established that $S \neq 0$ is necessary to account for *CP* violation. This condition is not enough, though. If any pair of quarks with the same charge would have equal mass, it would be possible to use transformations of the type $q_j \to q_j e^{i\phi}$ to cancel also the only remaining complex phase in the CKM matrix. Hence a necessary condition for *CP* violation to occur is

$$J = (m_t^2 - m_c^2)(m_t^2 - m_u^2)(m_c^2 - m_u^2)(m_b^2 - m_s^2)(m_b^2 - m_d^2)(m_s^2 - m_d^2)\, S \neq 0 \ . \qquad (2.27)$$

The constant J, appearing in the world of elementary particles, the smallest indivisible constituents of matter, can be related to the baryon asymmetry (2.13) of the Universe, the largest entity we can imagine. We will discuss this further in chapter 5.

Note: The CKM matrix can be parametrized with four parameters, the values of which must be experimentally determined. The unitarity of the matrix can be represented by the unitarity triangle. One of the free parameters of the CKM matrix is a complex phase which is within the Standard Model the only source of *CP* symmetry violation.

[26] This constant is often referred to as the Jarlskog invariant [6].

Chapter 3

Down the Rabbit Hole

3.1 Accelerating Science

3.1.1 Acceleration

Currently, the most prominent representatives of the Energy Frontier experiments are the experiments at the Large Hadron Collider (LHC) at CERN in Geneva. The collider is used to collide protons with protons, accelerated to the highest energy ever achieved by humans in an accelerator. Individual colliding protons have each an energy of 7 TeV. The accelerated protons are not continuously distributed along the collider. They are grouped into bunches. In each accelerated bunch there is around 10^{11} protons, and typically there are around 2800 bunches circulating in each direction along the collider[1]. Two general purpose experiments are positioned at the LHC to detect and analyse processes taking place in this high energy collisions: ATLAS (A Torodial LHC Apparatus) and CMS (Compact Muon Solenoid)[2]. Experiments in the Energy Frontier category search for new particles to be produced in collisions at the center-of-mass (CMS) energy E. The CMS frame is defined as the one in which the total momentum of particles under study is zero, $\sum_i \vec{p} = 0$. In the case of the LHC the laboratory frame (the frame in which the detectors reside, i.e. the Earth) coincides with the CMS frame, since the colliding protons have momenta equal in magnitude and of opposite directions. In principle at the CMS energy E a particle of mass $mc^2 = E$ can be produced. In principle, because typically processes are more complex resulting in (many) more than a single particle. Moreover, at such high energies interactions take place among constituents of protons instead of protons themselves. An example of such a process is the production of a Higgs boson, discovered by ATLAS and CMS in 2012, shown in Fig. 3.1. The Higgs boson is produced through an interaction of the constituents of the two colliding protons, quarks or gluons[3]. The remaining particles in a process (quarks from disintegrated protons) carry a part of the CMS energy. Hence the energy available for production of new particles is smaller than the total proton - proton collision energy.

[1] The energy of a single bunch of protons accelerated to 7 TeV is similar as the kinetic energy of a 1.5 t car driving at 45 km/h.

[2] Two more experiments are recording data at the LHC, the LHCb experiment devoted to precision measurements in physics of B mesons, and ALICE, predominantly studying processes in heavy ion collisions.

[3] Gluons are carriers of the strong interaction that binds the quarks inside a proton.

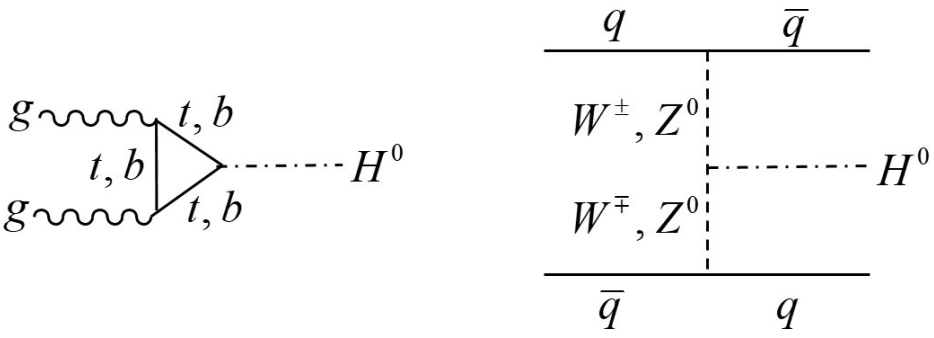

Figure 3.1: Feynman diagrams of dominant Higgs boson (H^0) production processes at the LHC.

Charged particles like protons are accelerated to high energies using electric field. A classic Coulomb force (electromagnetic interaction) experienced by a point electric charge e (particle) in an electric field of strength $\vec{E}$,

$$\vec{F}_C = e\vec{E} \ , \tag{3.1}$$

causes the charge to accelerate. When traversing a potential difference U its kinetic energy is increased by $(1/2)mv^2 - (1/2)mv_0^2 = eU$, as sketched in Fig. 3.2 (left). Gain in the energy

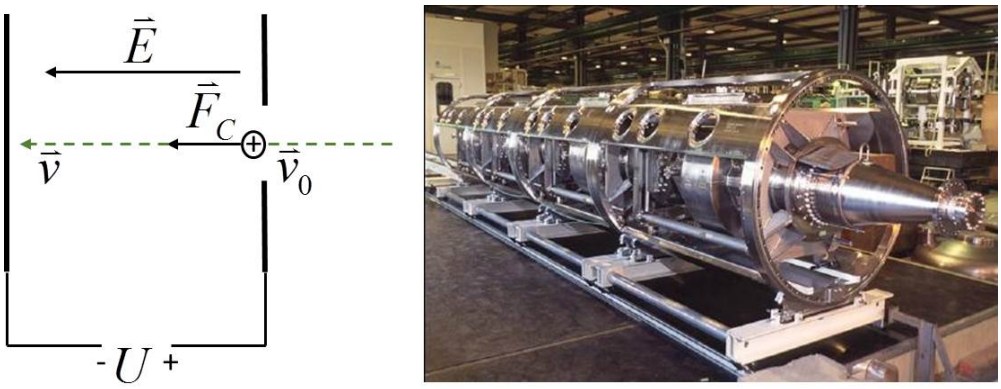

Figure 3.2: Left: Under the influence of a Coulomb force a charged particle is accelerated. Right: A superconducting radiofrequency cavity used at the LHC [7].

for a particle carrying the elementary charge $e_0 = 1.6 \cdot 10^{-19}$ As when traversing the potential difference of 1 V is 1 eV. Performing the acceleration to 7 TeV in a sketched way would be impossible, one would need a potential difference of $7 \cdot 10^{12}$ V. For this reason a different configuration of an electric field is used: electric field in a standing electromagnetic wave. Standing electromagnetic waves are produced in a resonator (similar as standing sound waves in an acoustic resonator) as the one shown in Fig. 3.2 (right). Charged particles entering such a resonator experience time and space dependent electric field of an electromagnetic wave. The time dependence of E is shown in Fig. 3.3. If a particle arrives into the cavity

at the right time (when the field is positive for positively charged particles or negative for negatively charged ones) the field accelerates it. Moreover, particles that are slower (arrive to the cavity at a later time) experience a larger field and are thus accelerated more, while the faster ones (arriving to the cavity at an earlier time) experience a lower field strength and are thus accelerated less. Typical frequencies of standing waves in the resonant cavities are

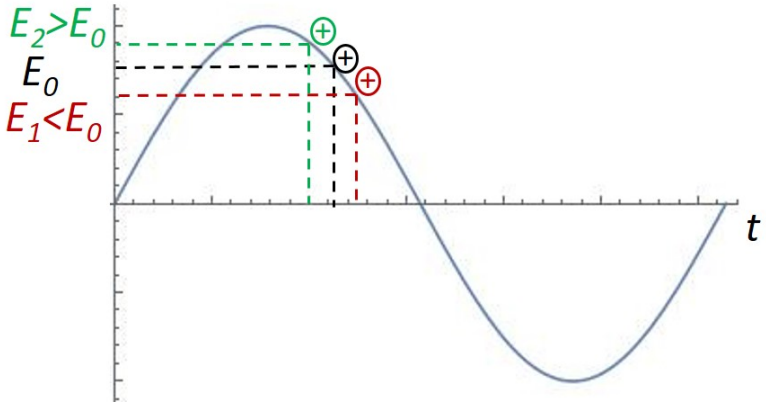

Figure 3.3: Time dependence of the electric field strength E in a radio-frequency resonant cavity. Particles arriving late experience a stronger field and are thus accelerated more.

of the order of 100 MHz. Hence the cavities are called radio-frequency (RF) cavities.

In order to keep the particles accelerated, passing through the RF cavities many times and to collide bunches of accelerated particles at high frequency, the particles' orbits are constrained to a circle. This is achieved by means of magnetic field in which a point charge experiences the magnetic part of the Lorentz force

$$\vec{F}_B = e\vec{v} \times \vec{B} \ , \tag{3.2}$$

where $\vec{B}$ is the magnetic flux density. Since this force is perpendicular to particle's velocity $\vec{v}$ it causes the trajectory to bend (see Fig. 3.4). Using dipole magnets the particles' trajectories can thus be made circular. Dipole magnets are not the only type of magnets used in contemporary accelerators. Accelerated bunches contain thousands of billions of charged particles (electrons, protons). Due to the same Coulomb force enabling their acceleration, there is a repulsion among particles of the same electric charge that would cause bunches to be blown up. Also, if such bunches collide, a collision probability for particles within the two bunches accelerated in the opposite directions is too small to produce collisions at an interesting rate. In order to keep the bunches spatially constrained and especially to squeeze them as much as possible in front of the designated interaction points, around which detectors are positioned, higher multipole (quadrupole, sextupole,...) magnets are used. The effect of those is to focus particles' trajectories in coordinates perpendicular to the direction of their velocity. Hence they perform a similar role as optical lenses do with the light.

In an accelerator one encounters a complicated lattice of RF cavities, magnets and other equipment (e.g. pumps to sustain a high vacuum in order for the accelerated particles not to interact with molecules of air), an example of which is shown in Fig. 3.5.

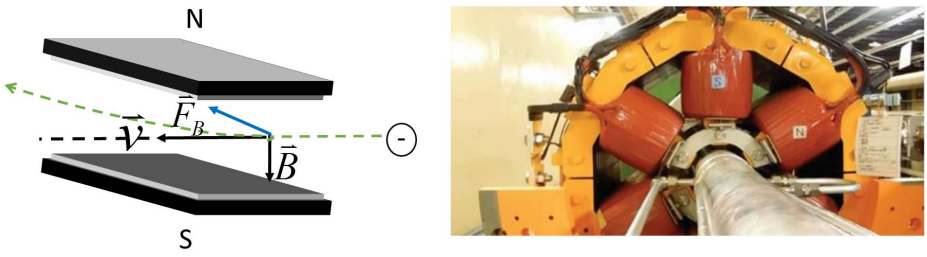

Figure 3.4: Left: Force acting on a point charge in a magnetic field $\vec{B}$. When passing through a magnetic field of a dipole magnet the trajectory of a charged particle is bent. Note that this example is shown for a negatively charged particle. Right: An example of a sextupole magnet, used in the SuperKEKB accelerator [9].

At the Intensity Frontier experiments the emphasize is on accurate measurements of processes that are typically rare within the SM. For such processes any NP contribution, even if tiny, might be relatively important compared to the SM one. Beside the experimental ingredient - a measurement of high accuracy - for the Intensity Frontier to be successful in the hunt for NP another component is needed: a firm theoretical prediction for the measurement result derived within the framework of the SM. Comparison of the two, or better to say any deviation between them can then be interpreted in terms of possible NP contributions.

Any experimental measurement unavoidably includes a finite precision by which the result - value of some physical observable - is determined from the data. The precision depends on the quality of data, measurement method, experimental conditions and other factors. All these needs to be evaluated in order to claim a reliable estimate of the accuracy of an individual result. In experimental particle physics it is common to separate an uncertainty of a measurement into a statistical and systematic part. The former is a consequence of performing a measurement using a dataset of limited size. Since processes in quantum world are subject to stohastic fluctuations a repeated measurement on a different dataset would yield a slightly different result. The statistical uncertainty is a measure of this variation and is decreased as the two data sizes are increased. For large enough datasets the relative statistical uncertainty of a measured quantity x decreases as

$$\frac{\sigma_{stat}(x)}{x} \propto 1/\sqrt{N} \ , \tag{3.3}$$

where N is the number of observations of a measured observable in a given dataset. The systematic part of the uncertainty depends on the properties of the apparatus used for the measurement, the method used in performing the measurement and interpreting the result. In mathematical terms it is less defined than the statistical uncertainty and it is hence important for each experiment to report as accurately as possible the way in which this part of the measurement uncertainty was determined.

The average rate at which a certain process occurs in collisions of particles in an accelerator is given by

$$\frac{dN_p}{dt} = \mathscr{L}\sigma_p \ . \tag{3.4}$$

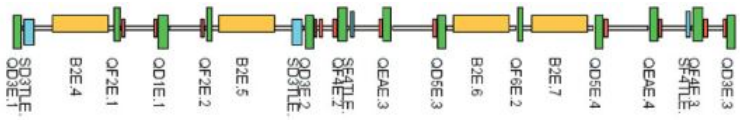

Figure 3.5: Schematics of a part of the SuperKEKB electron positron collider [8], showing a sophisticated lattice of magnets and other equipment. It should be noted that the part shown represents only around 2% of the full circular arrangement of one of the two beam lines (the one for electrons).

In the above equation $\mathscr{L}$ is the luminosity of the accelerator and σ_p is a cross-section for a process p. The product of the two yields the rate of the occurrence of events of such a process (N_p) in an interval of time (t).

Luminosity is a property of the accelerator and a measure of the intensity of its beams. For colliders[4] the luminosity can be expressed as

$$\mathscr{L} = \frac{N_1 N_2 \nu N_b}{2\pi\sigma_x\sigma_y} \quad . \tag{3.5}$$

Here, $N_{1,2}$ is the number of particles in the accelerated bunches, ν is the frequency of revolutions of a single bunch, and N_b is the number of bunches in a single beam. It is intuitive that the intensity of beams is proportional to these factors. On the other hand, probability of two particles inside opposite beams to collide is inversely proportional to dimensions of the colliding bunches in the plane perpendicular to the direction of acceleration (x and y) denoted by $\sigma_{x,y}$. The above equation is strictly correct for head-on bunch collisions of identical beams, assuming that the distribution of particles inside a bunch is Gaussian, i.e. that the density of particles inside a bunch follows a Gaussian distributions in the x and y coordinate[5]. Appropriate units in which the luminosity is measured are $\mathrm{cm}^{-2}\mathrm{s}^{-1}$. Luminosity of the LHC has currently reached around $2 \cdot 10^{34}$ $\mathrm{cm}^{-2}\mathrm{s}^{-1}$ and is expected to be significantly increased in the future. The record luminosity of a collider has been achieved by the KEKB electron positron collider, operating in Tsukuba, Japan, between 1999 and 2010. It reached the value of $2.1 \cdot 10^{34}$ $\mathrm{cm}^{-2}\mathrm{s}^{-1}$.

The final dataset available from an accelerator of course depends on the amount of time for which the accelerator is operating. Since a cross-section in Eq. 3.4 is a time independent quantity, integration of the equation yields the total number of events of a given process N_p,

$$N_p = \sigma_p \int_0^t \mathscr{L}\, dt \quad , \tag{3.6}$$

where t represents the time of accelerator operation. The quantity $\int_0^t \mathscr{L}\, dt$ is called the integrated luminosity.

[4] Colliders are accelerators in which particles accelerated in the opposite directions collide, as opposed to a fixed target experiments in which a beam of accelerated particles is directed onto a target of certain material, fixed in the laboratory frame.

[5] A Gaussian or a normal distribution means that a probability of finding a particle in such a bunch in an interval $[x, x+dx]$ is given by $dw = (dx/\sqrt{2\pi}\sigma_x)e^{-(x^2/2\sigma_x^2)}$.

While the luminosity in some way represents a technical specification of an accelerator, laws of physics are incorporated in the cross-section appearing in Eq. 3.4. Semi-classically one can think of a cross-section as of an area that can be hit by a projectile. For example, radius of a nuclei is roughly 10^{-15} m= 1 fm. A cross-sectional area covered by such a nucleus is $\pi r^2 = \pi$ fm^2. Hence a cross-section for a process to occur on such a nucleus would be π fm^2, or in more convenient units 0.0314 b. Here, b stands for "barn", b=10^{-28} m^2. In order to calculate a cross-section for a given quantum mechanical process quantum mechanics has to be applied. A cross-section is proportional to the amplitude squared of a given process, $|\mathscr{M}|^2$, like the one denoted in Fig. 1.9. Multipliying the cross-section σ_p with luminosity $\mathscr{L}$ yields the rate of the process p in units of s^{-1}.

Combining the dependence of the statistical uncertainty of a given measurement on the number of observations, Eq. 3.3, and the rate of a given process, Eq. 3.4, it becomes clear why the experiments performing high accuracy measurements are called Intensity Frontier. In order to decrease the statistical uncertainty one needs a large number of recorded process of a given type. This, on the other hand, is possible if the luminosity (intensity) of a collider is high.

Note: Charged particles can be accelerated by means of electric field, and constrained to move in circular orbits by means of magnetic field. The highest energies of accelerated particles were achieved at the Large Hadron Collider (CERN). Beside the energy, luminosity is an important property of a particle collider. The larger the luminosity, the larger is the rate of production of individual processes in the collisions of accelerated particles, and the better the precision by which these process can be measured.

3.1.2 *B* Factories

Prominent examples of the Intensity frontier experiments are the LHCb experiment at the LHC collider, and Belle II experiment at the SuperKEKB collider. The later is an electron positron collider, operating mainly at the CMS energy of 10.58 GeV. This energy corresponds to the rest energy of $\Upsilon(4S)$, a bound state of a $b\bar{b}$ quark pair. It's mass is just slightly larger than the sum of a pair of B^+B^- or $B^0\bar{B}^0$ mesons, $2 \cdot 5,28$ GeV= 10.56 GeV. The cross-section for an e^+e^- interaction at a given CMS energy is shown in Fig. 3.6. While generally decreasing with the CMS energy, the cross-section exhibits huge increases at certain energies, when the energy corresponds to a rest energy of a particle that can be produced in an e^+e^- collision. For example, at the energies around 90 GeV the cross-section increases due to the production of an intermediate neutral weak boson Z^0. The increase of the cross-section is due to the process shown in Fig. 3.7 (top left). Similarly, at the energy of around 10.5 GeV, the $\Upsilon(4S)$ state is produced (Fig. 3.7 (top right)). This bound state promptly[6], in more than 96 % of cases decays into a pair of $B\bar{B}$ mesons, where $B = B^+$ or $B = B^0_d$. Hence operating an electron positron collider at the energy of $\Upsilon(4S)$ resonance represents an abundant source of B mesons. We called the bound state of a $b\bar{b}$ pair, $\Upsilon(4S)$, a resonance[7]. The reason lies in a resonant energy shape of the cross-section in the vicinity of $m_{\Upsilon(4S)}$. The energy dependence

[6] Lifetime of $\Upsilon(4S)$ meson is around $3 \cdot 10^{-23}$ s [2].

[7] Another term, used specifically for bound states of b and $\bar{b}$ quarks, is bottomonium (an analogy with positronium, a bound state of e^+e^-).

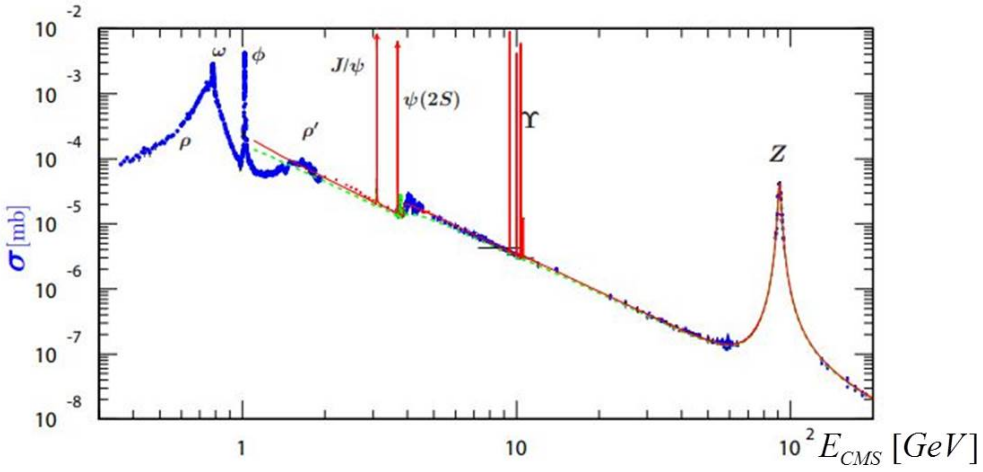

Figure 3.6: Cross-section for electron positron collisisons as a function of the CMS energy [2].

can be parametrized as $\sigma(E) = \sigma_{max}[\Gamma^2/4]/[(E-m_R)^2+\Gamma^2/4]$, with E denoting the CMS energy, m_R the rest energy of a short-lived intermediate state - resonance, like $\Upsilon(4S)$, and Γ the width of the curve at half maximum. The latter represents also a natural decay width of a resonance, related to the lifetime through $\tau = 1/\Gamma$. The described energy dependence is a typical resonance curve with a maximum at $E = m_R$. A closer look at the energy dependence of the cross-section is shown in Fig. 3.9. There, a graphic illustration of the cross-section division is presented. The resonant part, marked in red, corresponds to a production of $\Upsilon(4S)$ and its decay into a pair of B mesons (process in Fig. 3.7 (top right)). Beside the resonance production also an electromagnetic annihilation of the colliding electron and positron into a virtual photon[8] may occur (process in Fig. 3.7 (bottom)). In this case the final state is composed of lighter quark pairs ($q' = u,\ d,\ s$ or c), or charged leptons. As opposed to the resonant production the latter process is called the continuum production. The lower mass bottomonium states do not decay into pairs of B mesons because their mass is below the threshold of 2 m_B. Due to the properties of the strong interaction among quarks they never appear isolated in nature. Quarks are always bound within hadrons. In the case of a continuum production of lighter quarks, formation of hadrons from the initial quarks happens in the process of fragmentation. As the initial quark and anti-quark in the CMS move away from each other, new quark pairs are produced in the vacuum, combining with the already existing ones into final hadrons. The process is sketched in Fig. 3.8.

The resonant cross-section in the peak of the $\Upsilon(4S)$ resonance amounts to around 1.1 nb. The cross-section for the continuum production of $c\bar{c}$ or $u\bar{u}$ pairs is around 2.0 nb, while that for the $d\bar{d}$ or $s\bar{s}$ production is 0.5 nb.

At an electron positron collider with a luminosity of $2 \cdot 10^{34}$ cm^{-2}s^{-1} the cross section $\sigma(e^+e^- \to \Upsilon(4S) \to B\bar{B}) = 1.1$ nb means that around 20 $B\bar{B}$ meson pairs are produced every

[8] Virtual particle is a particle for which the usual relation $E = \sqrt{p^2+m^2}$ does not hold, see discussion in Sect. 1.2.3. In this specific case, the energy of the photon $E = E_{CMS}$, while its momentum in the CMS frame is zero.

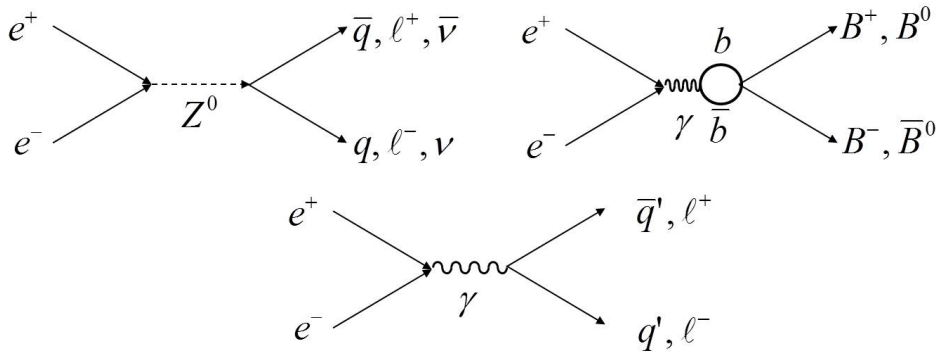

Figure 3.7: Top left: Electron positron annihilation into a neutral weak boson, producing $q\bar{q}$, $\ell^+\ell^-$ or $\nu\bar{\nu}$ pair (where $q = u,\ d,\ s,\ c$ or b, $\ell = e,\ \mu$ or τ, and $\nu = \nu_e,\ \nu_\mu$ or ν_τ). Top right: Electron positron collision producing $\Upsilon(4S)$, a bound state of $b\bar{b}$ which decays into a pair of B^+B^- or $B^0\bar{B}^0$ mesons. Bottom: Electron and positron can annihilate through a virtual photon to produce $q'\bar{q}'$ or $\ell^+\ell^-$ pair (where $q' = u,\ d,\ s$ or c, and $\ell = e,\ \mu$ or τ).

second (as well as, for example, around 35 $c\bar{c}$ pairs). By $B\bar{B}$ from now on we mean either B^+B^- or $B^0_d\bar{B}^0_d$ mesons, i.e. any B mesons that can be produced in the $\Upsilon(4S)$ decays. Also, we will use a short notation $B^0(\bar{B}^0)$ to denote $B^0_d(\bar{B}^0_d)$ meson. Heavier B mesons (B^0_s and B^+_c) are too heavy to be produced at this CMS energy: $m_{B_s} = 5.37$ GeV and $m_{B_c} = 6.27$ GeV. The most important ingredient of a collider called "B Factory", a production of B mesons at a high rate, is thus fulfilled by operating an e^+e^- machine at the $\Upsilon(4S)$ resonance. Moreover, at this precise energy, a $B\bar{B}$ meson pairs are produced without any additional final state particles, because the mass difference $m_{\Upsilon(4S)} - 2\,m_B \sim 20$ MeV does not allow for that. The B mesons from $\Upsilon(4S)$ are produced almost at rest in the CMS. B mesons are abundantly produced also in other processes, in proton proton collisions for example. The latter production is exploited by LHCb detector at the LHC collider. However, there are further specific properties, and requirements on the B meson production that must be satisfied for a successful operation of a B Factory, as discussed below.

The SuperKEKB collider is an upgrade of its predecessor, KEKB collider, which was in operation in the High Energy Accelerator Research Organization ("Koh-eh-nel-ghi ken-cue-kikoh", KEK for short) in Tsukuba, Japan, from 1999 until 2010. The collider had a twin brother named PEP-II operating in the Stanford Linear Accelerator Center (SLAC) in Stanford, USA, in the period 1999 - 2008. The description of the main ideas and methods behind the B Factories is common for the previous (KEKB and PEP-II) and present (SuperKEKB) generation of colliders. The difference is nevertheless huge: while the previous generation factories were colliding beams with luminosites of around $2 \cdot 10^{34}$ cm^{-2}s^{-1}, the present super B factory is expected to reach a 40 times higher luminosity, $\mathscr{L} = 8 \cdot 10^{35}$ cm^{-2}s^{-1} (remember that the highest luminosity ever achieved in any collider is $2.1 \cdot 10^{34}$ cm^{-2}s^{-1}!). At KEKB one gathered a dataset corresponding to an integrated luminosity (see Eq. (3.6)) of around 1 ab^{-1}. At SuperKEKB the plan is to reach a dataset of 50 ab^{-1}. The prefix "a" in ab denotes atto, a unit prefix of 10^{-18}. For a physics process with a cross-section of 1 nb, an integrated luminosity $\mathscr{L} = 1$ ab^{-1} corresponds to $N_p = 10^9$ events of the process under

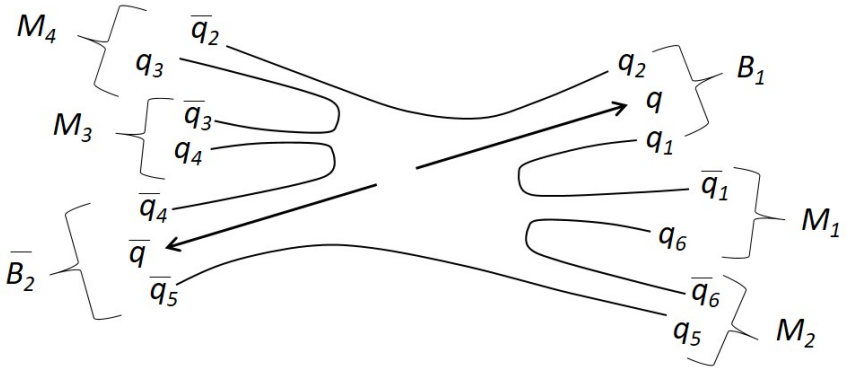

Figure 3.8: In the process of fragmentation the initial quarks $q\bar{q}$ are combined with new quark pairs produced in vacuum to form hadrons. M_i denotes a meson, and B_i a baryon.

question.

Belle II detector (Fig. 3.10) begun to take data in 2018, still awaiting a completion of its semiconductor detector. It is expected to reach an integrated luminosity of its predecessors in about a year time. In the book we discuss selected methods and results of the previous generation B Factories (KEKB and PEP-II, with the detectors recording data there, Belle and BaBar, respectively), applicable with some improvements also to the present one (SuperKEKB and Belle II detector). In the final chapter we also touch several expectations for the results from the latter. Interested readers with some advanced knowledge may find a comprehensive description of the detectors and measurement results of the B Factories in [5].

B Factories provide for an additional property of colliding electron and positron bunches, energy asymmetry. As will be discussed in Sect. 4.1, without the beam energy asymmetry the most important measurements at B Factories would not be possible. Colliding electrons have higher, and positrons lower energy in the laboratory frame. Denoting the former by E_- and the latter by E_+, the CMS collision energy is obtained as

$$\begin{aligned}(E_{CMS},0)^2 &= (E_+ + E_-, \vec{p}_+ + \vec{p}_-)^2 \\ E_{CMS}^2 &= 2m_e^2 + 2E_+E_- - 2\vec{p}_+\cdot\vec{p}_- \approx 4E_+E_- \quad .\end{aligned} \tag{3.7}$$

The first line above is the equality of the square of the momentum 4-vectors of colliding particles in the CMS frame and in the laboratory frame[9]. In the second line we neglected electron and positron rest energy in comparison to their total energy. Most of the time the KEKB collider operated with $E_- = 8$ GeV and $E_+ = 3.5$ GeV, and thus $E_{CMS} = 10.58$ GeV[10]. It should be understood, though, that the energy of electrons and positrons can be adjusted in some interval in order to yield various E_{CMS}. Perhaps most importantly, the CMS energy can be raised to the rest energy of $\Upsilon(6S)$, in decays of which beside B^+B^- and $B^0_d\bar{B}^0_d$ pairs also $B^0_s\bar{B}^0_s$ pairs are produced. At PEP-II, $E_- = 9$ GeV and $E_+ = 3.1$ GeV, and $E_{CMS} = 10.56$ GeV.

[9]Remember that a dot product of two 4-vectors, and hence also a square of any 4-vector, is a Lorentz invariant quantity.

[10]In this simplified calculation we neglected the finite crossing angle of electron and positron beams. The crossing angle at KEKB was 11 mrad, while at PEP-II the crossing angle was zero.

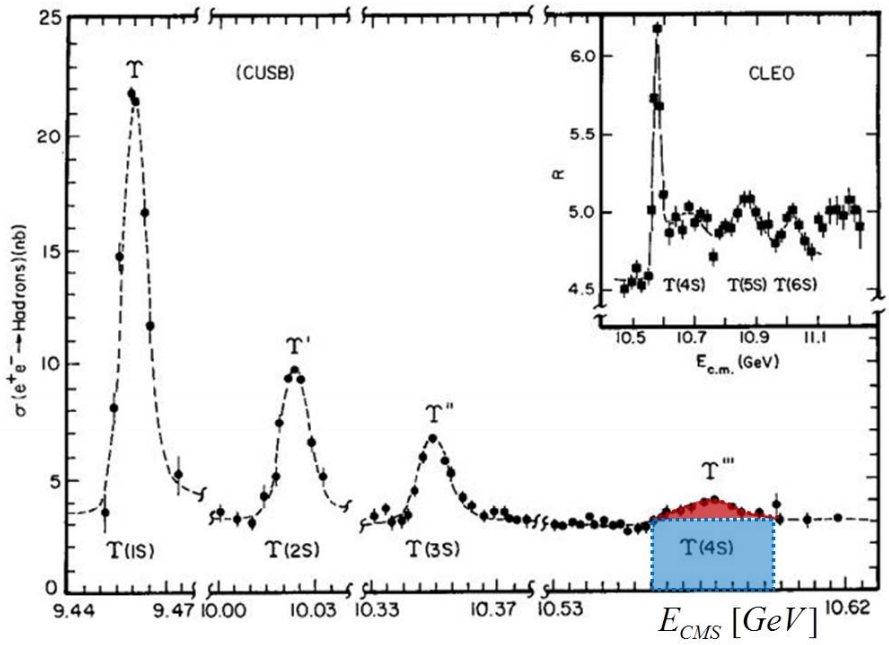

Figure 3.9: Measured cross-section for $e^+e^- \to$ hadrons at CMS energies around 10 GeV [10]. Prominent resonant peaks are observed, exposing four bound states of $b\bar{b}$, denoted by $\Upsilon(1-4S)$. The total cross-section at $E_{\text{CMS}} \sim m_{\Upsilon(4S)}$ is a sum of the resonant one (red), corresponding to the process in Fig. 3.7 (top right), and the continuum one (blue) for the process depicted in 3.7 (bottom).

Why the beam energy asymmetry is needed? Because in the CMS frame B mesons are produced almost at rest. If the CMS frame coincides with the laboratory frame (no energy asymmetry), B mesons have negligible momentum and decay at almost the same spot at which they were produced. With asymmetric beam energies the CMS frame is boosted with respect to the laboratory frame. Dimensionless velocity of $\Upsilon(4S)$ in the laboratory frame is $\beta = p_{4S}/E_{4S} = (p_- - p_+)/(E_- + E+) \approx (E_- - E_+)/(E_- + E_+) = 0.391$. Lorentz factor $\gamma = 1/\sqrt{1-\beta^2} = 1.086$ and hence $\beta\gamma = 0.425$ (at PEP-II the boost factor was even larger, $\beta\gamma = 0.56$). A $B\bar{B}$ meson pair is produced with a boost in the direction of the electron beam, and each of the B mesons travels a certain distance before decaying. The distance is indeed short, typically around 200 μm, nevertheless long enough to be reconstructed by precise semiconductor detectors, as described in Sect. 3.2.3.

Note: B Factories are electron positron colliders operating at the center-of-mass energy of $\Upsilon(4S)$ resonance which decays into a pair of B mesons. Due to the high accelerator luminosity, during their operation B mesons are produced abundantly at a rate of several tens per second. Asymmetric beam energies at B Factories enable measurements of B mesons' decay distance.

Figure 3.10: A photograph of Belle II detector. Photo: M. Friedl

3.2 Quantum measurements

In order to study processes involving B mesons produced at the B factories, particle detectors reconstructing their decay products are needed. Requirements for detectors depend on the physics goals of measurements to be performed and on the operating environment - the accelerator. Detectors at B factories were designed to measure CP violation in the system of B mesons, and in the course of a decade long data taking proved to be capable also of several other intriguing measurements. In the transition to the new generation of B factories (Belle II detector at the SuperKEKB collider) physicists profited from experiences with the previously operating detectors (Belle at KEKB and BaBar PEP-II) in development of improved instrumentation, capable of operation in harsher environment (significantly higher luminosity reflecting in higher radiation to be sustained by the detector) and of even more precise measurements.

Let us introduce the detectors first in general, to help the conceptual understanding, and explain some basic principles of operation afterwards. A schematic cross-section of the Belle and BaBar detectors are shown in Figs. 3.11 and 3.13, respectively. Each schematic illustration is followed by a photo of the detector. The detectors are of cylindrical shape built around the collision (or interaction) point of accelerated electrons and positrons. They are composed of a barrel part and two end-caps. For reasons to be explained below the detectors are placed in a strong[11] magnetic field pointing along the symmetry axis of the detector.

At the interaction point either the $\Upsilon(4S)$ resonance is formed, or fermion pairs are produced (see Sect. 3.1.2). The former immediately decays into a $B\bar{B}$ pair, and in the latter case in the process of fragmentation new pairs of quarks are formed, eventually grouped into various species of hadrons. B mesons have a lifetime of the order of ps and, as we

[11] The magnetic flux density is 1.5 T.

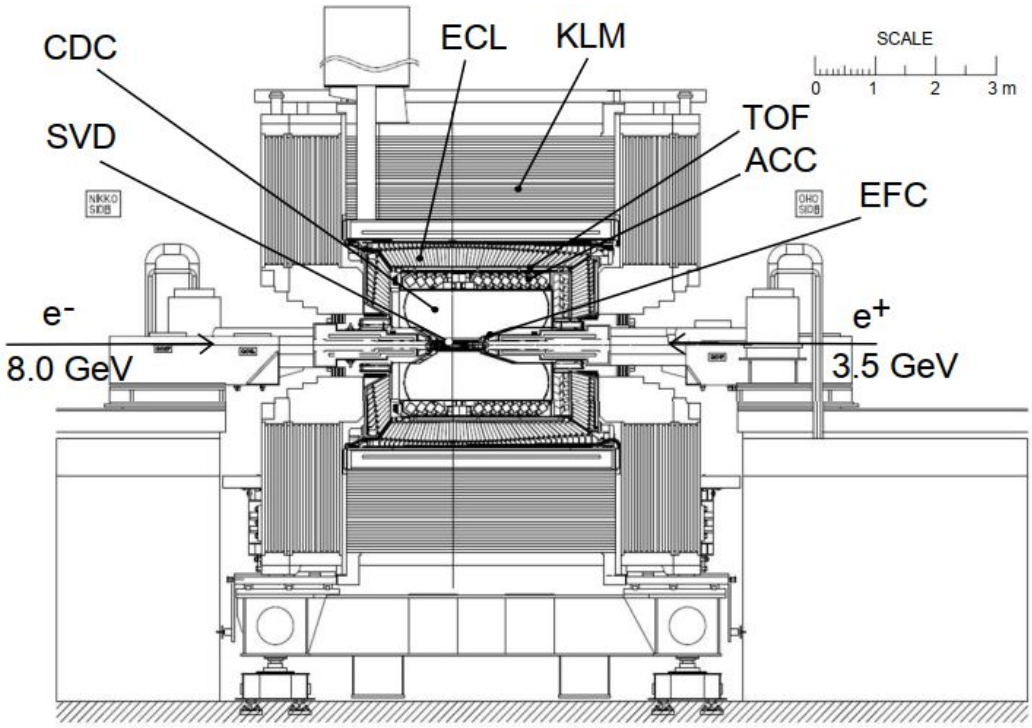

Figure 3.11: A cross-section of Belle detector [5]. Detector modules include Silicon Vertex Detector (SVD), Central Drift Chamber (CDC), Aerogel Cherenkov Counter (ACC) and Electromagnetic Calorimeter (ECL).

will discuss further in the next section, on the average decay at a distance of 200 μm. One can only detect hadrons and charged leptons[12] that have lifetimes long enough to reach the active parts of the detector. These particles are produced in decays of heavier, shorter lived particles or in fragmentation, and are listed in Tab. 3.1. Short lived particles produced in various physics processes are reconstructed from their decay products, detected in a detector. For such reconstruction typically an observable called the invariant mass is used. Consider a decay of an initial particle P to several final state particles f_i ($i = 1,...n$). The final state particles 3-momenta, $\vec{p}_i$, are measured in the detector. f_i's are also identified, i.e. as we clarify below, their masses m_i are determined. Energies of final state particles are thus known, $E_i = \sqrt{m_i^2 + p_i^2}$. 4-momentum of P, $(\sqrt{m_P^2 + p_P^2}, \vec{p}_P)$, is unknown. Since energy and momentum in decay are conserved, we can write:

$$(\sqrt{m_P^2 + p_P^2}, \vec{p}_P)^2 = \left[\sum_{i=1}^{n} (E_i, \vec{p}_i)\right]^2$$

$$m_P^2 = \sum_{i=1}^{n} m_i^2 + \sum_{j>i} 2(E_i E_j - \vec{p}_i \cdot \vec{p}_j) \quad . \tag{3.8}$$

[12] We specifically mention charged leptons, because neutral leptons - neutrinos - are not detectable with general purpose detectors described here. They only interact weakly and hence special detectors with a large amount of material are required for ν detection.

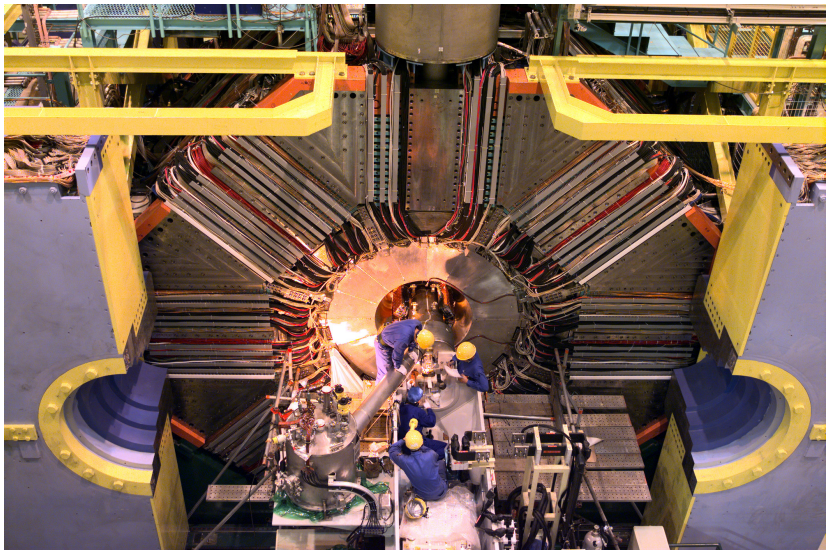

Figure 3.12: A view of one of the end-caps of Belle detector [11].

Mass of the initial state particle can be calculated using the measured momenta of its decay products. In this case m_P is called the invariant mass[13].

Taking into account the physics program of two international collaborations gathered around the Belle and BaBar detector[14], the detectors needed to fulfil some general requirements:

- ability to detect particles in the largest possible fraction of the solid angle around the e^+e^- interaction point (hermeticity);

[13]Invariant because it represents the square of a magnitude of a Lorentz vector, which is invariant under Lorentz transformations.

[14]Collaborations evolved during time, at the maximum each consisted of 500 to 600 collaborators, from more than 70 institutions worldwide.

particle	$c\tau$ [m]
e^-	∞
μ^-	659
π^-	7.8
K^-	3.7
K_L^0	15.3
p	∞
n	$2.6 \cdot 10^{11}$
γ	∞

Table 3.1: Particles stable enough to be detected in the detectors (corresponding anti-particles are implied). Their average decay length is $\gamma\beta c\tau$, where γ is an approriate Lorentz factor and β their velocity in units of the speed of light c. $c\tau = \infty$ means a stable particle.

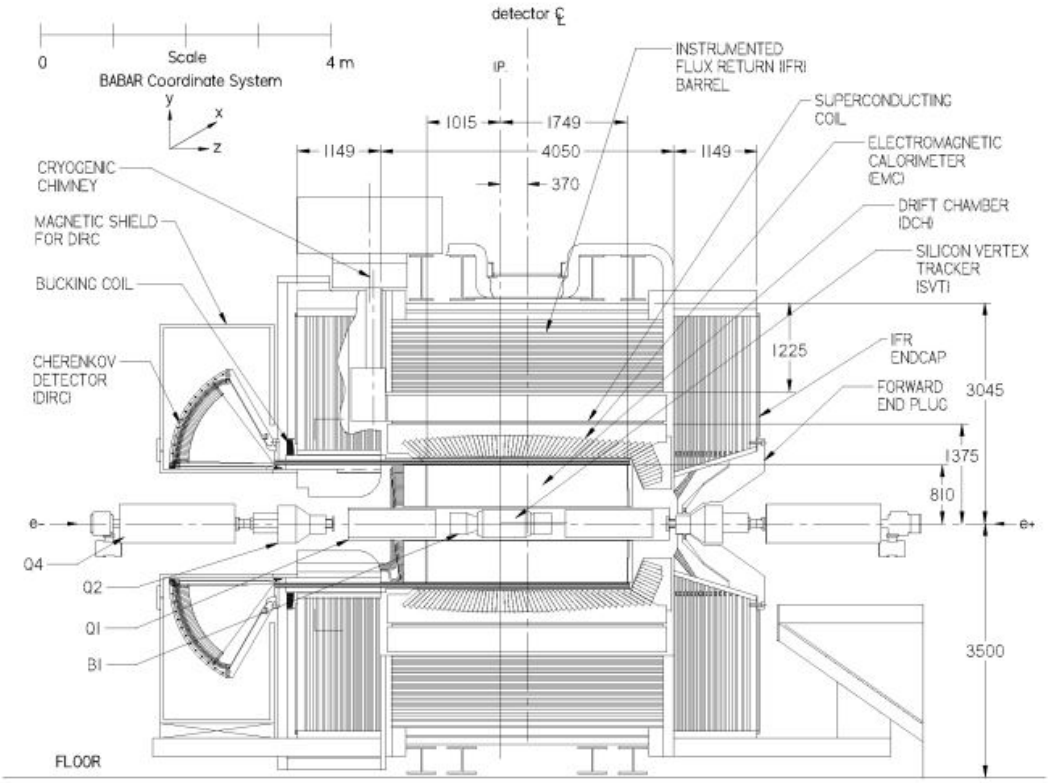

Figure 3.13: A cross-section of BaBar detector [5]. Various subdetectors are marked on the plot.

- excellent precision in spatial determination of B meson decay vertices, with resolution of around 100 μm (for decay time dependent studies);
- good separation among various types of particles, especially between kaons and pions (particle identification);
- capability of efficient and precise photon energy reconstruction (calorimetry).

For most of the particle detectors three groups of detector modules (subdetectors) are mandatory, performing three distinct tasks: charged particles momentum determination, charged particle identification, and neutral particle energy determination and identification.

3.2.1 Momentum

The first task from the list above is achieved using the already mentioned bending of charged particles trajectories in a magnetic field (Eq. (3.2)). Assuming the particle's initial velocity being perpendicular to the direction of magnetic field (Fig. 3.15 (left)), particle will travel

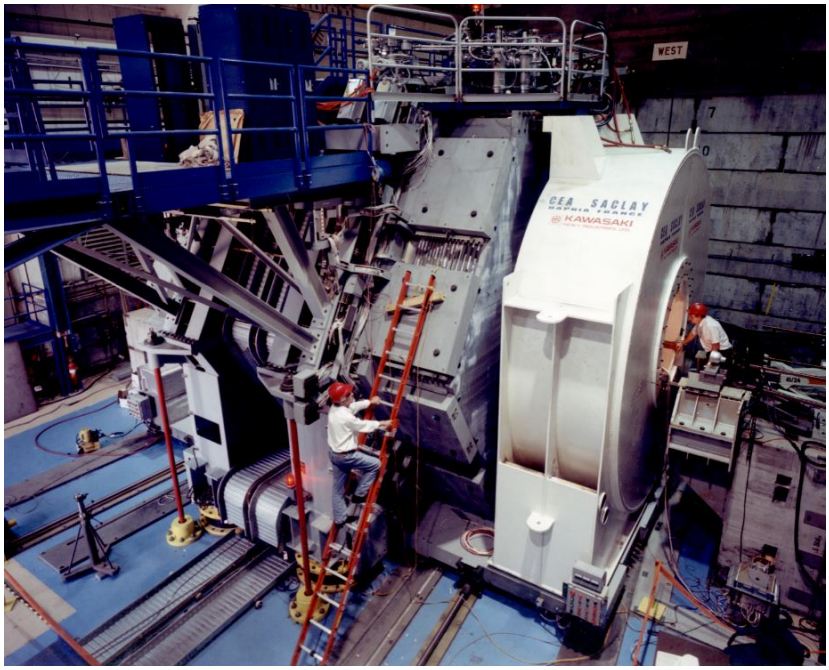

Figure 3.14: View of BaBar detector during installation [12].

along a circular orbit with radius R:

$$evB = m\frac{v^2}{R}$$
$$R = \frac{p}{eB} \quad , \tag{3.9}$$

where we used the centripetal acceleration v^2/R. Generalizing the expression to the case of non-perpendicular initial velocity, radius R is related to the component of momentum perpendicular to $\vec{B}$,

$$R = \frac{p_t}{eB} \quad . \tag{3.10}$$

In such a case a particle would travel along a 3-dimensional helix, as sketched in Fig. 3.15 (right). Hence by measuring the radius of a charged track in a magnetic field one can determine p_t. The component of momentum parallel to $\vec{B}$ can be obtained from the angle the track makes with the axis of the magnetic field

$$p_{\parallel} = p_t \tan\theta \quad . \tag{3.11}$$

Determination of charged particle's momentum thus reduces to spatial determination of its trajectory.

Trajectory of a charged particle is typically reconstructed using various types of gaseous detectors. A basic principle can be understood using an example of a cylindrical proportional counter cell (Fig. 3.16 (left)). A charged particle traversing the sensitive volume filled with gas ionizes gas molecules (primary ionization). An anode wire and a cathode enclosure

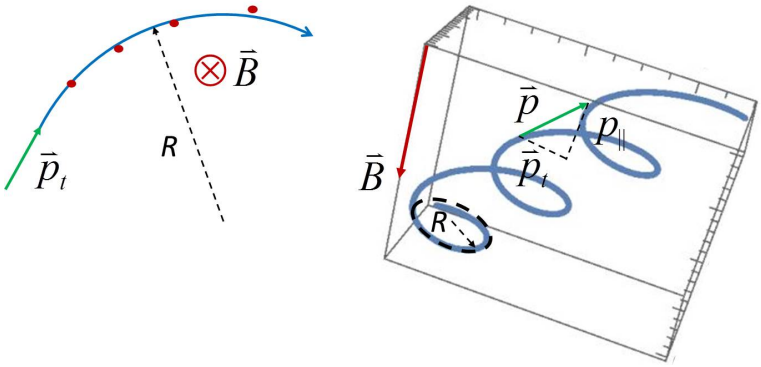

Figure 3.15: Left: In a plane perpendicular to the direction of magnetic field charged particle moves along a circular line. Right: In three dimensions the trajectory of a charged particle is a helix.

produce a radial electric field, with stregth $E = V_0/[r\log(b/a)]$, in which the ion pairs move. Due to collisions with the gas molecules the drift velocity of electrons and positive ions is approximately $v_{e,\text{ion}} = \mu_{e,\text{ion}}E$, where $\mu_{e,\text{ion}}$ denotes the electron or ion mobility. The effect of a specific radial dependence of the electric field strength in cylindrical geometry ($E \propto 1/r$) is multiplication of ion pairs, due to secondary ionization by electrons from the primary ionization, in the vicinity of the anode. Performance of such a counter can be extended by using several anode wires, as sketched in Fig. 3.16 (right). This constitutes a multiwire proportional chamber which enables determination of a spatial coordinate of the traversing ionizing particle. Invention of the latter is attributed to Georges Charpak, French physicist who at the time of invention worked at CERN. Multiwire proportional chambers caused a small revolution in experimental particle physics and played also an outstanding role in enabling new diagnostic methods in medicine. G. Charpak received the Nobel prize for physics in 1992. If the time of the ionizing particle's crossing is known, the position can be determined even more precisely by integration of ion pairs velocity over the time. In order to achieve a good accuracy with this method, the mobility of electrons and ions in the gas, as well as the electric field strength must be precisely known. Such variant of the chamber is called the drift chamber. Both Belle and BaBar detectors successfully used drift chambers as the main tracking devices to determine momenta of the charged particles. Belle II uses an upgraded version of the same device as used in Belle detector. A general idea on geometry of the devices is shown in Fig. 3.17 (left). The Belle Central Drift Chamber is denoted by CDC in Fig. 3.11, and BaBar's Drift Chamber by DCH in Fig. 3.13. Each of the chambers incorporated several thousands of anode wires. The accuracy by which the momentum of charged particles is measured depends mainly on two effects: the intrinsic resolution of a given device (determined by wire spacing, gas mixture used, etc.) and multiple scattering of ionizing particle. The latter is due to scattering of particle in the material of detector and causes its trajectory to deviate from an ideal helix. The first effect results in a relative

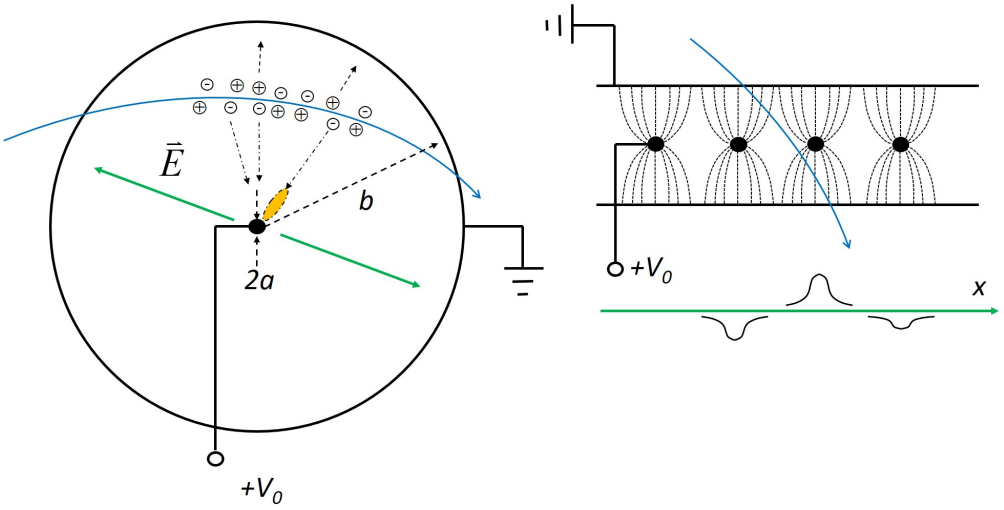

Figure 3.16: Left: A gaseous cylindrical proportional counter, with a charged track producing primary ionization. Electrons travel towards the anode and positive ions towards the cathode. In the vicinity of the anode a secondary ionization takes place. Right: A single counter cell can be evolved into a multiwire chamber that enables determination of a spatial coordinate.

accuracy of the transverse momentum component determination ($\sigma(p_t)/p_t$)) proportional to p_t. The second is inversely proportional to the velocity of the particle. The total relative accuracy is a quadratic sum of both terms:

$$\frac{\sigma(p_t)}{p_t} = \sqrt{(a\ p_t)^2 + (b/v)^2} \tag{3.12}$$

For Belle detector $a = 0.0019\ \mathrm{GeV}^{-1}$ and $b = 0.0030\ c$. For a charged pion with $p_t = 1$ GeV the relative accuracy is around 0.4%. In order to be able to deduce signals from all the anode wires, as well as to provide high voltage to them, a lot of cables must be connected to the back plate of a drift chamber. A photo of cables used for the drift chamber of Belle II detector is shown in Fig. 3.17 (right), and a nice example of reconstructed tracks in Belle CDC in Fig. 3.18 (left).

Note: Charged particles' momenta determination with a sub-percent relative accuracy is achieved by measuring the curvature of their trajectories in a magnetic field.

3.2.2 Identification

The second group of detector modules is used for charged particle identification (commonly abbreviated as PID). There are several physics principles to achieve this goal. But first we need to clarify what is meant by "identification". Individual hadrons and charged leptons are best distinguishable according to their mass. Once the mass of an individual particle is known, for example 106 MeV, 140 MeV or 494 MeV, one can easily deduce from the

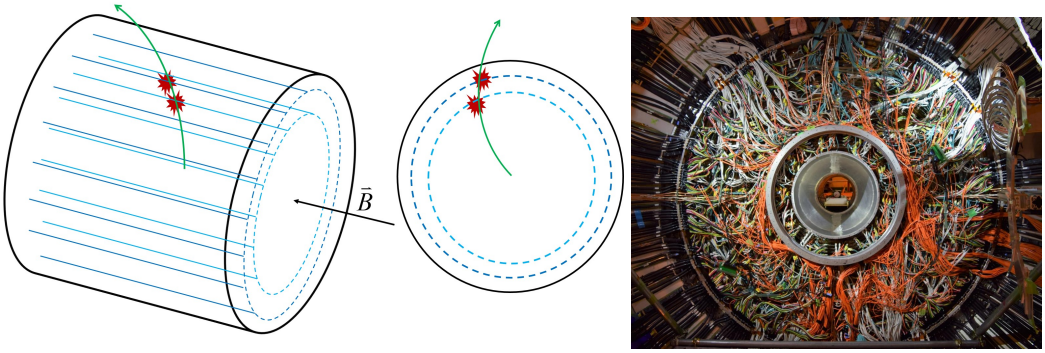

Figure 3.17: Left: Geometrical principle of momentum determination using drift chambers. Trajectory of a charged particle originating from the interaction point is curved due to magnetic field. The ionizing particle produces ionization in the gas of the chamber, which is detected by anode wires. Note that in realistic chambers the number of wires is much larger. Right: A view of Belle II CDC backward plane after connection of all cables. Photo: Van Thanh Dong.

already known particle properties that she is dealing with a muon, charged pion or charged kaon, respectively. On the other hand, once the momentum of a particle is known (from the measurements described before), the mass follows from the relation

$$\begin{aligned} p &= \gamma m v \\ m &= \frac{p}{\gamma v} \quad . \end{aligned} \tag{3.13}$$

The relation shows that in order to determine particle's mass, beside its momentum we need to know also the velocity. PID is hence a synonym for velocity measurements. Let us mention only one of the principles of velocity determination used in both, BaBar and Belle detectors.

The method is based on the effect of Cherenkov radiation. It is named after Pavel Cherenkov, a Russian physicist, who first experimentally observed this kind of radiation. It is emitted by any charged particle travelling through a medium at a speed greater than the speed of light in the same medium. By denoting the latter by c', to be distinguished from the speed of light in vacuum, c, we have the following relation between the two:

$$c' = \frac{c}{n} \quad . \tag{3.14}$$

The refractive index of a medium, n, is always greater than unity, and hence $c' \leq c$. With the velocity of a particle v greater than c' we have a situation sketched in Fig. 3.19 (top left). A charged particle emits radiation at an angle θ_C with respect to the direction of its velocity. If a particle emits a photon at $t = 0$, after δt it travels the distance $v\delta t$, while the photon in the same time moves by $c'\delta t = c\delta t/n$. Hence

$$\cos\theta_C = \frac{c/n}{v} = \frac{1}{\beta n} \quad . \tag{3.15}$$

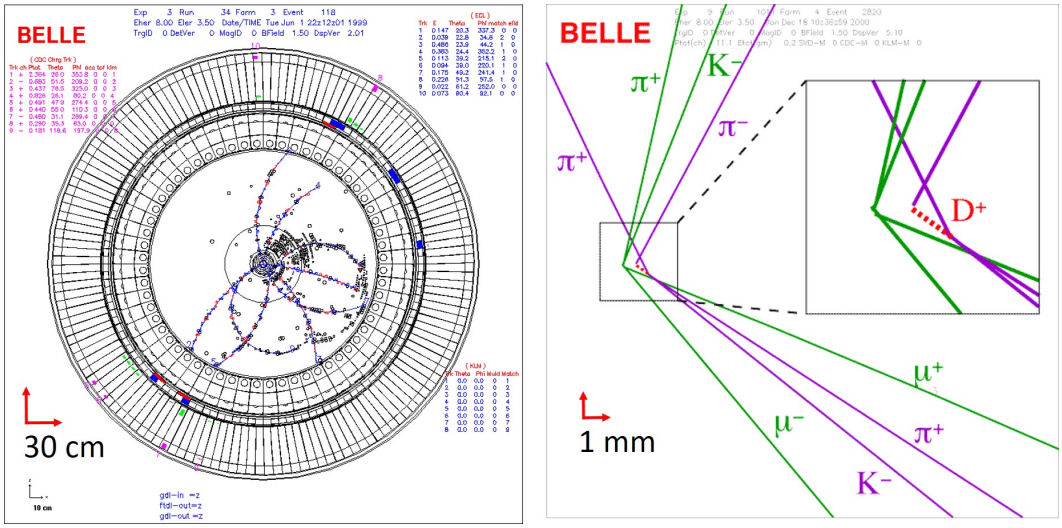

Figure 3.18: Left: Reconstructed tracks of charged particles in the volume of Belle CDC. Full lines are trajectories of particles fitted through the measured hits, represented by circles. Right: Zoom of interaction region with extrapolated tracks (the event is not the same as on the left plot). Note the change of scale between the plots, marked by red arrows. Points on particles tracks measured by SVD enable extremely precise determination of decay vertices of short lived particles. A sub-milimeter distance between decay vertices of two B mesons (one decaying into $K^-\pi^+\mu^-\mu^+$ and the other into $K^-\pi^+\pi^-\pi^+$) is clearly visible [23].

The light is only emitted if $v \geq c'$ or $\beta \geq 1/n$, and thus of course $\cos\theta_C \leq 1$. The angle θ_C is called the Cherenkov angle. P. Cherenkov was for his discovery awarded the Nobel prize in physics in 1958. He shared the prize with I. Tamm and I. Frank who described the effect theoretically.

Cherenkov angle, and Cherenkov effect in general depend on the velocity of a particle emitting the radiation. Determination of the Cherenkov angle (and knowledge of the material in which the radiation was generated, i.e. of the refractive index) leads to particle's velocity, and - in the sense of what was discussed just after Eq. (3.13) above - eventually to the mass of the particle.

In BaBar, the DIRC detector module (Detector of Internally Reflected Cherenkov Light) was performing exactly this - measurements of Cherenkov angle and by that identification of charged particles. The ingenious principle of operation is illustrated in Fig. 3.19 (top right). A charged particle entered an almost 5 m long quartz bar ($n \approx 1.5$) in which it emitted Cherenkov light[15]. The emitted photons propagated by means of internal reflection through the quartz to one end of the bar. At the end they were detected by photon detectors (photo-multipliers) measuring the position of the exiting photons as well as the time of their travel through the bar. From the measured Cherenkov photon information and known impact point of a charged track on the surface of the quartz bar one can reconstruct the Cherenkov angle. A geometrical configuration of the DIRC is sketched in Fig. 3.19 (bottom).

The performance of the DIRC subdetector is illustrated in Fig. 3.20 [24]. The efficiency

[15] If its velocity was larger than $c/1.5$, which is, for example, fulfilled for charged kaons with $p \geq 450$ MeV.

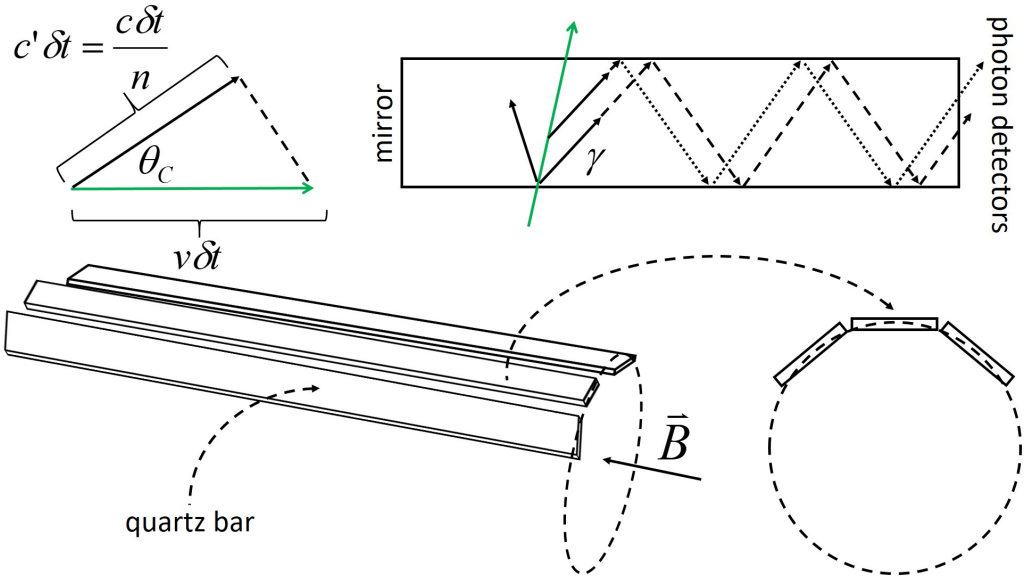

Figure 3.19: Top left: to derivation of the Cherenkov angle. Top right: Principle of BaBar DIRC operation. Bottom: A sketch of geometrical configuration of DIRC subdetector in BaBar detector. Note that the sketch is not to scale, DIRC was actually composed of 144 quartz bars.

for charged kaon identification, defined as the probability for a true kaon entering the DIRC system to be actually identified as such, is very high (> 95 %). It depends on the criteria (number of detected Cherenkov photons, accuracy of the Cherenkov angle determination, ...) used to select identified kaons, and should hence always be presented with another quantity, for example a probability for a charged pion to be identified as a kaon; with tighter selection criteria the efficiency drops, but also the latter probability is lower. The efficiency as well as the pion misidentification rate depend on the momentum of the particle. This follows from the dependence of the number of radiated Cherenkov photons on particle's velocity. It is proportional to $\sin^2\theta_C$:

$$N_\gamma \propto L\sin^2\theta_C = L\frac{(p^2/E^2)-(1/n^2)}{p^2/E^2}\quad , \tag{3.16}$$

where L is the distance travelled by the charged particle in the radiator material, and $\beta = p/E$ was used. Note that for a charged kaon with $p = 1$ GeV and in a material with $n = 1.5$, the average number of radiated Cherenkov photons is only around 220 cm^{-1} (thickness of the quartz bars in DIRC was around 1.7 cm). Due to a finite photon detection efficiency of photomultipliers the actual number of detected photons per charged track was only few tens in BaBar [25]. This is comparable to a sensitivity of a human eye (as one of the most sensitive light sensors), which responds to around 10 incident photons[16][26].

[16]The sensitivity strongly depends on the wavelength of the incident photons; human eye is most sensitive to green light, i.e. photons with wavelengths of around 550 nm. Photomultiplier tubes, on the other hand, at least the ones used in DIRC, are most sensitive to blue light, $\lambda \sim 450$ nm and less.

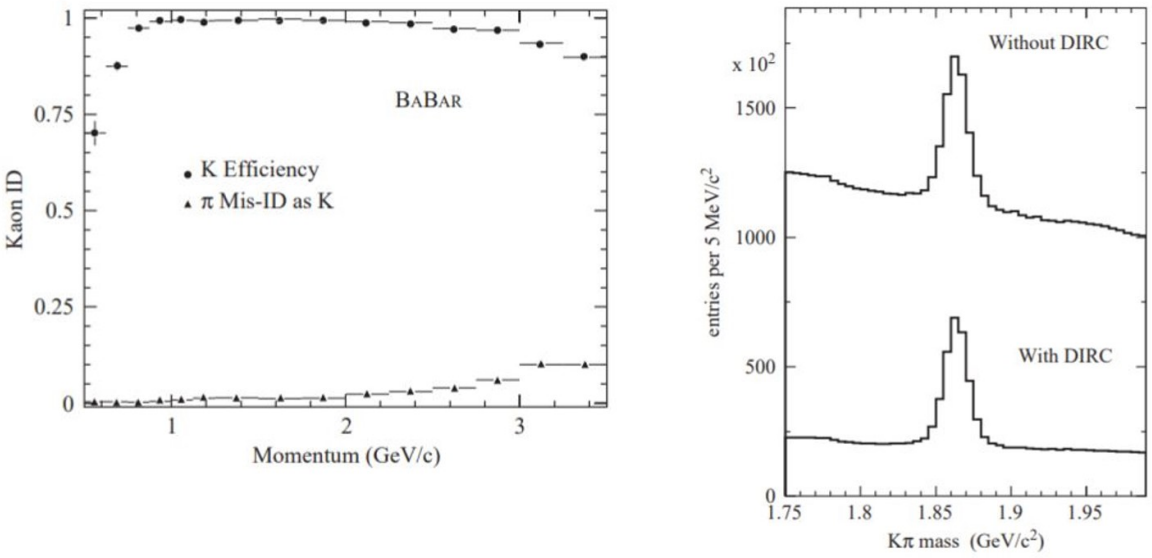

Figure 3.20: Left: Efficiency for correct identification of $K^{\pm}$ using DIRC subdetector in BaBar, and probability for misidentification of $\pi^{\pm}$ as $K^{\pm}$ [24]. Right: Invariant mass distribution for $D^0 \to K^-\pi^+$ decays, with or without using DIRC identification [24].

From the point of view of physics performance, Fig. 3.20 (right) shows an interesting comparison. The plot shows a distribution of invariant mass (Eq. (3.8)) of the final state particles in decays of charm mesons D^0 to $K^-\pi^+$ pairs. In case of correct reconstruction - combination of two reconstructed tracks which actually belong to a kaon and a pion from D^0 decay - the invariant mass equals the nominal mass of a D^0 meson. Such combinations form the observed peak at the mass of around 1.87 GeV. Wrong, mainly random combinations of tracks do not form such a peak but rather a smooth background distribution. When using the identification provided by DIRC, i.e. dividing the set of tracks to pions and kaons, the amount of such random combinations is largely reduced by a factor of $\sim$5, while the yield of correctly reconstructed decays is reduced by only a small fraction.

In Belle II detector a similar principle as in DIRC is used for PID. The internal reflection of light in quartz bars of Belle II detector is photographed in Fig. 3.21. Note though that what is seen in the photo is a laser light and not Cherenkov photons.

Note: Identification of charged particles - determination of their mass - is possible through various methods, one of the most accurate ones being a measurement of the Cherenkov radiation. It only appears for charged particles travelling through a medium at a speed greater than the speed of light in the same medium.

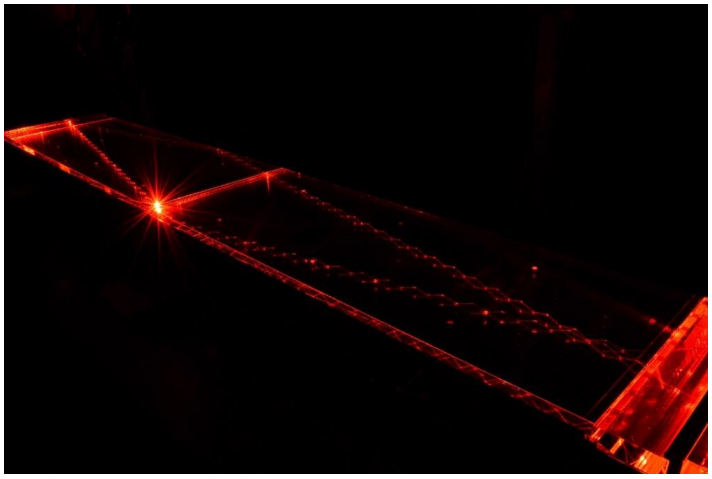

Figure 3.21: Laser light being internally reflected in a quartz bar of Belle II PID subdetector. Photo: K. Inami

3.2.3 Compactification

Looking at Fig. 3.11 and realizing that Belle CDC encompasses roughly 5 m^3 of gas[17], it's hard to imagine that in modern times, when everything is compact but yet capable and efficient, one needs such a relatively bulky device to perform a precise measurement. To perform measurements of quantum mechanical objects - particles momenta with a sub-percent relative precision, at an affordable price, such a device is nevertheless needed. However, compactification has been present in experimental particle physics long before than in smart phones. Semiconductor detectors are used in many experiments, also in Belle and BaBar. These detectors are denoted as SVD (Silicon Vertex Detector) in Fig. 3.11 and as SVT (Silicon Vertex Tracker) in Fig. 3.13. As the name suggest they are made of semiconductor - Silicon. Principle of operation is rather similar as in gaseous detectors. In semiconductor an ionizing particle instead of ion pairs produces electron - hole pairs. In a junction of a p- and n-doped semiconductor (a p-n junction) a region depleted of any free charge carriers (electrons or holes) is established. Across the depleted region an electric field is built up which, similarly as in a cylindrical proportional counter, scrolls electrons and holes to the appropriate side of the junction. Thin metallic electrodes on the surface of the semiconductor act in a similar manner as the cathodes and anodes in a drift chamber. In contemporary detectors orthogonal strips of heavily doped semiconductor (denoted as p^+ and n^+) are implanted on each side of the bulk of semiconductor material (Fig. 3.22). By this a 2-dimensional information on the coordinate can be obtained, and such detectors are called Double Sided Silicon Detectors (DSSD).

Semiconductor detectors are capable of measuring trajectories of charged particles with significantly better precision then gaseous detectors. Typical distances among the wires in drift chambers are of the order of 10 mm, while the widths of semiconducting strips and their separations are of the order of 0.1 mm. This delicate and precise devices are installed closest to the interaction point. A longitudinal and transverse cross-section of BaBar's SVT is shown

[17] The gas in CDC was 50% He and 50% C_2H_6.

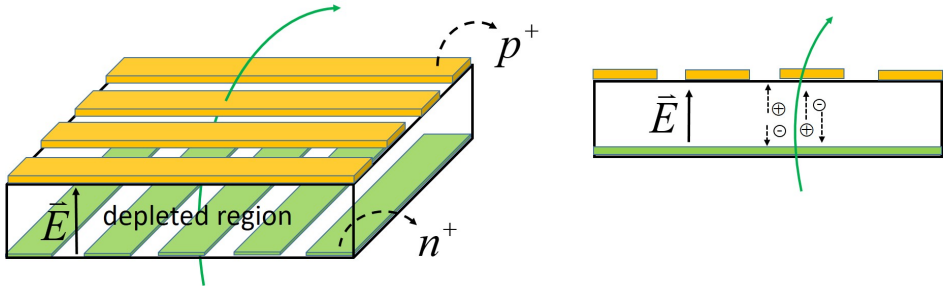

Figure 3.22: A schematic illustration of a double sided silicon strip detector. p^+ and n^+ denote a heavily p- and n-doped semiconductor, respectively. A traversing ionizing particle produces electron-hole pairs in a depleted region, and the released charge carriers are moving in the electric field across the region.

in Fig. 3.23. By extrapolation of tracks reconstructed with the help of silicon detectors it is

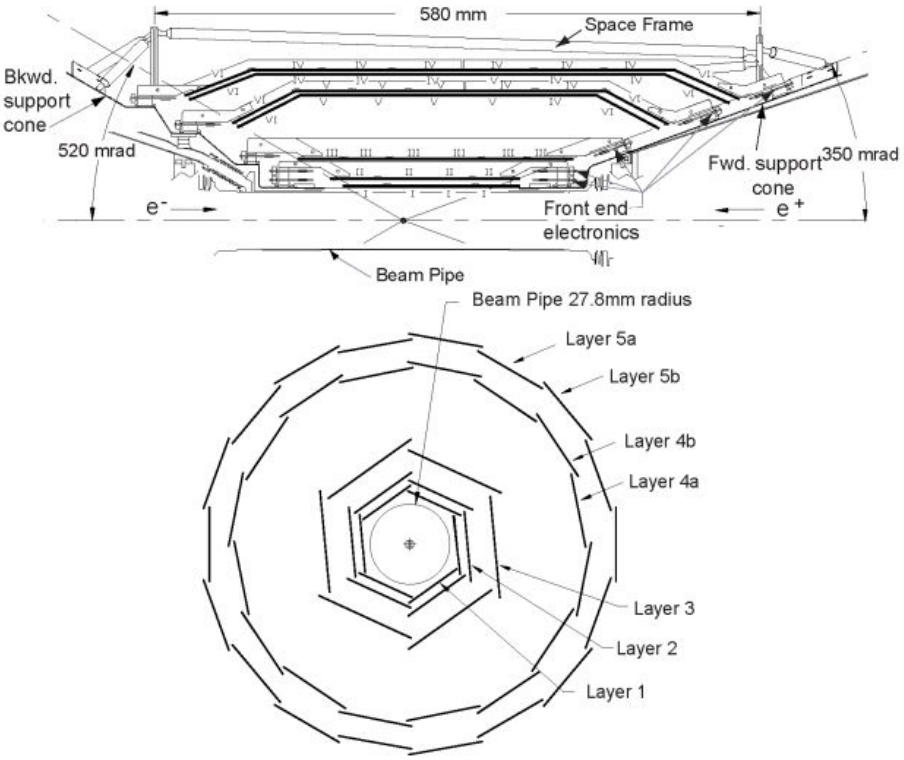

Figure 3.23: Longitudinal (top) and transverse (bottom) cross-section of BaBar's SVT [5]. It consisted of five cylindrical layers of double sided silicon detectors, extending in radius from around 3 cm to around 15 cm.

possible to determine intersections of groups of particles originating from decays of a single short lived particle, like a B mesons. These common points are called vertices. An example of such a vertex reconstruction is presented in Fig. 3.18 (right).

Belle II is equipped with four layers of DSSD and in addition two innermost layers of new type of detectors, in which strips are replaced by pixels. The latter provide even more precise spatial information. A photo of the assembled half-shell of these semiconductor detectors is shown in Fig. 3.24 (left), together with BaBar's SVT during maintenance (right).

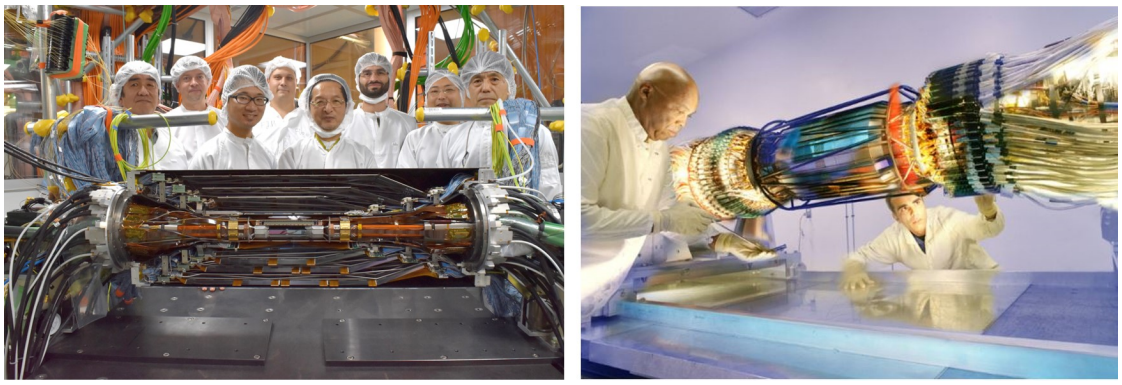

Figure 3.24: Left: An assembled half-shell of Belle II vertex detector, composed of pixel and double sided silicon strip detectors [27]. Right: BaBar's SVT (together with magnets of interaction region) during maintenance [5].

Precision of tracking can be verified using cosmic rays penetrating through the detector. Track reconstruction algorithm reconstructs tracks from the interaction point outwards. This is true also for a cosmic ray particle, the track of which is hence reconstructed as two independent halves. Any discrepancy between the starting points of the half-tracks is a measure of the tracking resolution. Resolution of Belle SVD determined with such a method is shown in Fig. 3.25. In both independent coordinates ($r-\phi$ in the plane perpendicular to the direction of magnetic field, and z in the direction of $\vec{B}$) the accuracy reaches around 30 μm for particles momenta above 2 GeV.

Note: Semiconductor detectors enable precise determination of B meson decay vertices, with a spatial precision below 100 μm.

3.3 Entanglement

3.3.1 BBbar

In decays of $\Upsilon(4S)$ pairs of B mesons are produced. These pairs are not just any pairs of B mesons, they posses some special properties enabling specific methods for studies of CP violation. Every pair of B mesons from $\Upsilon(4S) \to B\bar{B}$ carries the same quantum numbers as $\Upsilon(4S)$, specifically spin $J=1$, parity $P=-1$, charge conjugation parity $C=-1$, and beauty $B=0$[18]. Parity and C-parity of $\Upsilon(4S)$ can be deduced from the explanations in Sect. 2.1,

[18] We use the same symbol B to denote the baryon number and the beauty quantum number. The reader should be careful not to confuse the two.

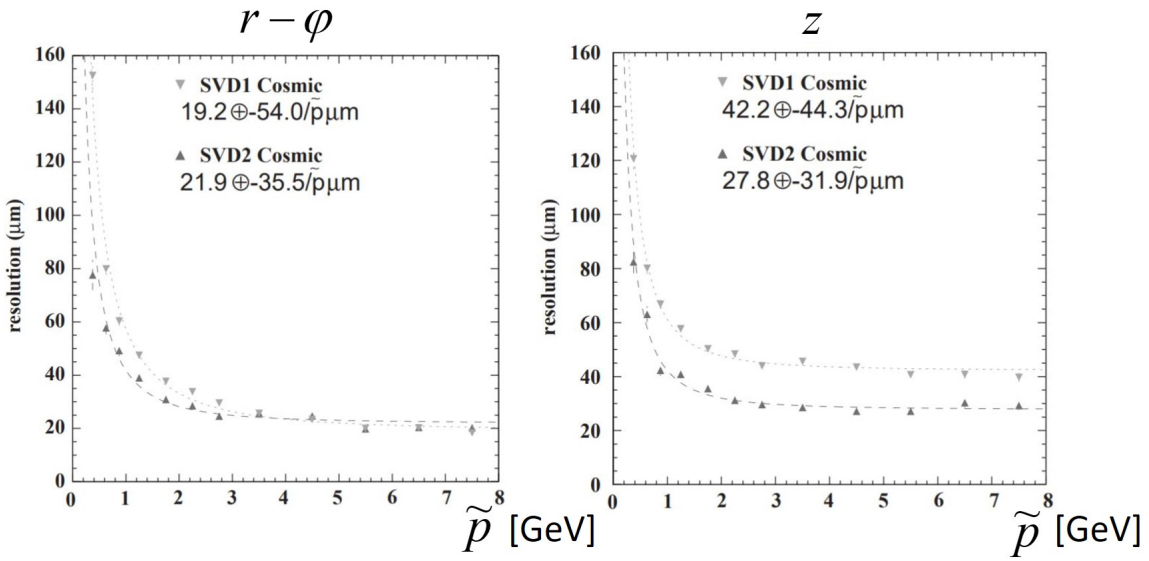

Figure 3.25: Tracking resolution in $r-\phi$ and z coordinate at Belle estimated using cosmic rays [28].

taking into account that the quark pair in the meson is in a spin 1 state. The transfer of C and P from $\Upsilon(4S)$ to a pair of B mesons is possible because the decay is mediated by the strong interaction which conserves both parity and C parity. Hence any pair of B mesons produced in a decay of $\Upsilon(4S)$ must be treated as a unique quantum system, and not as a pair of individual mesons. Such a pair is an example of quantum entanglement. It means that properties of an individual meson in a pair are not independent of the properties of the other meson, because together they have to be in agreement with the properties of the $\Upsilon(4S)$. To illustrate the fact, let us consider a production of a pair of neutral B mesons, $B^0\bar{B}^0$, in an $\Upsilon(4S)$ decay. First, in order the two final state mesons with spin 0 to conserve the angular momentum (remember, the spin of $\Upsilon(4S)$ is 1), they must carry a relative orbital angular momentum $L=1$. According to the discussion in Sect. 2.1 a quark (fermion) and an anti-quark (anti-fermion) in a meson have opposite intrinsic parities. Hence a B^0 as well as $\bar{B}^0$ have negative intrinsic parity - as stated in the mentioned section, bosons and corresponding anti-bosons have the same intrinsic parity. The total parity of the meson pair is $P_{B^0}P_{\bar{B}^0}(-1)^L=-1$, the same as the one of the mother $\Upsilon(4S)$ meson. A very similar argument follows for the C parity of the mesons system. Exchanging $B^0 \leftrightarrow \bar{B}^0$, which is what the $\hat{C}$ operator does, effectively swaps the positions of the two mesons and hence the effect is the same as that of the parity operation: it introduces a factor $(-1)^L$ to the eigenvalue of C parity. The C parity of the final state is thus -1, in agreement with $C_{\Upsilon(4S)}$. Last but certainly not least, $\Upsilon(4S)$ composed of a $b\bar{b}$ quark pair has beauty quantum number $B=0$. In the final state this is divided between the B^0 (composed of a $\bar{b}$ anti-quark) with $B_{B^0}=1$ and the $\bar{B}^0$ (composed of a b quark) with $B_{\bar{B}^0}=-1$. The total beauty of the final state is thus 0.

The mentioned facts simply represent conservation of various quantum numbers and are not related to quantum entanglement. Now remember a phenomenon briefly described in Sect. 1.2.3, the neutral meson oscillations (see also Fig. 1.11). Although rare, the process

may cause one of the B mesons, e.g. B^0, to oscillate into its anti-particle, $\bar{B}^0$. Does this mean that at a certain point the final state of an $\Upsilon(4S)$ decay is a $\bar{B}^0\bar{B}^0$ and not $\bar{B}^0B^0$? And that $B=-2$, different than the one of $\Upsilon(4S)$? No, because the quantum entanglement prevents it. In case one of the mesons oscillates, simultaneously also the other meson oscillates into its anti-particle. This is the meaning of what we said earlier: the properties of the two mesons in an entangled pair are not independent but correlated. Hence the final state remains composed of a B^0 and $\bar{B}^0$ as long as one of the two mesons doesn't decay. At that time the coherence of the final state wave function is destroyed, the wave function of a quantum entangled state collapses.

The question of quantum entanglement played (and actually still does) an important role in the history of quantum mechanics development. Even the great Albert Einstein had difficulties with contra-intuitive fact that one of the objects in an entangled state "knows" what are the properties of the other, or better to say "feels" when a partner object was being measured and its properties revealed to an outside observer. And all this regardless of the distance between the two objects, on a time scale in which a signal - even if travelling with the speed of light - can not travel the distance between the two objects. It was a subject of the so called Einstein-Podolsky-Rosner (EPR) paradox, which the three great minds described in a scientific paper in 1935 [29]. Since then it has been experimentally proven on many occassions (among else also with the measurements at the B Factories [30]) that the quantum entanglement is a fact of Nature.

The quantum entanglement and the neutral (B) meson oscillations lie in the heart of the most prominent CP violations studies at the B Factories. In the following we will take a slightly deeper look into the time evolution of any short-lived neutral meson P^0 undergoing oscillations. A more impatient reader can jump to Eq. (3.46) in which the time evolution is given.

Assume an initial state $|\psi(t=0)\rangle$ which is a superposition of a neutral meson P^0 and its anti-particle $\bar{P}^0$:

$$|\psi(t=0)\rangle = a(0)|P^0\rangle + b(0)|\bar{P}^0\rangle \ . \tag{3.17}$$

Note that the above equation includes cases when the initial state is a pure $|P^0\rangle$ or $|\bar{P}^0\rangle$ (i.e. $a(0)$ or $b(0)$ equals 0), and may obtain the other component at a later time. In time the state - considering possibility of oscillations as well as decays - will evolve and obtain parts corresponding to various possible decay final states, $|\psi(t)\rangle = a(t)|P^0\rangle + b(t)|\bar{P}^0\rangle + \sum_i c_i(t)|f_i\rangle$, where f_i's represent possible final states that $|\psi\rangle$ can decay into. For the moment we are not interested in any specific final state but rather only in $|P^0\rangle$ and $|\bar{P}^0\rangle$ components of $|\psi(t)\rangle$. In this case one can use a simplified description, by writing components of $|\psi(t)\rangle$ in the subspace of $|P^0\rangle$ and $|\bar{P}^0\rangle$ only:

$$|\psi(t)\rangle = \begin{bmatrix} a(t) \\ b(t) \end{bmatrix} \ . \tag{3.18}$$

The time evolution of the state is governed by an effective Hamiltonian

$$\hat{H} = \boldsymbol{M} - \mathrm{i}\frac{\boldsymbol{\Gamma}}{2} \ . \tag{3.19}$$

The effective Hamiltonian $\hat{H}$ is represented by a 2×2 complex matrix, and as such can

be written as a sum of two Hermitian matrices $\boldsymbol{M}$ and $\boldsymbol{\Gamma}$[19]. The diagonal elements of $\hat{H}$ describe the flavour-conserving transitions $|P^0\rangle \to |P^0\rangle$ and $|\bar{P}^0\rangle \to |\bar{P}^0\rangle$, and the off-diagonal elements the flavour-changing oscillations $|P^0\rangle \leftrightarrow |\bar{P}^0\rangle$. Since $\boldsymbol{M}$ and $\boldsymbol{\Gamma}$ are hermitian, $\boldsymbol{M}^\dagger = \boldsymbol{M}$ and $\boldsymbol{\Gamma}^\dagger = \boldsymbol{\Gamma}$, their elements satisfy $M_{12}^*(\Gamma_{12}^*) = M_{21}(\Gamma_{21})$. We can calculate expectation values $\langle P^0|\hat{H}|P^0\rangle$ and $\langle \bar{P}^0|\hat{H}|\bar{P}^0\rangle$:

$$\begin{aligned}\langle P^0|\hat{H}|P^0\rangle &= [1,0]\begin{bmatrix} M_{11}-\mathrm{i}\Gamma_{11}/2 & M_{12}-\mathrm{i}\Gamma_{12}/2 \\ M_{12}^*-\mathrm{i}\Gamma_{12}^*/2 & M_{22}-\mathrm{i}\Gamma_{22}/2\end{bmatrix}\begin{bmatrix}1\\0\end{bmatrix} = M_{11}-\mathrm{i}\Gamma_{11}/2 \\ \langle \bar{P}^0|\hat{H}|\bar{P}^0\rangle &= [0,1]\begin{bmatrix} M_{11}-\mathrm{i}\Gamma_{11}/2 & M_{12}-\mathrm{i}\Gamma_{12}/2 \\ M_{12}^*-\mathrm{i}\Gamma_{12}^*/2 & M_{22}-\mathrm{i}\Gamma_{22}/2\end{bmatrix}\begin{bmatrix}0\\1\end{bmatrix} = M_{22}-\mathrm{i}\Gamma_{22}/2 \ . \end{aligned} \tag{3.20}$$

The conservation of CPT symmetry (see discussion around Eq. (2.16)) requires equality of masses and lifetimes for a particle and its antiparticle, and hence $M_{11} = M_{22}$ and $\Gamma_{11} = \Gamma_{22}$.

The oscillations are described by

$$\langle P^0|\hat{H}|\bar{P}^0\rangle = M_{12} - \mathrm{i}\Gamma_{12}/2 \ . \tag{3.21}$$

The eigenvectors of $\hat{H}$, which are written as linear combinations

$$|P_{1,2}\rangle = p|P^0\rangle \mp q|\bar{P}^0\rangle \ , \tag{3.22}$$

have well defined masses and decay widths, expressed in terms of the elements of $\boldsymbol{M}$ and $\boldsymbol{\Gamma}$. Parameters p and q must satisfy the normalization condition $|p|^2 + |q|^2 = 1$. In the $|P^0\rangle$, $|\bar{P}^0\rangle$ basis the eigenvectors are written as

$$|P_1\rangle = \begin{bmatrix} p \\ -q\end{bmatrix} \ , |P_2\rangle = \begin{bmatrix} p \\ q\end{bmatrix} \ . \tag{3.23}$$

The eigenvector and eigenvalue problem

$$\hat{H}|P_{1,2}\rangle = \lambda_{1,2}|P_{1,2}\rangle \tag{3.24}$$

involves solving the determinant equation

$$\begin{vmatrix} M_{11}-\mathrm{i}\Gamma_{11}/2-\lambda_{1,2} & M_{12}-\mathrm{i}\Gamma_{12}/2 \\ M_{12}^*-\mathrm{i}\Gamma_{12}^*/2 & M_{11}-\mathrm{i}\Gamma_{11}/2-\lambda_{1,2}\end{vmatrix} = 0 \ , \tag{3.25}$$

resulting in the eigenvalues

$$\lambda_{1,2} = M_{11} - \mathrm{i}\Gamma_{11}/2 \pm \sqrt{(M_{12}-\mathrm{i}\Gamma_{12}/2)(M_{12}^*-\mathrm{i}\Gamma_{12}^*/2)} \ . \tag{3.26}$$

With these eigenvalues one can determine q and p from Eq. (3.24) written as

$$\begin{bmatrix} M_{11}-\mathrm{i}\Gamma_{11}/2 & M_{12}-\mathrm{i}\Gamma_{12}/2 \\ M_{12}^*-\mathrm{i}\Gamma_{12}^*/2 & M_{22}-\mathrm{i}\Gamma_{22}/2\end{bmatrix}\begin{bmatrix} p \\ \mp q\end{bmatrix} = \lambda_{1,2}\begin{bmatrix} p \\ \mp q\end{bmatrix} \ . \tag{3.27}$$

[19] It should be understood that this effective Hamiltonian is not Hermitian; a corresponding time evolution in the chosen 2-dimensional subspace is not unitary and consequently the probability density $|\psi(t)|^2$ is not conserved.

After some algebra this brings us to

$$\left(\frac{q}{p}\right)^2 = \frac{M_{12}^* - \mathrm{i}\Gamma_{12}^*/2}{M_{12} - \mathrm{i}\Gamma_{12}/2} \ . \tag{3.28}$$

Together with the normalization condition the above expression fixes values of q and p in terms of $\boldsymbol{M}$ and $\boldsymbol{\Gamma}$ elements; hence the eigenvectors (3.22) and their eigenvalues (3.26) are determined. The latter we write as a sum of a real and an imaginary part,

$$\lambda_{1,2} \equiv m_{1,2} - \mathrm{i}\Gamma_{1,2}/2 \ , \tag{3.29}$$

where $m_{1,2}$ and $\Gamma_{1,2}$ are masses and decay widths of the eigenstates $|P_{1,2}\rangle$, respectively. The time evolution of these states is simple,

$$|P_{1,2}(t)\rangle = e^{-\mathrm{i}\lambda_{1,2}t}|P_{1,2}(t=0)\rangle = e^{-\mathrm{i}(m_{1,2}-\mathrm{i}\Gamma_{1,2}/2)t}|P_{1,2}(t=0)\rangle \ . \tag{3.30}$$

Time dependent probability density is

$$|\langle P_{1,2}(t=0)|P_{1,2}(t)\rangle|^2 = e^{-\Gamma_{1,2}t} \tag{3.31}$$

Hence the eigenstates $|P_{1,2}(t)\rangle$ exhibit a simple exponential time evolution. Note that this is true for the eigenstates of the effective Hamiltonian $\hat{H}$, but not for the physical states $|P^0(t)\rangle$, $|\bar{P}^0(t)\rangle$, which are the states of definite flavour (for example B^0 and $\bar{B}^0$).

Time evolution of states $|P^0(t)\rangle$ and $|\bar{P}^0(t)\rangle$ is, on the other hand, nontrivial because of a possibility of oscillations. It can be derived by reverting the expression Eq.(3.22) which is valid at any time:

$$\begin{aligned} |P^0(t)\rangle &= \frac{1}{2p}\left[|P_2(t)\rangle + |P_1(t)\rangle\right] \\ |\bar{P}^0(t)\rangle &= \frac{1}{2q}\left[|P_2(t)\rangle - |P_1(t)\rangle\right] \ . \end{aligned} \tag{3.32}$$

To make the time evolution explicit we introduce new parameters:

$$\begin{aligned} m &\equiv \frac{m_1+m_2}{2}, \ \ \Gamma \equiv \frac{\Gamma_1+\Gamma_2}{2} \\ \Delta m &\equiv m_1 - m_2, \ \ \Delta\Gamma \equiv \Gamma_1 - \Gamma_2 \ . \end{aligned} \tag{3.33}$$

We assume $m_1 > m_2$ and hence $\Delta m > 0$. This is a choice we are free to make, but once this is assumed the sign of $\Delta\Gamma$ must be experimentally determined. The fact that the choice $\Delta m > 0$ can be made may perhaps not be completely obvious. There is an observable distinction between $|P_1\rangle$ and $|P_2\rangle$: if $p = q$ (a limit in which CP is conserved, as we will show below) it follows from Eq. (3.22) that $\hat{C}\hat{P}|P_{1,2}\rangle = \pm|P_{1,2}\rangle$. $|P_1\rangle$ and $|P_2\rangle$ are thus even and odd eigenstates of $\hat{C}\hat{P}$, respectively. In the case of neutral K mesons (see Sect. 2.2 and discussion there), $|K_1^0\rangle$ decays into 2π and $|K_2^0\rangle$ decays to 3π. Even if CP symmetry is not conserved ($\varepsilon \neq 0$ in Eq. (2.9)), $|K_S^0\rangle$ decays predominantly to two pions and $|K_L^0\rangle$ decays to three pions in majority of decays. It may seem we've arbitrarily decided that the mass of one state (which is CP-even in case of CP conservation) is larger than the mass of the other (which is

	K^0	D^0	B_d^0	B_s^0
$\Delta m/\Gamma$	1	$5 \cdot 10^{-3}$	0.8	27
$\Delta\Gamma/\Gamma$	-2	0.02	0	0.1

Table 3.2: Approximate values of Δm and $\Delta\Gamma$ (in units of the average decay width Γ) for various neutral mesons.

CP-odd). However, one should note that the eigenvalue problem in Eq. (3.27) yields $(q/p)^2$, and hence we have a choice of sign for the physical solution of q/p. Beside $q/p = 1$ also $q/p = -1$ leads to *CP* conservation, causing an interchange $|P_1\rangle \leftrightarrow |P_2\rangle$ with respect to the former case. Hence the choice of the sign for Δm doesn't constrain and is not in a potential conflict with any of the observable. The sign of $\Delta\Gamma$ and the answer whether the heavier state is more *CP*-even or *CP*-odd is left to the experiment.

In the neutral kaon system the long-lived component ($|K_L^0\rangle$, which is predominantly *CP*-odd) has obviously a much smaller width than the short-lived component ($|K_S^0\rangle$, which is predominantly *CP*-even). On the other hand, $|K_L^0\rangle$ is slightly heavier than $|K_S^0\rangle$. With positive Δm this means $\Delta\Gamma < 0$. In the system of B_d^0 mesons the width (or equivalently the decay time) difference between the two mass eigenstates is much smaller. The sign of $\Delta\Gamma$ has so far not been determined yet[20]. We have made an explicit notation for the B_d^0 mesons since for the B_s^0 mesons the situation is somewhat different. There, $\Delta\Gamma$ has been measured rather precisely and is known to be positive. Also in the system of neutral D mesons the more *CP* even component is heavier and has a shorter decay time. Approximate vales of Δm and $\Delta\Gamma$ for various neutral meson systems are given in Tab. 3.2.

Using (3.26) and (3.33) with some algebra[21] we can also relate Δm, $\Delta\Gamma$, M_{12} and Γ_{12}:

$$\begin{aligned} (\Delta m)^2 - \frac{1}{4}(\Delta\Gamma)^2 &= 4|M_{12}|^2 - |\Gamma_{12}|^2 \\ \Delta m \Delta\Gamma &= 4\,\mathrm{Re}(M_{12}\Gamma_{12}^*) \end{aligned} \tag{3.34}$$

It should be noted that Δm and $\Delta\Gamma$ are measurable quantities, as explained later.

Note: Pairs of B mesons produced at B factories are an example of quantum entanglement. Specifically, a neutral B meson from such a pair can freely oscillate only after its partner decayed. Entanglement and oscillations lead to a non-trivial decay time dependence of decay rates.

[20] Current experimental results [2] show that $\Delta\Gamma/\Gamma$ for B_d^0 mesons is less than around 1%.

[21] Relations that are helpful in the derivation are $\mathrm{Re}(z^2) = (\mathrm{Re}(z))^2 - (\mathrm{Im}(z))^2$ and $\mathrm{Im}(z^2) = 2\mathrm{i}\,\mathrm{Re}(z)\,\mathrm{Im}(z)$, for any complex number z.

3.3.2 Evolution in time

Returning to the time evolution of flavour states, it can be economically written as

$$\begin{aligned} |P^0(t)\rangle &= g_+(t)|P^0(t=0)\rangle - \frac{q}{p}g_-(t)|\bar{P}^0(t=0)\rangle \\ |\bar{P}^0(t)\rangle &= g_+(t)|\bar{P}^0(t=0)\rangle - \frac{p}{q}g_-(t)|P^0(t=0)\rangle \ , \end{aligned} \tag{3.35}$$

with $g_\pm(t)$ given by

$$g_\pm(t) = \frac{1}{2}e^{-im_1 t}e^{-\Gamma_1 t/2}\left[1 \pm e^{i\Delta m t}e^{\Delta\Gamma t/2}\right] \ . \tag{3.36}$$

Time dependent states $|P^0(t)\rangle$ and $|\bar{P}^0(t)\rangle$ denote the states which were $|P^0\rangle$ and $|\bar{P}^0\rangle$, respectively, at time $t=0$ (because $g_+(t=0)=1$ and $g_-(t=0)=0$). In order to reduce the notation we can skip the "$(t=0)$" to emphasize the state at an initial time, and simply write $|P^0\rangle$ and $|\bar{P}^0\rangle$.

Consider, for example, a decay $P^0 \to f$, where f is a final state accessible only to P^0 and not to $\bar{P}^0$ (i.e. $\langle f|\bar{P}^0\rangle = 0$). Such final states are called flavour specific, because from detecting $|f\rangle$ or $|\bar{f}\rangle$ one can deduce whether the decaying meson was a $|P^0\rangle$ or a $|\bar{P}^0\rangle$. A time dependent decay width for decay to such a final state is

$$\frac{d\Gamma(P^0\to f)}{dt} = \mathcal{N}_+|\langle f|P^0(t)\rangle|^2 = \mathcal{N}_+|g_+(t)|^2|\langle f|P^0\rangle|^2 \ . \tag{3.37}$$

$\mathcal{N}_+$ denotes the necessary normalization, ensuring $\int_0^\infty \frac{d\Gamma(P^0\to f)}{dt}dt = |\langle f|P^0\rangle|^2$. The instantaneous probability $|\langle f|P^0\rangle|^2$ is related to the decay branching fraction, $Br(P^0\to f) \propto |\langle f|P^0\rangle|^2$. Performing the integration one finds[22]

$$\mathcal{N}_+ = \frac{2}{\Gamma}\frac{[1+(\Delta m/\Gamma)^2][1-(\Delta\Gamma/2\Gamma)^2]}{2+(\Delta m/\Gamma)^2-(\Delta\Gamma/2\Gamma)^2} \tag{3.38}$$

An explicit calculation of the decay width yields

$$\frac{d\Gamma(P^0\to f)}{dt} = \mathcal{N}_+ e^{-\Gamma t}\left[\cosh\left(\frac{\Delta\Gamma t}{2}\right) + \cos(\Delta m t)\right]|\langle f|P^0\rangle|^2 \ . \tag{3.39}$$

The time dependence is exponential (depending on the average decay width Γ), but modulated by the cosine and hyperbolic cosine terms; these appear because of possibility of oscillations, i.e. intermediate transitions of $|P^0\rangle \to |\bar{P}^0\rangle$ and vice versa. They depend on Δm and $\Delta\Gamma$, which are often called the mixing parameters[23]. The decay rate for $\bar{P}^0$ is analogous with reversed sign of the cosine term.

The time dependence of the derived decay width is shown in Fig. 3.26 as a solid line. It is an oscillatory function, with its amplitude decreasing exponentially (the exponential envelope is shown with a green dotted line). One notices time intervals at which decay rate

[22] The following equation is written in a form usually used when further notation reduction is exploited, using $x \equiv \Delta m/\Gamma$ and $y \equiv \Delta\Gamma/2\Gamma$. Then, $\mathcal{N}_+ = (2/\Gamma)(1+x^2)(1-y^2)/(2+x^2-y^2)$.

[23] Mixing indicates the fact that an initial $|P^0\rangle$ state is at a later time a mixture of $|P^0\rangle$ and $|\bar{P}^0\rangle$.

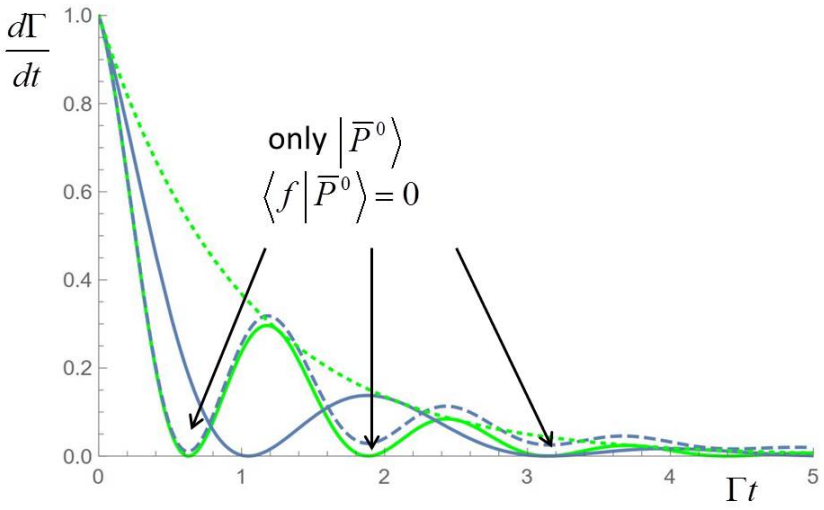

Figure 3.26: The time dependent decay width $d\Gamma/dt$ (Eq. (3.39)). Solid green line shows the time dependence for $\Delta m/\Gamma = 5$ and $\Delta\Gamma/\Gamma = 0.1$. Dotted green line is the exponential envelope. Solid blue line is the same function with $\Delta m/\Gamma = 3$ and $\Delta\Gamma/\Gamma = 0.1$ (note the reduced frequency of oscillations in this case), and blue dashed line for $\Delta m/\Gamma = 5$ and $\Delta\Gamma/\Gamma = 0.9$.

is low. At given instances the rate drops to 0, since the initial $|P^0\rangle$ at that times exists as a pure $|\bar{P}^0\rangle$, which does not decay to $|f\rangle$. The effect of Δm, acting as the frequency of oscillations, can also be seen in the figure by comparing the examples for different values of $\Delta m/\Gamma$. Time dependent probability to find an initially produced $|P^0\rangle$ after time t in a $|P^0\rangle$ or $|\bar{P}^0\rangle$ state is illustrated in Fig. 3.27 for various neutral meson systems. The plot exposes a diversity of oscillation phenomena among various meson species. To make the described oscillations less abstract, Fig. 3.28 (left) shows results of one of the measurements, performed by the LHCb experiment [31]. It demonstrates the rapidity of oscillations of B_s^0 mesons on one hand, and on the other the clearness by which the semiconductor detectors (see Sect. 3.2.3) are able to reconstruct the decay vertices and by that the decay time of such mesons.

Decay-time dependent rate (3.39) can be used to measure Δm and $\Delta\Gamma$. Examples of flavour specific decays of B mesons are $B^0 \to D^-\pi^+$ and $\bar{B}^0 \to D^+\pi^-$, semileptonic decays $B^0 \to \ell^+\nu_\ell X$ and $\bar{B}^0 \to \ell^-\bar{\nu}_\ell Y$, and many others. By reconstructing decays of this type it is possible to group B meson pairs at B Factories into unmixed, $B^0\bar{B}^0$, and mixed, $\bar{B}^0\bar{B}^0$ or B^0B^0, where at least one of the B mesons undergoes an oscillation after the other decayed. An asymmetry between the number of decays belonging to each group, defined as $\mathscr{A}_{\rm flav} = (N_{\rm unmix}(t) - N_{\rm mix}(t))/(N_{\rm unmix}(t) + N_{\rm mix}(t))$ has the following time dependence:

$$\mathscr{A}_{\rm flav} = \frac{\cos(\Delta m t)}{\cosh\left(\frac{\Delta\Gamma t}{2}\right)} \ , \tag{3.40}$$

which for small $\Delta\Gamma$ reduces to

$$\mathscr{A}_{\rm flav} = \cos(\Delta m t) \ . \tag{3.41}$$

Measured asymmetry by BaBar (using semileptonic decays) is shown in Fig. 3.28 (right) [32]. Two clarifications should be made: as we explain below, at B factories instead of time t ac-

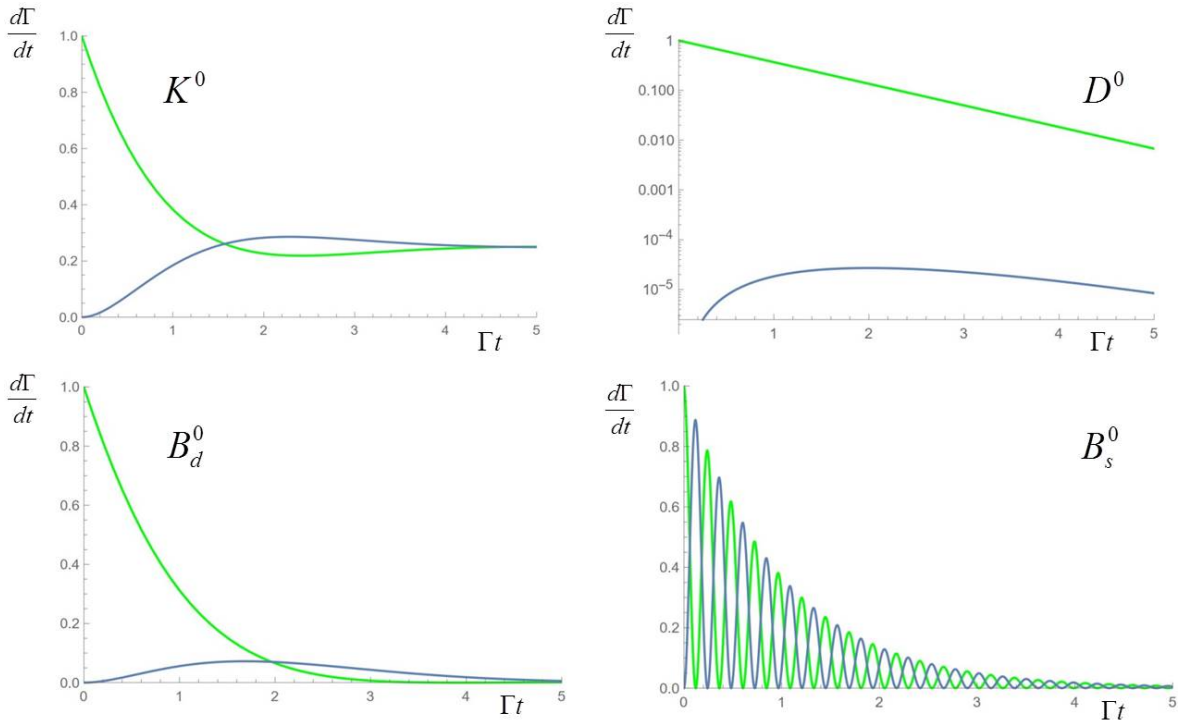

Figure 3.27: Probability for an initially produced oscillating meson $|P^0\rangle$ to be found in its original state (green) or in a state of its anti-particle (blue) after time t (i.e. $|\langle P^0|P^0(t)\rangle|^2$ and $|\langle \bar{P}^0|P^0(t)\rangle|^2$, respectively) for various mesons. Note that the vertical axis for the case of D^0 mesons is logarithmic.

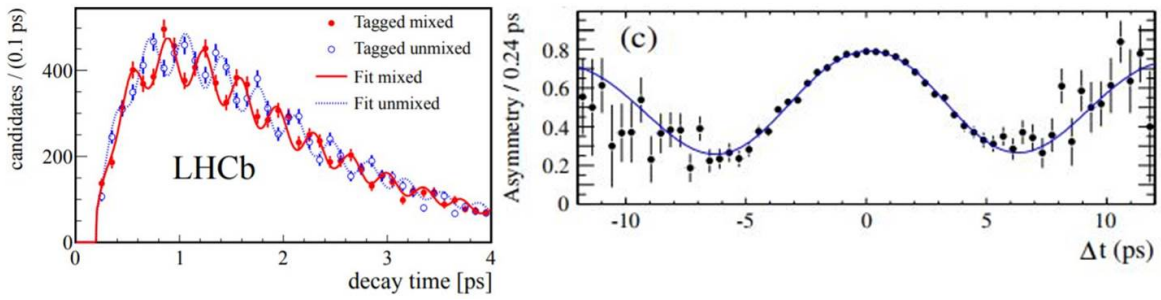

Figure 3.28: Left: Measurement of B_s^0 oscillation frequency (Δm) [31]. Data points represent number of decays of B_s^0 mesons in a given decay time interval. Red data points denote decays of B_s^0 mesons which oscillated and decayed as $\bar{B}_s^0$, and blue points those which decayed as B_s^0. Deviations from theoretical probability shown in Fig. 3.27 (bottom right), especially the truncated exponential envelope at low decay times, is a consequence of detection capability (efficiency of reconstruction). In comparison note that the full scale (4 ps) corresponds to around 2.7 units in Γt. Right: Asymmetry $\mathscr{A}_{\text{flav}}$ (3.40) [32] measured by BaBar using B meson semileptonic decays. The asymmetry exhibits a pure cosine behaviour with the oscillation frequency Δm, indicating that $\Delta\Gamma \approx 0$.

tually the time difference between decays of two B mesons in a pair, Δt, appears. Second, the asymmetry shown was fitted[24] with $\Delta\Gamma = 0$ approximation for $\mathscr{A}_{\text{flav}}$. Because $\Delta\Gamma$ for B^0_d mesons is small, decays into self conjugated final states are more sensitive to it than decays to flavour specific final states, as we also explain below. As indicated in Tab. 3.2, current averages of measurements of Δm and $\Delta\Gamma$ yield values of 0.770 ± 0.004 and -0.002 ± 0.010, respectively [2]. $\Delta\Gamma$ is thus within the measurement accuracy consistent with 0.

The time dependence of the decay width is even richer if one considers a final state into which both, $|P^0\rangle$ and $|\bar{P}^0\rangle$ can decay. Let us denote such a state by f_{CP}. An example of such a state, to be specific, is $J/\psi K^0_s$, into which B^0 and $\bar{B}^0$ can decay (see Fig. 3.29). The subscript CP in f_{CP} signifies that the chosen type of final state is an eigenstate of CP.

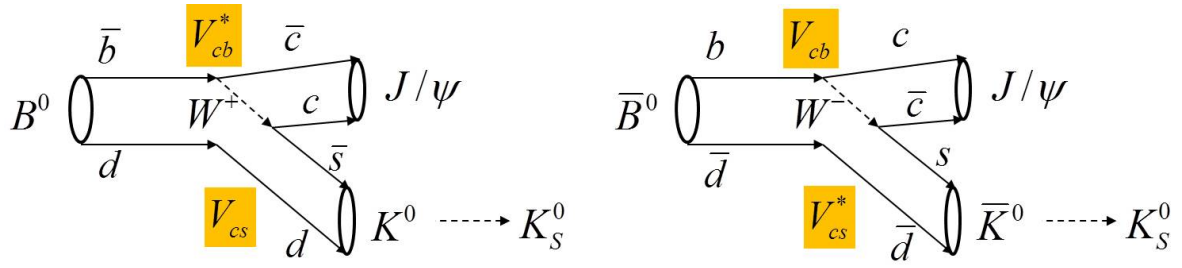

Figure 3.29: Decay of B^0 and $\bar{B}^0$ to $J/\psi K^0_S$. The CKM matrix elements entering the amplitude are shown. The dashed line denotes a time evolution of a neutral kaon.

Considering the specific example of $f_{CP} = J/\psi K^0_S$: charmonium state J/ψ is an eigenstate of CP as discussed in Sect. 2.1. On the other hand, K^0_S is not an eigenstate of CP, due to CP violation described by the parameter ε in Eq. (2.9). However, since $\varepsilon \sim \mathscr{O}(10^{-3})$ we can neglect a small component of $|K^0_2\rangle$ in $|K^0_S\rangle$, as long as we are discussing effects significantly larger than ε. As we will see this is indeed the case when discussing CP symmetry violation in the system of neutral B mesons. For this purpose $|K^0_S\rangle$ can be regarded as a CP eigenstate; so is the $J/\psi K^0_S$ in this approximation. Angular momentum conservation in $B^0(S=0) \to J/\psi(S=1)\, K^0_S(S=0)$ requires orbital angular momentum of $L=1$ in the final state (spins of involved particles are written in parenthesis). Hence $CP(J/\psi K^0_S) = C(J/\psi)C(K^0_S)(-1)^L \approx C(J/\psi)C(K^0_1)(-1)^L = -1\cdot 1\cdot(-1) = 1$.

In obtaining the time dependence of P^0 and $\bar{P}^0$ decays to f_{CP} we proceed as in derivation of (3.39); one starts from (3.35), which for f_{CP} leads to

$$\begin{aligned}\frac{d\Gamma(P^0 \to f_{CP})}{dt} &= \mathscr{N}\left|g_+(t)\langle f_{CP}|P^0\rangle + \frac{q}{p}g_-(t)\langle f_{CP}|\bar{P}^0\rangle\right|^2 \\ \frac{d\Gamma(\bar{P}^0 \to f_{CP})}{dt} &= \mathscr{N}\left|g_+(t)\langle f_{CP}|\bar{P}^0\rangle + \frac{p}{q}g_-(t)\langle f_{CP}|P^0\rangle\right|^2 \ .\end{aligned} \tag{3.42}$$

To reduce the amount of necessary writing it is custom to use a shorthand notation for the instantaneous amplitudes $\langle f_{CP}|P^0\rangle \equiv A_f$ and $\langle f_{CP}|\bar{P}^0\rangle \equiv \bar{A}_f$. In addition, once through the

[24] Actually, in the measurement time dependence of mixed and unmixed pairs is fitted; the function shown in Fig. 3.28 (right) is not a fit but just the ratio of the two functions fitted to individual groups of decays.

derivation, we would realize that parameters q, p, A_f and $\bar{A}_f$ enter in a single form, as

$$\lambda = \frac{q}{p}\frac{\bar{A}_f}{A_f} \ . \tag{3.43}$$

Throughout the derivation we need to keep in mind that all the quantities entering λ are complex. At the end of calculation - a good exercise in complex calculus - we arrive at

$$\begin{aligned}
\frac{d\Gamma(P^0 \to f_{CP})}{dt} &= \frac{1}{2}|A_f|^2 \mathcal{N} e^{-\Gamma t}\Big[(1+|\lambda|^2)\cosh\left(\frac{\Delta\Gamma t}{2}\right) + (1-|\lambda|^2)\cos(\Delta m t) + \\
&\quad +2\,\mathrm{Re}(\lambda)\sinh\left(\frac{\Delta\Gamma t}{2}\right) - 2\,\mathrm{Im}(\lambda)\sin\Delta(mt)\Big] \\
\frac{d\Gamma(\bar{P}^0 \to f_{CP})}{dt} &= \frac{1}{2}|\bar{A}_f|^2 \mathcal{N} e^{-\Gamma t}\Big[(1+|\lambda|^{-2})\cosh\left(\frac{\Delta\Gamma t}{2}\right) + (1-|\lambda|^{-2})\cos(\Delta m t) + \\
&\quad +2\,\mathrm{Re}(\lambda^{-1})\sinh\left(\frac{\Delta\Gamma t}{2}\right) - 2\,\mathrm{Im}(\lambda^{-1})\sin\Delta(mt)\Big] \ .
\end{aligned} \tag{3.44}$$

Because of $\sinh(\Delta\Gamma t/2)$ term (for $\Delta\Gamma t \ll 1$ this term is just $\Delta\Gamma t$), self-conjugated final states f_{CP} are more sensitive to $\Delta\Gamma$ than flavour specific, which include a $\cosh(\Delta\Gamma t/2) \approx 1 - (1/2)(\Delta\Gamma t/2)^2$ term.

We started the section with a discussion about the entangled B meson pairs produced in $\Upsilon(4S)$ decays. We continued with the calculations of time dependent decay widths, for neutral mesons that are not in any way constrained in undergoing the oscillations (i.e. not entangled). It is time to ask the question in what way does the entanglement influence the so far derived decay rates in Eq. (3.44). In description of an entangled B meson pair we should consider decay times of both mesons, t_1 and t_2. Instead, one can describe the decay rate as a function of $\bar{t} \equiv t_1 + t_2$ and $\Delta t \equiv t_1 - t_2$. Double differential rate (in $\bar{t}$ and Δt) can be integrated over $\bar{t}$ for a fixed value of Δt. By that the decay rate as a function of the time difference Δt between the two B meson decays is obtained. Without going through such a detailed calculation we can reveal that the effect is exactly the same as by a simple replacement of t by Δt in Eq. (3.44). Also the reason may be understood: in discussion of entangled B meson pairs we concluded that any oscillation of a single B meson in such a pair is accompanied by a reverse oscillation of the second meson in the pair. In other words, a true unconstrained oscillations of one of the mesons may only occur once the other meson has decayed. Decays of such unconstrained mesons into a final state f_{CP} are described by the time dependent decay rate of (3.44). Clearly, $t = 0$ occurs at the very moment of the first meson decay, and hence t is actually the above mentioned Δt.

Beside $t \to \Delta t$ replacement[25] there is also a simplification one can make in Eq. (3.44) to describe the neutral B mesons. $\Delta\Gamma$ for B^0_d mesons is significantly smaller than Δm. Hence we can take into account only the basic term in Taylor expansion, $\cosh(\Delta\Gamma t/2) \approx 1$ and

[25] There's an additional small but important difference when discussing the time evolution of an entangled pair. Interval of Δt spans from $-\infty$ to ∞, as oposed to the interval of t ($[0,\infty]$). The exponential factor becomes $e^{-\Gamma|\Delta t|}$, since decays with large Δt, either positive or negative, are suppressed.

$\sinh(\Delta\Gamma t/2) \approx 0$. By this we arrive at

$$\begin{aligned}
\frac{d\Gamma(P^0 \to f_{CP})}{d(\Delta t)} &= \frac{1}{2}|A_f|^2 \mathcal{N} e^{-\Gamma|\Delta t|}\Big[(1+|\lambda|^2)+(1-|\lambda|^2)\cos(\Delta m\Delta t) - 2\,\mathrm{Im}(\lambda)\sin(\Delta m\Delta t)\Big] \\
\frac{d\Gamma(\bar{P}^0 \to f_{CP})}{d(\Delta t)} &= \frac{1}{2}|\bar{A}_f|^2 \mathcal{N} e^{-\Gamma|\Delta t|}\Big[(1+|\lambda|^{-2})+(1-|\lambda|^{-2})\cos(\Delta m\Delta t) - \\
&\quad -2\,\mathrm{Im}(\lambda^{-1})\sin(\Delta m\Delta t)\Big] \ . \qquad (3.45)
\end{aligned}$$

We can make the above two equations easier comparable by factorizing from the first a factor of $1+|\lambda|^2$ and from the second a factor of $1+|\lambda|^{-2}$. Realizing $|\bar{A}_f|^2(1+|\lambda|^{-2}) = |A_f|^2|p/q|^2(1+|\lambda|^2)$ one gets

$$\begin{aligned}
\frac{d\Gamma(P^0 \to f_{CP})}{d(\Delta t)} &= \frac{1}{2}|A_f|^2(1+|\lambda|^2)\mathcal{N} e^{-\Gamma|\Delta t|}\Big[1+\frac{1-|\lambda|^2}{1+|\lambda|^2}\cos(\Delta m\Delta t) - 2\frac{\mathrm{Im}(\lambda)}{1+|\lambda|^2}\sin(\Delta m\Delta t)\Big] \\
\frac{d\Gamma(\bar{P}^0 \to f_{CP})}{d(\Delta t)} &= \frac{1}{2}|A_f|^2(1+|\lambda|^2)|\frac{p}{q}|^2\mathcal{N} e^{-\Gamma|\Delta t|}\Big[1-\frac{1-|\lambda|^2}{1+|\lambda|^2}\cos(\Delta m\Delta t) + \\
&\quad +2\frac{\mathrm{Im}(\lambda)}{1+|\lambda|^2}\sin(\Delta m\Delta t)\Big] \ . \qquad (3.46)
\end{aligned}$$

At this point we should remind the reader to the discussion about the CP violation at the end of Sect. 2.3.1. Any difference between $d\Gamma(P^0 \to f)/dt$ and $d\Gamma(\bar{P}^0 \to \bar{f})/dt$ signals violation of CP symmetry. For the case $f = \bar{f} = f_{CP}$, any difference between the time dependent decay widths of Eq. (3.46) is related to CP violation. Depending on the source of a difference one talks about various types of CP violation. The two expressions are equal only if the following is true:

$$|\frac{p}{q}| = 1 \qquad (3.47)$$

If $|p/q|$ deviates from unity this is called CP violation in mixing.

The next necessary condition for $d\Gamma(P^0 \to f_{CP})/dt = d\Gamma(\bar{P}^0 \to f_{CP})/dt$ is $|\lambda| = 1$, which taking into account (3.47) reduces to

$$|\frac{\bar{A}_f}{A_f}| = 1 \qquad (3.48)$$

If this condition is not met we talk about the CP violation in decay.

The last condition is

$$\mathrm{Im}(\lambda) = 0 \qquad (3.49)$$

If λ does have an imaginary component we are dealing with CP violation in the interference between decays without and decays with mixing.

Most of the things discussed in the book so far somehow culminate in the equations (3.46):

- we live in the Universe where matter dominates over anti-matter;
- a necessary condition for the Universe to evolve into such a state is violation of CP symmetry;

- *CP* violation occurs in weak interaction processes, and is described by the CKM matrix proposed by Kobayashi and Maskawa;
- it manifests (among else) through differences in decay time dependent rates of particles' and anti-particles' decays;
- among the contemporary colliders we have machines capable of production of an abundant number of B mesons, heavy particles decaying through weak interaction processes, and detectors with capability to determine their decay points with $\sim 100\ \mu$m spatial precision;
- precise measurements of B meson decays and comparison with Eqs. (3.46) allow us to determine parameters ($|p/q|,\ \lambda$) describing *CP* violation.

To visualize any possible deviation between $d\Gamma(P^0 \to f_{CP})/d(\Delta t)$ and $d\Gamma(\bar{P}^0 \to f_{CP})/d(\Delta t)$ one can form an asymmetry

$$\mathscr{A}_{CP}(\Delta t) \equiv \frac{d\Gamma(\bar{P}^0 \to f_{CP})/d(\Delta t) - d\Gamma(P^0 \to f_{CP})/d(\Delta t)}{d\Gamma(\bar{P}^0 \to f_{CP})/d(\Delta t) + d\Gamma(P^0 \to f_{CP})/d(\Delta t)} \tag{3.50}$$

Inserting expressions (3.46), and taking into account an experimental fact that to a good approximation for the B^0_d meson system $|p/q| = 1$, we get for the asymmetry

$$\mathscr{A}_{CP}(\Delta t) = S \sin \Delta m \Delta t + A \cos \Delta m \Delta t \quad , \tag{3.51}$$

where

$$\begin{aligned} S &= 2\frac{\mathrm{Im}(\lambda)}{1+|\lambda|^2} \\ A &= -\frac{1-|\lambda|^2}{1+|\lambda|^2} \quad . \end{aligned} \tag{3.52}$$

If $\mathrm{Im}(\lambda) = 0$ then $S = 0$, and hence $S \neq 0$ signals *CP* violation in the so called interference between a decay without and a decay with mixing. Since $\sin(\Delta m \Delta t)$ is an odd function of Δt, integration of the asymmetry over all Δt causes this term to diminish. Hence in time-integrated measurements, where one only measures a possible asymmetry in decay-time integrated rates, this type of *CP* violation doesn't appear. On the other hand, $A \neq 0$ appears if $|\lambda| \neq 1$ and hence signals either *CP* violation in decay ($|\bar{A}_f/A_f| \neq 1$) or *CP* violation in mixing ($|p/q| \neq 1$). As $\cos(\Delta m \Delta t)$ is an even function of Δt the term does not disappear when integrating over Δt and this type of *CP* violation may appear also in time integrated measurements. Since *CP* violation in interference between decays with and without mixing ($\mathrm{Im}(\lambda) \neq 0$) can be observed only in decay-time dependent rates, this type of *CP* violation is sometimes referred to as the time-dependent *CP* violation.

It may be important to note that in order for *CP* violation to be observed in some process, either through decay-time dependent or time integrated asymmetry measurements, at least two amplitudes leading from a chosen initial to a single final state are required. This may be understood due to the fact that *CP* symmetry breaking is due to the complex phase of

coupling constants entering the amplitudes. If only a single amplitude contributes, probabilities related to the process are proportional to the modulo of amplitude in which the phase is lost. Hence *CP* violating effects are observable only in interference effects. Let us assume a process $|i\rangle \to |f\rangle$, where two amplitudes contribute to the transition from an initial state $|i\rangle$ to a final state $|f\rangle$. Denoting the two amplitudes by $\mathscr{M}_1$ and $\mathscr{M}_2$, we can write

$$\mathscr{M}_{1,2} = |\mathscr{M}_{1,2}| e^{\mathrm{i}\varphi_{1,2}+\mathrm{i}\delta_{1,2}} \ . \tag{3.53}$$

We denoted the phase of CKM matrix elements entering the amplitudes by $\varphi_{1,2}$. On the other hand there may be another complex phase of each amplitude, $\delta_{1,2}$, not related to CKM matrix. For charge-conjugated process, $|\bar{i}\rangle \to |\bar{f}\rangle$, we have

$$\bar{\mathscr{M}}_{1,2} = |\bar{\mathscr{M}}_{1,2}| e^{-\mathrm{i}\varphi_{1,2}+\mathrm{i}\delta_{1,2}} \ . \tag{3.54}$$

The difference between the two types of phases now becomes evident: while the complex phase of CKM matrix elements changes sign for charge-conjugated process, the sign of the other phase, called a strong phase, is not altered. A probability for the process is

$$P_{i\to f} \propto |\mathscr{M}_1 + \mathscr{M}_2|^2 = |\mathscr{M}_1|^2 + |\mathscr{M}_2|^2 + 2|\mathscr{M}_1|\,|\mathscr{M}_2|\,\cos(\delta_1 - \delta_2 + \varphi_1 - \varphi_2) \ , \tag{3.55}$$

and for the charge conjugated process

$$P_{\bar{i}\to\bar{f}} \propto |\bar{\mathscr{M}}_1 + \bar{\mathscr{M}}_2|^2 = |\bar{\mathscr{M}}_1|^2 + |\bar{\mathscr{M}}_2|^2 + 2|\bar{\mathscr{M}}_1|\,|\bar{\mathscr{M}}_2|\,\cos(\delta_1 - \delta_2 - \varphi_1 + \varphi_2) \ . \tag{3.56}$$

Assuming $\mathscr{M}_{1,2} = \bar{\mathscr{M}}_{1,2}$ any asymmetry of the form

$$\mathscr{A} = \frac{P_{i\to f} - P_{\bar{i}\to\bar{f}}}{P_{i\to f} - P_{\bar{i}\to\bar{f}}} \tag{3.57}$$

is

$$\mathscr{A} = \frac{\cos(\delta_1 - \delta_2 + \varphi_1 - \varphi_2) - \cos(\delta_1 - \delta_2 - \varphi_1 + \varphi_2)}{\cos(\delta_1 - \delta_2 + \varphi_1 - \varphi_2) + \cos(\delta_1 - \delta_2 - \varphi_1 + \varphi_2)} \ . \tag{3.58}$$

Using trigonometric identities this can be written as

$$\mathscr{A} = \tan(\delta_1 - \delta_2)\tan(\varphi_2 - \varphi_1) \ . \tag{3.59}$$

What becomes evident is that not only two amplitudes are necessary for any *CP* violating effect to become observable, the two amplitudes also need to have different weak phases (i.e. phases arising from CKM matrix elements, $\varphi_1 \neq \varphi_2$) as well as different strong phases ($\delta_1 \neq \delta_2$).

Note: Oscillations are observed for all neutral mesons systems which are not self-conjugated, and have different quantitative properties for each of the meson species. The familiar exponential decay law of short-lived particles is more complex in such a case and involves an oscillating component. Differences in decay rates between B^0 and $\bar{B}^0$ are signals of various types of *CP* violation.

Chapter 4

Outcome

4.1 Method...

Colliders - B Factories - provide for an abundant source of entangled B meson pairs. There are few experimental steps to be taken in order to measure the decay rate of $B^0(\bar{B}^0) \to f_{CP}$ as given by Eqs. (3.46). They are sketched in Fig. 4.1 and described in the following. In the figure, the two B mesons produced in an $\Upsilon(4S)$ decay are denoted as the signal B meson (B_{sig}, i.e. the one decaying into f_{CP}; the final state in the example is $J/\psi K^0_S$) and the tagging B meson (B_{tag}, the one used to tag the flavour of B_{sig}).

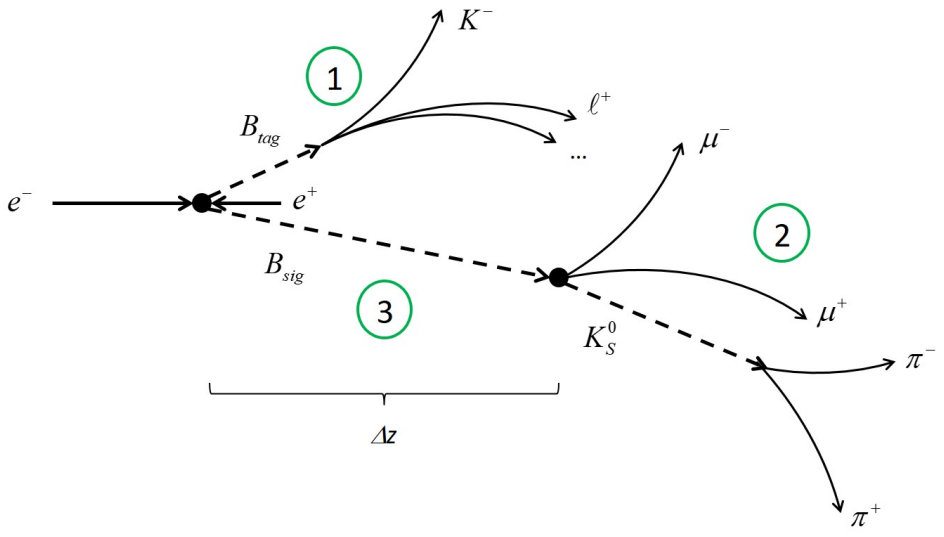

Figure 4.1: Experimental steps in measuring decay-time dependent rates of $B^0 \to f_{CP}$. 1: Flavour tagging; 2: Signal B meson reconstruction; 3: determination of Δt.

4.1.1 ...①,...

First, we need to know whether it was a B^0 or $\bar{B}^0$ that decayed into a CP eigenstate[1]. This is achieved by means of flavour tagging. The method exploits the hierarchy of CKM elements magnitudes (see Sect. 1.2.3), making decays of B mesons leading to a specific final state particles more probable than others. In the CKM matrix column related to b quark processes (the third column in Eq. (1.13)) the element with the largest magnitude is V_{tb}, followed by V_{cb}. Since a b quark cannot decay into a t quark, the most probable quark subprocess in $\bar{B}$ meson decays is $b \to c$. In the second row of CKM matrix, among the elements related to c quark decays, the one with the largest magnitude is V_{cs}. The most probable - Cabibbo allowed - decay chain in b quark processes is thus $b \to c \to s$. Roughly speaking it is around one hundred times more probable than for example $b \to u \to d$ process, and around twenty times more probable than $b \to c \to d$. For a B meson composed of a $\bar{b}$ quark, the most probable subprocess is $\bar{b} \to \bar{c} \to \bar{s}$. Strange quarks (anti-quarks) compose negative (positive) kaons. Hence a B ($\bar{B}$) decay with a large probability ends up in a final state with a K^+ (K^-). This is illustrated in Fig. 4.2. If among a final state products of a B meson decay one finds

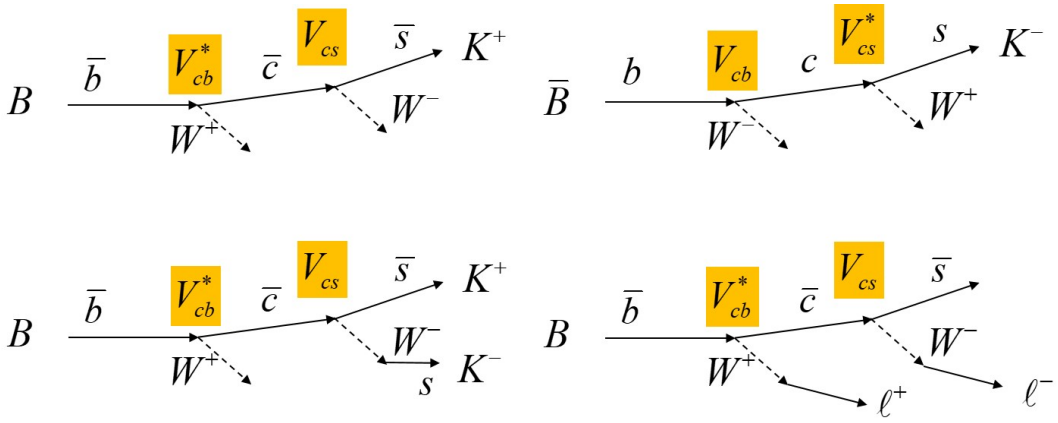

Figure 4.2: Most probable Cabibbo allowed decay chain of a B (top left) and $\bar{B}$ (top right) meson leading to a K^+ or K^- meson in the final state, respectively. Charged kaons can also be produced in a different way, leading to an opposite charge than in the case of $\bar{b} \to \bar{c} \to \bar{s}$ decay chain (bottom left). For a B meson flavour determination - flavour tagging - also charge of a lepton from semileptonic decay can be used (bottom right).

a charged kaon, a probability for the B meson being a particle or an anti-particle can be assigned based on the kaon's charge. The procedure by which the assignment is made is called flavour tagging (it tags the flavour - beauty - of a B meson). Other processes can be used for flavour tagging, for example semileptonic B meson decays. In a $\bar{b} \to \bar{c}$ process a positively charged lepton can be produced (Fig. 4.2 (bottom right)). Identification of such a lepton is also an indication of a B meson decay (and an ℓ^- is an indication of a $\bar{B}$ meson decay).

[1] Note that such a final state is self conjugated, and as such - and as opposed to flavour specific final states - does not allow to determine the flavour of the mother particle.

Clearly, flavour tagging is based on probabilities and as such is not free of erroneous tagging, called mistagging. For example, in the mentioned example of a semileptonic decay, also a $\bar{c}$ quark[2] may produce a lepton, of an opposite charge than the one produced in a $\bar{b}$ decay (Fig. 4.2 (bottom right)). If one mistakenly considers such a lepton as the one from a B meson decay, the assignment of flavour would be wrong. Leptons from semileptonic b and c quark decays can be distinguished by kinematical properties, typically the former have larger momenta than the latter ones. Also charged kaons can be produced in different ways than the one illustrated in Fig. 4.2 (top), e.g. in decay of a charmed meson in $B^0 \to D^-(\to K^-K^+\pi^-)\pi^+$ (Fig. 4.2 (bottom left)). The charge of the kaon in this case is opposite than the charge of the kaon arising from the $\bar{b} \to \bar{c} \to \bar{s}$ chain. Charged kaons produced in various processes are again distinguished based on their kinematic properties. The full flavour tagging method at B Factories relies on numerous information inputs, such as the mentioned examples. To process this information and produce the final flavour tag for a B meson the algorithms use artificial neural network or multidimensional tables. The quality of tagging is quantified by the effective tagging efficiency $Q = \varepsilon_{tag}(1-2w)^2$, where ε_{tag} is the fraction of B mesons decays in which the flavour assignment is possible, and w is the fraction of events in which the assigned flavour is wrong. Typical effective tagging efficiencies at B Factories are around 30%.

We should relate the tagging of the flavour of a B meson to the Δt dependent decay rates. The first of the two equations (3.46) yields Δt dependent decay rate for a meson that at $\Delta t = 0$ is a B^0. Hence the tagging B meson is $B_{tag} = \bar{B}^0$. The second of equations (3.46) is for $\bar{B}^0$ at $\Delta t = 0$, and thus $B_{tag} = B^0$. One can re-write the two equations using a tagging variable q:

$$q = \begin{cases} +1 & B_{tag} = B^0 \\ -1 & B_{tag} = \bar{B}^0 \end{cases} \tag{4.1}$$

With this, Eqs. (3.46) can be written as a single equation,

$$\frac{d\Gamma(B \to f_{CP})}{d(\Delta t)} \propto e^{-\Gamma|\Delta t|}\left[1 + q\left(-\frac{1-|\lambda|^2}{1+|\lambda|^2}\cos(\Delta m \Delta t) + 2\frac{\mathrm{Im}(\lambda)}{1+|\lambda|^2}\sin(\Delta m \Delta t)\right)\right] \quad , \tag{4.2}$$

or using (3.52) even shorter:

$$\mathscr{P}(\Delta t,\, q;\, A,\, S) = \frac{d\Gamma(B \to f_{CP})}{d(\Delta t)} \propto e^{-\Gamma|\Delta t|}\left[1 + q\left(A\cos(\Delta m \Delta t) + S\sin(\Delta m \Delta t)\right)\right] \quad , \tag{4.3}$$

Note: The first step required to measure the time dependent decay rate of entangled pairs of B^0 mesons is flavour tagging, determination of flavour of one of the B mesons at the time of its decay. The tagging method exploits specific B meson final states to determine a probability that the decaying meson was a B^0 or a $\bar{B}^0$.

4.1.2 ...②,...

Another step in the measurement is a reconstruction of the signal B meson. In Fig. 4.1 an example of $B^0 \to J/\psi K^0_S$ decay is shown, where the charmonium state J/ψ decays into a

[2] A $\bar{c}$ quark composes a charm ($\bar{D}$) anti- meson.

pair of muons. Reconstruction of any short-lived decaying particle typically means reconstruction of its invariant mass from the measured decay products, as given in Eq. (3.8). For charged particles their energy is determined as $E = \sqrt{m^2 + |\vec{p}|^2}$ using the mass of a particle as assigned in the process of particle identification (see Sect. 3.2.2). Momenta of decay products are measured with a finite accuracy and hence the resulting invariant mass also suffers from a finite resolution. At B Factories the resolution of B mass reconstruction is improved by exploiting the fact that the energy of produced B mesons in the CMS is known to be exactly the beam energy of colliding electrons and positrons, $E_B = E_{\text{beam}}$. The mass of a B meson is hence

$$M_{bc} = \sqrt{E_{\text{beam}}^2 - \sum_i |\vec{p}_i^*|^2} \ , \tag{4.4}$$

where the sum runs over all decay products of a meson, and $*$ denotes momenta in the CMS. Using E_{beam} instead of $\sum_i \sqrt{m_i^2 + |\vec{p}_i|^2}$ reduces the dependence of M_{bc} on $\vec{p}_i$ and by this improves the resolution. M_{bc} is called a beam-constrained mass to emphasize the usage of beam energy in its determination[3]. Another specific property of beam constrained mass is its independence (see Eq. (4.4)) of the masses assigned to the B meson decay products[4].

Another quantity enabling identification of B meson decay products is an energy difference,

$$\Delta E = E_B^* - E_{\text{beam}} \ . \tag{4.5}$$

Here, E_B^* is the reconstructed B meson energy in CMS, $E_B^* = \sum_i \sqrt{m_i^2 + |\vec{p}_i^*|^2}$. Contrary to M_{bc}, ΔE does strongly depend on masses of final state particles, and within the resolution equals zero for correctly reconstructed B mesons.

Examples of reconstructed M_{bc} and ΔE are shown in Fig. 4.3, where several properties of the two observables are evident. The example shown is for decays $B^+ \to \bar{D}^0 K^+$, where D meson decays to $K_S^0 \pi^+ \pi^-$[33]. When speaking about a specific decay mode from now on we implicitly include a charge conjugated decay, unless explicitly stated otherwise. For the example in question this means that the distributions are shown for the mentioned decay as well as for the $B^- \to D^0 K^-$. In the distribution of M_{bc} one observes a prominent peak at the nominal mass of $B^\pm$ mesons, 5.28 GeV, corresponding to correctly reconstructed decays. In addition, there is also a small peak at the same mass (dark green) arising from $B^+ \to \bar{D}^0 \pi^+$ decays, where a pion was wrongly identified as a kaon (and hence assigned a kaon mass). However, since M_{bc} is independent of final state particles masses, such decays contribute to the signal peak. Furthermore there is a smooth contribution of various background processes, mainly arising from $e^+e^- \to c\bar{c}$ continuum process (black; see Sect. 3.1.2). In the process of fragmentation D mesons are formed, which together with a random kaon from such an event yield M_{bc} as shown in the plot. In the distribution of the energy difference, the peak centred at $\Delta E = 0$ corresponds to the correctly reconstructed signal decays. Another peak at $\Delta E \approx 50$ MeV (dark green) arises from $B^+ \to \bar{D}^0 \pi^+$ decays, which in this case are shifted

[3] At BaBar a similar quantity, called beam-energy substituted mass was used, $M_{ES} = \sqrt{(E_{\text{CMS}}^2/2 + \vec{p}_0 \sum_i \vec{p}_i)^2 / E_0^2 - (\sum_i \vec{p}_i)^2}$, where $(E_0, \vec{p}_0)$ is a four-momentum of the CMS in the laboratory frame.

[4] There is a small residual dependence because of the need to boost momenta of the B meson decay products into the CMS. M_{ES} is free of this dependence as well.

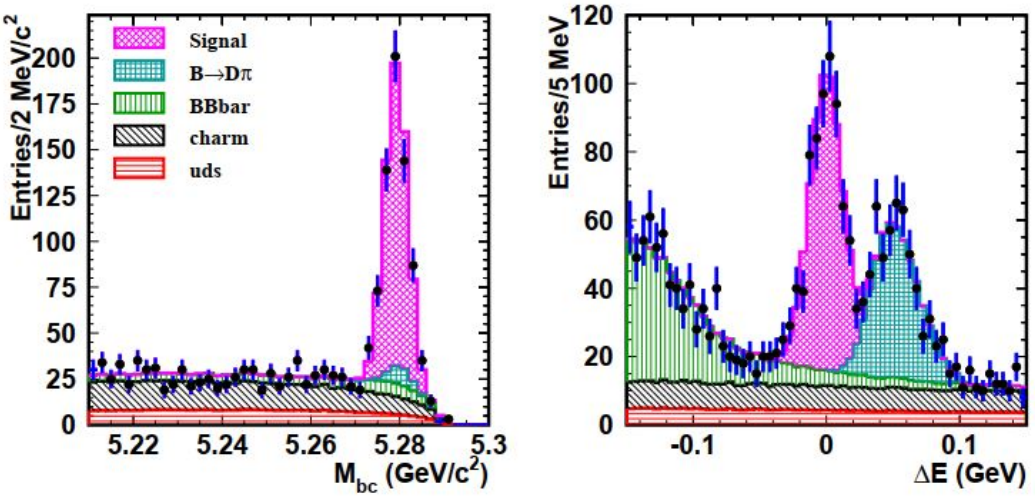

Figure 4.3: M_{bc} (left) and ΔE for $B^+ \to \bar{D}^0(\to K^0_S\pi^+\pi^-)K^+$ decays [33]. Data are represented as points with error bars, and fitted contributions of individual processes as coloured histograms. Apart from correctly reconstructed decays peaking at $M_{bc} \approx 5.28$ GeV and $\Delta E \approx 0$ several other features can be observed, as described in the text.

with respect to the true signal due to ΔE dependence on the mass of final state particles[5]. Various other B meson decays (light green) with more final state particles populate negative ΔE region. In these decays one or more final state particles are not taken into account in ΔE calculation, hence the calculated E^*_B is lower than the actual one, and $\Delta E < 0$.

By fitting the measured distributions one can obtain the amount of signal and background decays in a given interval of M_{bc} and ΔE. Of course in order to fit the data a model describing the signal as well as various backgrounds must be assumed. Signals are usually well described using one or more Gaussian functions, while for the backgrounds different empirical functions (polynomial, exponential, etc.) are used[6].

Note: To study B decays, mesons must be reconstructed from their decay products. For this purpose at B Factories beam-constrained mass and energy difference are used, variables enabling isolation of correctly reconstructed mesons from backgrounds.

4.1.3 and ③

The last stone in the mosaic of time-dependent decay rate measurements is the determination of Δt, the time difference between decays of the two B mesons. In description of the procedure it is important first to remember that a B meson produced in an $\Upsilon(4S)$ decay is almost at

[5] It should be noted that the M_{bc} distribution in the figure is shown only for decays for which $|\Delta E| < 30$ MeV, and ΔE distribution is shown for $M_{bc} > 5.272$ GeV. This is the reason for different amount of $B^+ \to \bar{D}^0\pi^+$ decays in the two distributions.

[6] For the case of M_{bc} a somewhat special function is used to describe the backgrounds, mainly due to the end point arising from the fact $M_{bc} \leq E_{\text{beam}}$ (see Eq. (4.4). Function is called the Argus function [34], because it was first used by the Argus experiment at Desy.

rest in the CMS. More precisely, each of the B mesons carries a momentum $p_B^* \approx 300$ MeV. Due to asymmetric beam energies (see Sect. 3.1.2) each of the B mesons is boosted in the direction of the electron beam. Comparison illustrating B meson's momentum in the CMS and the laboratory frame is shown in Fig. 4.4. In general momentum of a B meson in the CMS

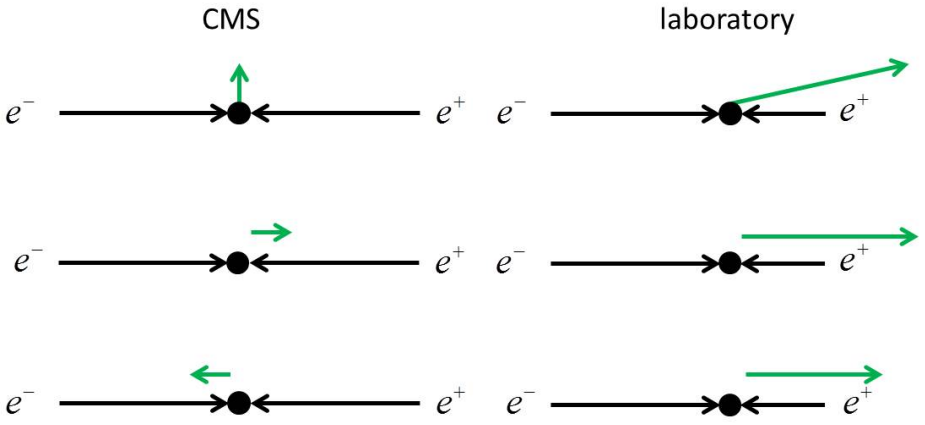

Figure 4.4: Illustration of B meson's momentum in the CMS (left) and laboratory frame (right), for three extreme cases of meson's polar angle in the CMS ($\theta^* = 90°$ (top), $\theta^* = 0°$ (middle) and $\theta^* = 180°$ (bottom)). Black arrows denote momenta of colliding electrons and positrons, and green arrows momentum of one of the produced B mesons.

is $\vec{p}_B^* = p_B^*(\cos\theta^*, \sin\theta^*)$, if θ^* denotes the polar angle of the meson in this frame. The first component is the one along the beam direction (z) and the second the transverse one. Using a Lorentz transformation from the CMS to laboratory frame (with Lorentz factors $\gamma\beta = 0.425$ as discussed in Sect. 3.2.1) one finds

$$\vec{p}_B = (\gamma\beta\sqrt{m_B^2 + p_B^{*2}} + \gamma p_B^* \cos\theta^*, p_B^* \sin\theta^*) \ . \tag{4.6}$$

The largest transverse momentum of a B meson in the laboratory frame is thus $p_{Bt} \approx 300$ MeV, compared to the smallest z component of $p_{Bz} \approx 1.9$ GeV. In other words, B mesons in the laboratory frame fly predominantly along the z axis, i.e. in the direction of the electron beam.

Displacement between the decay and the production point of a particle with a proper decay time t is

$$\vec{r}_{\text{dec}} - \vec{r}_{\text{prod}} = \vec{v}t = \frac{\vec{p}}{m}t \ , \tag{4.7}$$

where in the last step we wrote dimensionless velocity $\vec{\beta} = \vec{p}/m$ and comply with the previous understanding on the usage of natural units ($c = 1$). Displacement along the z-axis for a B meson is thus

$$z_{\text{dec}} - z_{\text{prod}} = \frac{\vec{p}_{Bz}}{m_B}t = \left[\gamma\beta\sqrt{1 + \frac{p_B^{*2}}{m_B^2}} + \gamma\frac{p_B^*}{m_B}\cos\theta^*\right]t \ . \tag{4.8}$$

Factor $p_B^*/m_B \approx 0.06$; neglecting small terms we obtain a simplified expression

$$z_{\text{dec}} - z_{\text{prod}} = \gamma\beta t \quad . \tag{4.9}$$

A distance between the two decay vertices of a pair of B mesons is thus

$$\Delta z = z_{\text{dec}}^{tag} - z_{\text{dec}}^{sig} = \gamma\beta\Delta t \quad . \tag{4.10}$$

It should be noted that Eqs. (3.46) are valid for any sign of Δt, i.e. for $\Delta t > 0$ and $\Delta t < 0$. The order of B_{tag} and B_{sig} decays doesn't play a role[7].

Decay vertices of B_{sig} and B_{tag} are determined by finding a most probable common origin point of tracks assigned to arise from either of the mesons. Depending on the specific final state also some neutral particles (e.g. K_S^0), reconstructed from their decay products, can be used in the vertex determination. Typical dimensions related to Δz are denoted in Fig. 4.5. Individual steps in decay vertex reconstruction are illustrated in the figure. Through detected spatial points in the detector (top) individual tracks are fitted (middle top; see Sects. 3.2.1 and 3.2.3). Invariant masses of subsets of reconstructed particles may reveal some intermediate short lived states, either charged of neutral (middle bottom; examples shown are $K_S^0 \to \pi^+\pi^-$ and $J/\psi \to \mu^+\mu^-$). By fitting the tracks and reconstructed neutral particles arising from an individual B meson to a common point one finds its decay vertex (bottom). Fitting tracks from distinct vertices into a single point results in a degraded resolution (example of B_{tag} vertex).

Accuracy by which Δz is determined depends on the accuracy of z_{dec}^{tag} and z_{dec}^{sig} reconstruction. Accuracy of individual decay vertex reconstruction is proportional to the precision of spatial points of individual tracks. The more precise the detector is, the more accurate is Δz reconstruction. Resolution is also improved with an increased number of reconstructed hits per track, and is better if more tracks are arising from and are fitted

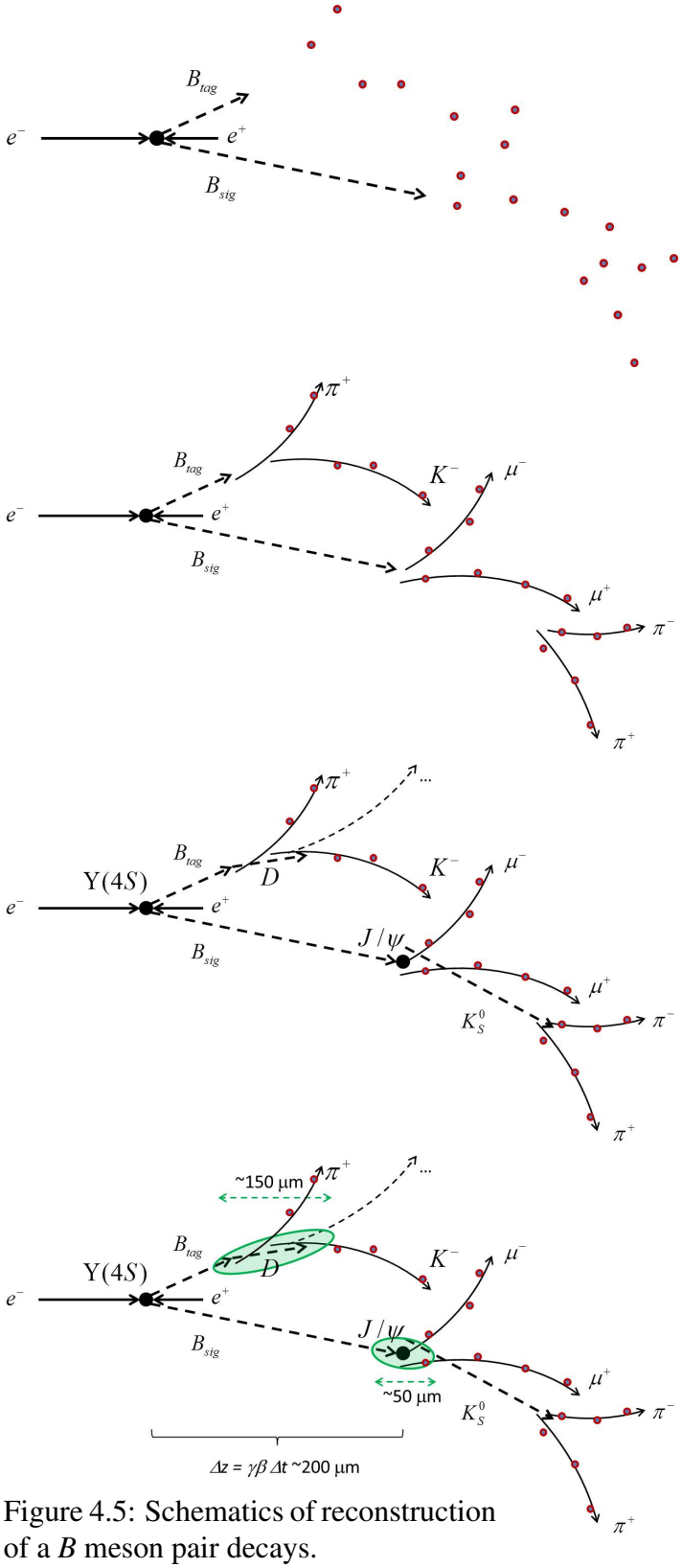

Figure 4.5: Schematics of reconstruction of a B meson pair decays.

[7] Because once the flavour and decay time of one of the B mesons is determined, the known time dependence of meson oscillations extrapolates back or forth in time to yield a probability that the other B was either a meson or an anti-meson at a given t.

to a common vertex. Last but not least, the resolution in Δz determination is improved by having some spatial points as close as possible to the decay vertices.

The signal B meson decay vertex is usually determined with a better accuracy, since all final state particles must be reconstructed correctly (in order to give a correct M_{bc}). A typical resolution by which the z coordinate of the B_{sig} decay vertex is determined is 50 μm. On the tagging side, the B meson most probably decays into a charm D meson with a finite decay length (D mesons have, depending on the quark accompanying a c quark in the meson, decay lengths $c\tau$ from 120 μm to 310 μm). Since no attempt is made to reconstruct decay of a B_{tag}, tracks are fitted into a common vertex. In addition, there is a non-negligible probability for some final state particles of B_{tag} to escape undetected and hence fewer tracks may be used to reconstruct the decay vertex. A typical resolution on $z_{\rm dec}^{tag}$ is 150 μm. Accuracy of Δz and by that Δt determination depends on a specific kinematic properties of final state particles and varies from process to process. The uncertainty of Δt is estimated for each B_{sig} decay from known uncertainties on 3-momenta of tracks used in the vertex fit. A distribution of these accuracies in $B^0 \to J/\psi K_S^0$ and some related decay modes is shown in Fig. 4.6 (top left). The most probable $\sigma_{\Delta t}$ is around 0.5 ps. This finite accuracy in Δt de-

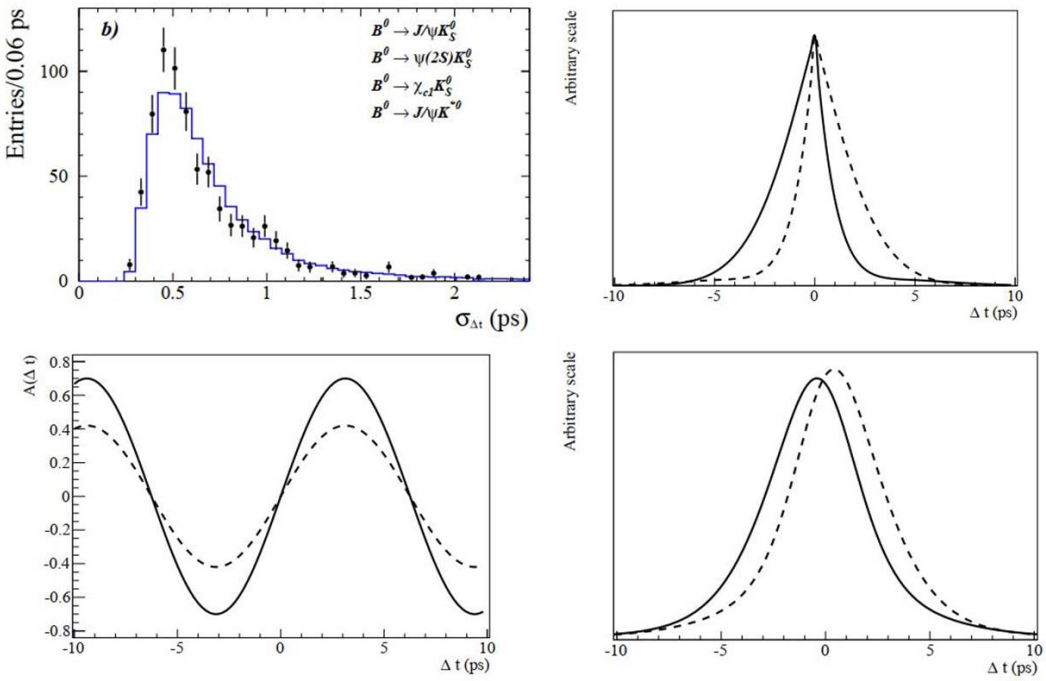

Figure 4.6: Top left: Distribution of uncertainties on Δt, estimated for each $B^0 \to J/\psi K_S^0$ decay and some similar less probable decay modes [35]. Bottom left: Asymmetry (3.51) for $S = 0.7$ and $A = 0$ (solid line) and effect of mistagging (dashed line; $w = 0.2$) [5]. Top right: Δt dependent decay rate (Eqs. (3.46)) for $S = 0.7$ and $A = 0$ [5]. Solid line represents the distribution for $B_{tag} = \bar{B}^0$ and dashed line for $B_{tag} = B^0$. Bottom right: Same as top right, including effects of finite resolution in determination of Δt and mistagging [5].

termination must be taken into account when interpreting the measured distributions. Since

$\sigma_{\Delta t}$ is clearly non-negligible compared to the B meson lifetime (~ 1.5 ps) or even the oscillation period ($2\pi/\Delta m \sim 12$ ps) one expects the effect of finite resolution to be important. It is illustrated in Fig. 4.6 (top right, bottom right). The theoretically expected curves from Eqs. (3.46) are widened due to a finite resolution on Δt. This widening is easy to understand; visualize, for example, each of decays occurring at given Δt_0 being randomly shifted around this value (effect of finite precision measurement; Fig. 4.7). The result is a widened distribution of measured Δt's.

The effect of mistagging is most obviously observable in the asymmetry (3.50). Decays with mistagged B^0 ($\bar{B}^0$) meson contribute to the asymmetry in a dual way: they lower the number of $P^0 \to f_{CP}$ ($\bar{P}^0 \to f_{CP}$) decays at a given Δt, and increase the number of $\bar{P}^0 \to f_{CP}$ ($P^0 \to f_{CP}$) decays at the same Δt. Taking into account the functional shape of $\mathscr{A}(\Delta t)$ (3.51) it is easy to understand that any non-zero value of mistag probability w causes a reduction of the amplitude of the asymmetry. This is illustrated in Fig. 4.6 (bottom left). Experimental effects need to be taken into account when interpreting measurement results. Here, "interpretation of results" refers mainly to fits of measured data distributions with the aim of determination of some underlying parameters. For example, from measured Δt distributions one can determine parameters A and S (or $|\lambda|$ and $\mathrm{Im}(\lambda)$), by fitting the expected distributions to data. However, such a fit is only possible by properly taking into account experimental effects which significantly change the expected theoretical distributions. This is achieved by means of a resolution function with which the expected theoretical distributions are convolved. In its simplest form a resolution function may be a single Gaussian, $G(x'|x,\sigma) = (1/\sqrt{2\pi}\sigma)e^{-(x'-x)^2/2\sigma^2}$. It represents a probability density function for a measurement to yield a value of x' when determining a quantity x, and σ is the measurement resolution. If the (theoretically) expected distribution of x is $p(x)$, the measured distribution is a convolution $q(x') = \int_{-\infty}^{\infty} p(x)G(x'|x,\sigma)dx$.

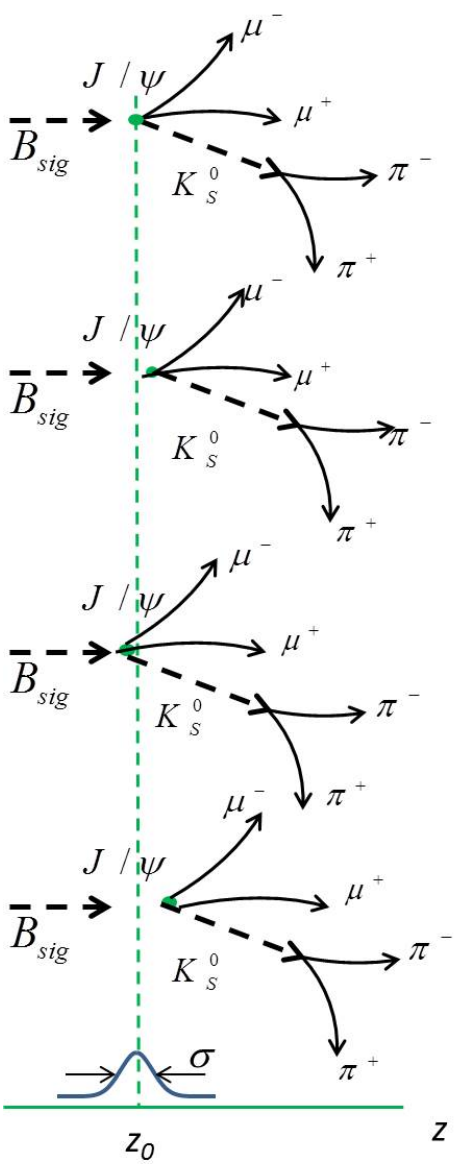

Figure 4.7: Effect of widening z_{dec} distribution due to a finite detector resolution. Plot at the top represents a decay with ideally reconstructed tracks and resulting vertex. Finite resolution in track reconstruction, as illustrated in plots below, reflects in scattered reconstructed z_{dec}.

In $\Delta t = (z_{\mathrm{dec}}^{tag} - z_{\mathrm{dec}}^{sig})/\gamma\beta$ measurements at B Factories resolution functions are more complex. They take into account resolutions in determination

of $z_{\rm dec}^{tag}$ and $z_{\rm dec}^{sig}$ as a consequence of finite tracking precision, a resolution on $z_{\rm dec}^{tag}$ due to a finite D meson flight distance, the approximation of Δz done in Eq. (4.9)[8], as well as the uncertainty on the $\gamma\beta$ factor determined from the measured energies of electron and positron beams. Resolution functions depend on a specific decay mode under study (mainly on the number of tracks used for the B_{sig} vertex reconstruction), and their width (σ) is calculated from the uncertainties on momenta of final state particles for each individual decay.

By performing the described steps in the measurement of Δt dependent decay rate and taking into account experimental effects, one hence expects measured distributions of oppositely tagged B^0 decays to a charge conjugated final state f_{CP} of the form shown in Fig. 4.6 (bottom right). If $S \neq 0$ and $A = 0$, that is, i.e. if CP symmetry violation occurs in the interference between a decay without and a decay with mixing, and CP violation in decays and in mixing is negligible (see Eqs. (3.47)-(3.49)). Examples of other scenarios would reflect in distributions shown in Fig. 4.8. Note a difference in heights and area of expected distributions in cases where $A \neq 0$. As explained at the end of Sect. 3.3.2, a consequence of $A \neq 0$ is a different total (time integrated) number of decays of B^0 and $\bar{B}^0$ decays.

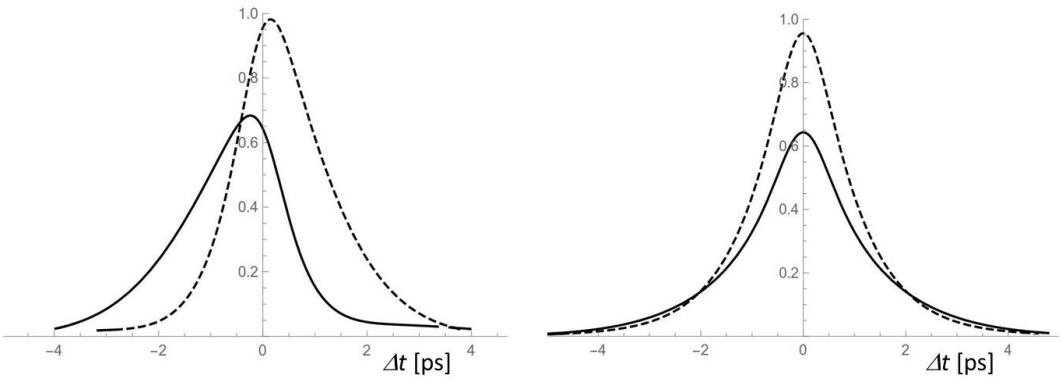

Figure 4.8: Approximate expected Δt dependent B meson decay rates into f_{CP}, for $(S,A) = (0.7, 0.2)$ (left) and $(0, 0.2)$ (right). Solid line represents the distribution, including resolution effects, for $B_{tag} = \bar{B}^0$ and dashed line for $B_{tag} = B^0$.

Note: In order to measure decay-time dependent decay rates of B^0 mesons decaying to a self-conjugated state f_{CP}, also decay distance between the decay vertices of two neutral B mesons must be measured. Finite resolution affects the distributions and must be properly taken into account.

[8] At BaBar for many measurements a more involved expression for Δt was used, $\Delta t = (\Delta z - \gamma\alpha\tau_B \cos\theta)/(\gamma\beta \pm \gamma\alpha\cos\theta)$, with $\alpha = p_B^*/m_B$. This results in an improved resolution by around 5 % [5].

4.2 Result

4.2.1 First numbers

Violation of *CP* symmetry was experimentally discovered in 1964 (see Sect. 2.2) in the system of neutral kaons. Since then *CP* violation was a subject of theoretical description (most notably by Kobayashi and Maskawa, see Sect. 2.3.2); there was no experimental evidence, however, that it is related to weak interaction and not just a (strange, indeed) property of kaons. After establishing the Kobayashi-Maskawa mechanism, *B* Factories were envisioned to test the hypothesis of *CP* symmetry breaking by weak interaction. A most important test, one should say, considering the already known potential relation between the phenomena and baryon asymmetry of the Universe (Sakharov conditions, see Sect. 2.3.1).

In 2000, at an international conference on high energy physics in Osaka, Belle and BaBar collaborations presented first results of their measurements, which started a year before that. The most eagerly awaited results were those on time dependence of neutral B meson decays to $J/\psi K^0_S$. They are presented in Fig. 4.9. BaBar presented their result in a form of distributions (3.46), which taking into account experimental effects were expected to look like in Fig. 4.6 (or 4.8, for example). Belle presented the results in a form of a sum $\mathscr{P}(\Delta t,\ q=+1)+\mathscr{P}(-\Delta t,\ q=-1)$ (see Eq. (4.3)). Both experiments fitted expected distributions, depending on S and neglecting A, to their data. With the data sample available at that time no significant difference between decays with $B_{tag}=B^0$ and $B_{tag}=\bar{B}^0$ has been observed, and S was consistent with zero within the measurement uncertainty.

To put it in a nut shell, by 2000 still no experimental evidence of *CP* violation was obtained, apart from the 1964 result. The situation changed in 2001. At two large international conferences of that year both, Belle and BaBar presented convincing experimental evidence for the phenomena believed to have an important role in the Universe evolution. Results of $B^0\to J/\psi K^0_S$ measurements using a larger sample of recorded data revealed an asymmetry between B^0 and $\bar{B}^0$ tagged decays. Results are presented in Fig. 4.10.

Even by eye one can spot an asymmetry between the two classes of decays. Numerically, results arising from fitting the expected distributions to data, again with an assumption $A=0$, were $S=0.59\pm0.14\pm0.05$ (BaBar, [38]) and $S=0.99\pm0.14\pm0.06$ (Belle, [39]). In results, the first quoted uncertainty is statistical ($\sigma_{\text{stat.}}$) and the second systematic ($\sigma_{\text{syst.}}$). Total uncertainties, calculated as $\sigma=\sqrt{\sigma^2_{\text{stat.}}+\sigma^2_{\text{syst.}}}$, are around 0.15[9]. Significances of results, calculated in a simplified way as $\kappa=S/\sigma$, are around 4 and 6.5, respectively. Probability that a repeated measurement, with the same accuracy as the performed one, would yield a value of S with a significance κ, assuming that the true value of S is null, can be obtained by integrating a Gaussian function: $\varepsilon=[1/(\sqrt{2\pi}\sigma)]\int_S^\infty e^{-x^2/(2\sigma^2)}dx\ =(1/2)[1-\text{Erf}(\kappa/\sqrt{2})]$. $\text{Erf}(x)$ is the error function; inserting the values of significances we arrive at probabilities of around $3\cdot10^{-5}$ and below 10^{-10}. These probabilities are low enough to justify the statements of collaboration representatives in the proceedings of 2001 conferences: "It is now clear that *CP* violation occurs in the *B*-meson system as well as in the *K*-meson system." [39], and "37 years after the discovery of *CP* violation in the Kaon system, BaBar has established *CP*

[9] The reason for adding two uncertainties in quadrature is a convolution of two Gaussian functions, with widths σ_1 and σ_2, which is also a Gaussian function with the width $\sigma=\sqrt{\sigma_1^2+\sigma_2^2}$.

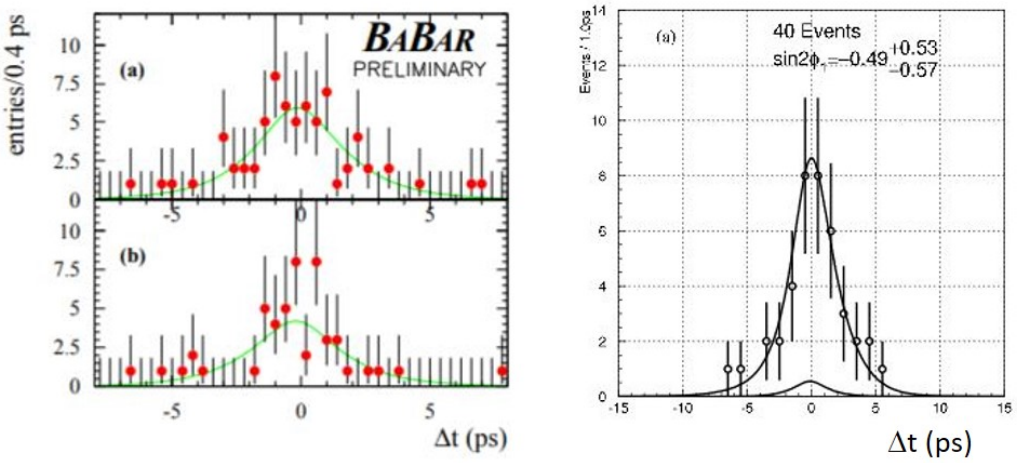

Figure 4.9: Left: measurement of Δt dependent B decay rate to self-conjugated final state $J/\psi K_S^0$ by BaBar experiment, at the Osaka conference in 2000 [36]. The upper plot is for $B_{tag} = \bar{B}^0$ and the lower for $B_{tag} = B^0$. Right: measurement by Belle [37] at the same conference. Results are presented in a slightly different form, as the sum of $\mathscr{P}(\Delta t,\ q = +1) + \mathscr{P}(-\Delta t,\ q = -1)$ (see Eq. (4.3)).

violation in the B system...” [38].

Note: In 2001 Belle and BaBar experiments presented evidence for CP violation in the system of B mesons, thus experimentally proving that the phenomena is more general and not limited to a system of neutral kaons, where it has been discovered 37 years before that.

4.2.2 The Meaning

Described results were actually only among the first in a row of findings arising from the two experiments in the following decade. A careful reader may have noticed no mentioning of Kobayashi-Maskawa mechanism and weak interaction in the above quotes. Measurements have proven that $S \neq 0$ and hence (see Eq. (3.49)) that CP violation occurs in the B meson system. To prove correct the description through the CKM matrix required further measurements.

First, we need to look for a relation between the measured parameter S and the elements of the CKM matrix. The observable S is related to λ through (3.52). λ, in turn, is $(q/p)(\bar{A}_{J/\psi K_S^0}/A_{J/\psi K_S^0})$, see (3.43). By inspection of diagrams in Fig. 3.29 one can convince herself that the amplitudes differ only in the elements of CKM matrix, $\bar{A}_{J/\psi K_S^0}/A_{J/\psi K_S^0} = V_{cb}V_{cs}^*/V_{cb}^*V_{cs}$.

Equation (3.21) suggest that M_{12} and Γ_{12} can be calculated from the amplitude of a $\bar{P}^0 \to P^0$ transition. In principle this is true. Such an amplitude, however, does not include only processes depicted in the so called box diagram of Fig. 1.11. A transition can occur

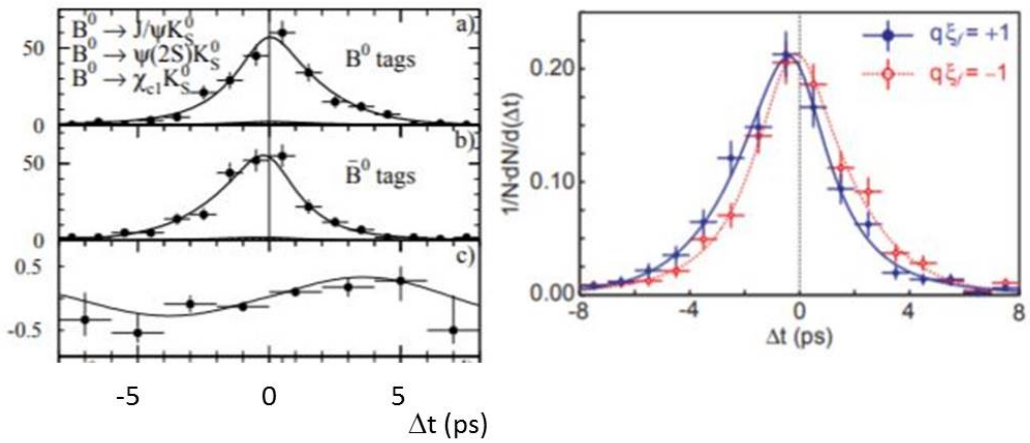

Figure 4.10: Results of Δt distribution measurements for $B \to f_{CP}$ decays in 2001. Left: Results from BaBar [38], the upper panel showing decays with $B_{tag} = B^0$ and middel panel decays with $B_{tag} = \bar{B}^0$. The bottom panel represents the asymmetry $-\mathscr{A}_{\mathscr{C}\mathscr{P}}$, as defined in (3.51). Right: analogous result by Belle [39]. Blue points are for $B_{tag} = \bar{B}^0$ and red points for $B_{tag} = B^0$.

also through all final states $|n\rangle$ accessible to both, P^0 and $\bar{P}^0$, by $\sum_n \langle P^0|\hat{H}|n\rangle\langle n|\hat{H}|\bar{P}^0\rangle$. An example is schematically shown in Fig. 4.11. While the amplitude of a former process can be calculated rather precisely, the amplitudes for a transition through all common final states are difficult to determine because of non-perturbativness of quantum chromodynamics[10]. These

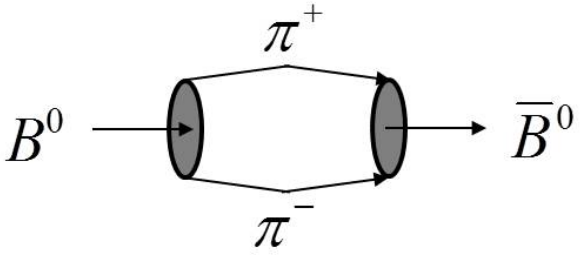

Figure 4.11: An example of a common final state for B^0 and $\bar{B}^0$, leading to oscillations.

contributions are important in calculating M_{12} and Γ_{12} in the systems of neutral kaons and D mesons. They are, however, small compared to contributions of box diagrams for B^0_d and B^0_s mesons. It turns out that for B mesons Γ_{12} is strongly suppressed ($|\Gamma_{12}|/|M_{12}| \ll 1$) and M_{12} can be well predicted within the Standard Model.

[10]Quantum chromodynamics, theory of strong interaction, is limited in methods because the strong interaction coupling constant increases at lower energies. A consequence is a bad or even non-existent convergence of perturbative series in the coupling constant, a usual method of calculations related to weak and electromagnetic interactions. Solutions include calculations in the framework of various models or quantum chromodynamics on the lattice.

In the system of B_d^0 mesons $\Delta\Gamma \ll \Delta m$ (see Sect. 3.3.2). Hence $(\Delta m)^2 - (1/4)(\Delta\Gamma)^2 \approx (\Delta m)^2$. If one can moreover neglect Γ_{12} several expressions simplify; the first equation of (3.34) becomes

$$\Delta m = 2|M_{12}| \ , \tag{4.11}$$

and relations (3.21) and (3.28) depend solely on M_{12}:

$$\begin{aligned} \langle P^0|\hat{H}|\bar{P}^0\rangle &\approx M_{12} \\ \left(\frac{q}{p}\right)^2 &\approx \frac{M_{12}^*}{M_{12}} = e^{-2i\phi_M} \ . \end{aligned} \tag{4.12}$$

Phase of M_{12} is thus the phase of $\bar{B}^0 \to B^0$ transition. The reverse transition is shown in Fig. 1.11. Any up-like quark can be exchanged in the loop. However, a more involved calculation shows that the amplitude is proportional to the mass of the exchanged quark. Since m_t is much larger than mass of any other quark, the t quark contribution is by far dominant in B^0 mixing. Then the elements of CKM appearing in the amplitude can be read off the diagram as $(V_{td}V_{tb}^*)^2$. For an opposite process, $\bar{B}^0 \to B^0$, one has $(V_{td}^*V_{tb})^2$. From this we conclude that the factor q/p entering λ is

$$\frac{q}{p} = \frac{V_{td}V_{tb}^*}{V_{td}^*V_{tb}} \ . \tag{4.13}$$

Another factor enters λ for $B^0 \to J/\psi K_S^0$. K^0 produced in a decay undergoes a time evolution (as K_S^0) including a possibility of mixing. Hence a factor analogous to q/p for B^0 oscillations must be included also for K^0 oscillations. To do so, it may be helpful to graphically present the decay and factors entering the amplitude. This is shown in Fig. 4.12. A

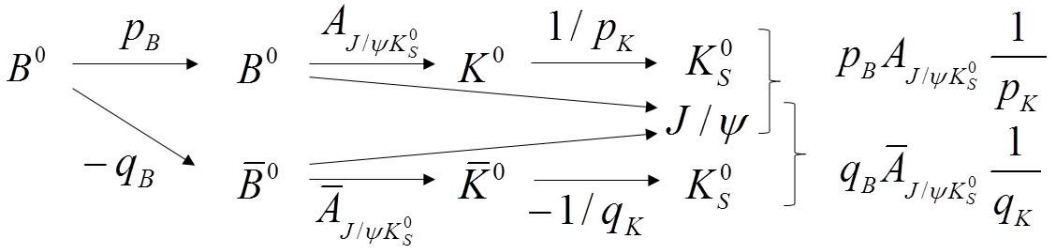

Figure 4.12: Graphical presentation of B decay to $J/\psi K_S^0$. The process may proceed without mixing of B^0 (upper part) or through mixing into $\bar{B}^0$ (lower part). Produced K^0 or $\bar{K}^0$ should decay as a K_S^0. Individual factors entering the amplitude for the process are marked in the scheme and explained in the text.

produced B^0 meson evolves in time, the amplitude to find it after some time t in a state B^0 ($\bar{B}^0$) is p ($-q$), as apparent from Eq. (3.35). The decay to $J/\psi K^0$ ($J/\psi \bar{K}^0$) adds a factor $A_{J/\psi K_S^0}$ ($\bar{A}_{J/\psi K_S^0}$). In the neutral kaon system we neglect CP violation, since it is small compared to CP violating effects in the B meson system, as we will see. Hence $|K_S^0\rangle = |K_1^0\rangle$ (see

(2.9)). For K^0 ($\bar{K}^0$) to decay as a K_S^0 a factor $1/p$ ($-1/q$) for the kaon system must be added to the amplitude, see (3.32). The full expression is thus

$$\lambda = \left(\frac{q}{p}\right)_B \frac{\bar{A}_{J/\psi K_S^0}}{A_{J/\psi K_S^0}} \left(\frac{p}{q}\right)_K \quad , \tag{4.14}$$

where we used indices B, K to indicate to which system q/p refers to.

To determine $(p/q)_K$, we note that B^0 is composed of $\bar{b}d$ and K^0 from $\bar{s}d$; hence one has to make a replacement $b \to s$. Conclusion that the additional factor is $V_{td}^* V_{ts}/V_{td} V_{ts}^*$ (by comparison to (4.13)) is premature. For B^0 oscillations we argued that the top quark contribution is dominant since $m_t \gg m_q$ for any other quark. This of course holds also for K^0 oscillations, however there a c quark exchange in the loop is actually much more important. This is due to $|V_{td}V_{ts}| \ll |V_{cd}V_{cs}|$[11]. The factor $(p/q)_K$ is thus $V_{cd}^* V_{cs}/V_{cd} V_{cs}^*$.

Putting it all together, we arrive at the expression for λ in $B^0 \to J/\psi K_S^0$ decays:

$$\lambda = \underbrace{\frac{V_{cb}V_{cs}^*}{V_{cb}^*V_{cs}}}_{\bar{A}_{J/\psi K_S^0}/A_{J/\psi K_S^0}} \underbrace{\frac{V_{td}V_{tb}^*}{V_{td}^*V_{tb}}}_{(q/p)_B} \underbrace{\frac{V_{cd}^*V_{cs}}{V_{cd}V_{cs}^*}}_{(p/q)_K} = \frac{V_{td}V_{tb}^*}{V_{td}^*V_{tb}} \frac{V_{cb}V_{cd}^*}{V_{cb}^*V_{cd}} \tag{4.15}$$

We realize that $|\lambda| = 1$, and hence $S = \mathrm{Im}(\lambda)$. Also, since $|\lambda| = 1$ the imaginary part is just $\mathrm{Im}(\lambda) = \sin(\mathrm{Arg}[\lambda])$[12]. In order to determine $\mathrm{Arg}[\lambda]$ we need to identify the phase of (4.15).

By inspection of the unitarity triangle in Fig. 2.8 (left) one realizes that the complex number $(V_{td}V_{tb}^*)/(V_{cb}^*V_{cd})$ has an argument $\pi - \varphi_1$:

$$\pi - \varphi_1 = \mathrm{Arg}\left[\frac{V_{td}V_{tb}^*}{V_{cb}^*V_{cd}}\right] \quad . \tag{4.16}$$

Noting that $\mathrm{Arg}[1/x] = -\mathrm{Arg}[x]$ and $\mathrm{Arg}[x_1x_2] = \mathrm{Arg}[x_1] + \mathrm{Arg}[x_2]$ we can write

$$\varphi_1 = \pi - \mathrm{Arg}\left[\frac{V_{td}V_{tb}^*}{V_{cb}^*V_{cd}}\right] = \mathrm{Arg}\left[-\frac{V_{cb}^*V_{cd}}{V_{td}V_{tb}^*}\right] = \mathrm{Arg}\left[\frac{V_{td}V_{tb}^*}{V_{cb}^*V_{cd}}\right] \quad , \tag{4.17}$$

in accordance with Eq. (2.25). Phase of λ can be identified as

$$\mathrm{Arg}[\lambda] = 2\,\mathrm{Arg}\left[\frac{V_{td}V_{tb}^*}{V_{cb}^*V_{cd}}\right] = 2\varphi_1 \quad , \tag{4.18}$$

and hence

$$S = \sin(2\varphi_1) \quad . \tag{4.19}$$

Measurement of S in $B^0 \to J/\psi K_S^0$ decays represents determination of one of the angles of the unitarity triangle.

If the final state is changed from $J/\psi K_S^0$ to $J/\psi K_L^0$, and again neglecting CP violation in the neutral kaon system ($|K_L^0\rangle = |K_2^0\rangle$), only a small but important change in the expression

[11] Using values from (1.13) one gets $|V_{td}V_{ts}|/|V_{cd}V_{cs}| = 0.0017$.

[12] Argument of a complex number, written in a form $|z|e^{i\phi}$, is ϕ.

for λ appears: $1/q_K$ appears with a reversed sign due to $\langle K_2^0|\bar{K}^0\rangle \propto -1/q$ (3.32), and hence $\lambda_{J/\psi K_L^0} = -\lambda_{J/\psi K_S^0}$. In general it holds that λ depends also on the CP eigenvalue of the final state f_{CP}. This is usually incorporated into the expression for S:

$$S = -\eta_f \sin(2\varphi_1) \ , \tag{4.20}$$

where η_f denotes the CP value of the final state. According to discussion in Sect. 2.1, J/ψ composed of a c and $\bar{c}$ quarks has $P = -1$ and $C = -1$, and hence $CP = +1$. K_S^0 also has $CP = +1$ as argued in Sect. 2.2. $J/\psi K_S^0$, appearing in the decay of a B^0, have an angular momentum of $L = 1$ (since spin of J/ψ is $S = 1$), and the value of η_f is hence $CP_{J/\psi} CP_{K_S^0} (-1)^L = -1$. Because of opposite CP values of K_S^0 and K_L^0, $J/\psi K_L^0$ final state has $\eta_f = +1$.

A final note is in order: a careful reader may want to relate the above explanations with the argument given at the end of Sect. 3.3.2, about CP violating observables being a consequence of at least two non-vanishing phase differences, a weak and a strong one (see Eq. (3.59)). In discussion above we clarified the contribution of weak phase, i.e. the one arising from the elements of CKM matrix. How about the strong phase? This is taken care of by oscillations, specifically by the phase $\Delta m \Delta t$. This does not change under charge-conjugation and hence plays a role of a strong phase difference.

Note: A measurement of time-dependent decay rate of neutral B meson decays to self-conjugated states f_{CP} enables determination of one of the angles of the unitarity triangle.

4.2.3 Recent Numbers

The most recent measurements of $\sin(2\varphi_1)$ are shown in Fig. 4.13 [40, 41]. In the measurements both, CP-even and CP-odd final states were used. The former are represented by $J/\psi K_L^0$, and the latter by $J/\psi K_S^0$, $\psi(2S)K_S^0$ and $\chi_{c1} K_S^0$[13]. For all these decay modes the underlying quark process (c.f. Fig. 3.29) is the same, $b \to c\bar{c}s$. Results show a clear reversal of the CP asymmetry sign for the two types of final states, as discussed around Eq. (4.20). Numerically, results for $\sin(2\varphi_1)$ are $0.667 \pm 0.023 \pm 0.012$ and $0.687 \pm 0.028 \pm 0.012$. We quote the results in order to be compared to the results of measurements back in 2001. The statistical uncertainties have been reduced by a factor of $\sqrt{20}$ to $\sqrt{30}$, because of the corresponding increase of the detected sample of B meson decays (see Eq. (3.3)). Also the systematic part of the uncertainties is significantly reduced, pointing to a much improved understanding of detectors and measurement methods. The most significant contribution to systematic uncertainties arises from a limited knowledge of resolution functions (see Sect. 4.1.3) describing the measured Δt distribution. Compared to the first measurements scientists have specifically gained in understanding which decay vertices (i.e. in which decay modes of B_{tag}) are reconstructed more and which less precisely, and adjusted the resolution function depending on this.

Last but not least, the more recent measurements of $B^0 \to f_{CP}$ decay-time distributions allow also for a possibility of $A \neq 0$ in (3.51). The measured Δt distributions are thus fitted

[13] $\psi(2S)$ and $\chi c1$ are two additional charmonium states, similar to J/ψ.

using a complete expression (4.3), convolved with a resolution function. The results quoted for A are $0.006 \pm 0.016 \pm 0.012$ [40] and $0.024 \pm 0.020 \pm 0.016$ [41]. Within the measurement uncertainty parameter A is consistent with a null value, confirming to a good accuracy $|\lambda| = 1$.

In derivation of λ we neglected CP violation in the neutral kaon system by assuming $|K_S^0\rangle \approx |K_1^0\rangle$, i.e. neglecting an addition of $|K_2^0\rangle$ in $|K_S^0\rangle$ of the order of $|\varepsilon| \sim 2 \cdot 10^{-3}$ (2.9). The resulting CP asymmetry in the neutral B meson system is found to be of the order of one, $\mathrm{Im}(\lambda) = \sin(2\varphi_1) \approx 0.7$. The approximation is hence justified.

Within the framework of Kobayashi-Maskawa mechanism experimental confirmation of $\sin(2\varphi_1) \neq 0$ proves that the unitarity triangle in Fig. 2.8 has a finite area, and that the complex phase of CKM matrix is non-vanishing (Sect. 2.3.2). Results prove that the CP asymmetries in the processes involving b quarks (B mesons) are much larger than those involving s quarks (K mesons). They show that $|\lambda| \approx 1$ in $B^0 \to J/\psi K_S^0$ decays. All these experimental results make a strong statement about the correctness of the Kobayashi-Maskawa picture, but are still just determinations of some apriori unknown parameters of the theory. A basic prediction arising from CKM matrix is the existence of the unitarity triangle (non-degenerate one, i.e. of non-vanishing area). Measurements of $B^0 \to J/\psi K_S^0$ decays provide for only one of the angles in this triangle. To further prove the theory some over-constrained measurements, as explained in the following, are needed.

In the complex plane of Wolfenstein parameters, defined in Eq. (2.22), a measurement of S represents an area between lines of constant φ_1 denoted in Fig. 4.14 (top). Because $\sin(\alpha) = \sin(\pi - \alpha)$ and $\sin(\alpha) = \sin(\alpha + 2\pi)$, determination of $\sin(2\varphi_1)$ in terms of φ_1 specifies four possible values, beside φ_1 also $\pi/2 - \varphi_1$, $\varphi_1 + \pi$ and $3\pi/2 - \varphi_1$.

In discussion of decays to flavour specific states around Eq. (3.41) we already mentioned some measurements, also related to parameters ρ and η. Such a measurement is the determination of B^0 oscillation frequency, Δm. According to (4.11) Δm is proportional to $|M_{12}|$. The latter is the amplitude for a $\bar{B}^0 \to B^0$ transition, and hence $M_{12} \propto (V_{td} V_{tb}^*)^2$. Using the Wolfenstein parametrization

$$\Delta m \propto |V_{td} V_{tb}^*|^2 = |A\lambda^3(1 - \rho - \mathrm{i}\eta)|^2 \propto (1-\rho)^2 + \eta^2 \quad . \tag{4.21}$$

In the (ρ, η) plane the measured value of Δm (with some finite accuracy) represents an area between circles centred at $\rho = 1$, as sketched in Fig. 4.14 (top).

Measurements of S in $B^0 \to J/\psi K_S^0$ decays and of Δm represent over-constrained measurements. They can both be interpreted in terms of values of ρ and η. And, if the underlying theoretical interpretation is correct, they have to yield the same values of unknown parameters. In graphical terms, the areas representing one and the other measurement must overlap.

A reader may argue that it is easy to assure an overlapping region of a circle, centred at $(1,0)$ and a line starting at the exact same point. Which is of course quite true. The mentioned two variables merely provide for possible values of ρ and η. A serious test arises when one adds another measurement related to the two parameters.

Returning to Fig. 1.10 we remember that rates of B meson decays with a $b \to u$ quark subprocess depend on the magnitude of V_{ub} element of CKM matrix. For example, measured probability of $B^+ \to \pi^+ \pi^0$ decays is proportional to $|V_{ub}|^2$. Without going into any details of

$|V_{ub}|$ determination from the measured charmless decays[14] of B mesons, we note that (2.22)

$$|V_{ub}|^2 = A^2\lambda^6(\rho^2+\eta^2) \ . \tag{4.22}$$

Determination of $|V_{ub}|$ represents another circle in the (ρ,η) plane, this one centred at $(0,0)$. Addition of this measurement in over-constraining possible parameters values makes the test non-trivial. As sketched in Fig. 4.14, regions of the three so far mentioned measurements may not (middle) or may (bottom) overlap.

The above examples round up our presentation of over-constraining the unitarity triangle parameters with the aim of testing the Kobayashi-Maskawa theoretical explanation of *CP* violation[15]. It is time to turn to the real measurements. The current knowledge on the unitarity triangle is presented in the colourful Fig. 4.15 [42]. Every individual coloured region represents an average of measurements of a single observable related to CKM matrix elements. They represent a 95% confidence region of an individual variable[16]. The averages are input to a minimization procedure in which a likelihood function depending on the measured variables ($\vec{o}$) and their theoretical interpretation ($\vec{f}(\vec{p})$), $\mathscr{L}(\vec{o}-\vec{f}(\vec{p}))$ is minimized in order to obtain the most probable values of underlying parameters (ρ and η in our case). There are 24 observables used in the fit (not all shown in Fig. 4.15). Actually, most of the input variables are averages of number of individual measurements. For example, Δm value used as an example above, enters the fit as an average of 32 individual measurements, performed by experiments at the LEP collider[17], at the Tevatron collider[18], at KEKB and PEP-II, as well as at the LHC.

All of the measurements intersect at a single point (a tiny region, actually) in the (ρ,η) plane: $\bar{\rho} = 0.1577^{+0.0096}_{-0.0074}$, $\bar{\eta} = 0.3493^{+0.0095}_{-0.0071}$ (for clarification regarding the difference between (ρ,η) and $(\bar{\rho},\bar{\eta})$ see the footnote at page 35; the quoted uncertainties include experimental statistical and systematic uncertainties, as well as uncertainties of theoretical predictions). Now, this is an overconstrained measurement of the CKM matrix parameters! Numerous processes studied at a number of experiments is experimentally verified to be in agreement with expectations using CKM matrix.

It was the tests described above that persuaded the physics community in the correctness of the *CP* violation description in the world of elementary particles as proposed by Makoto Kobayashi and Toshihide Maskawa (Fig. 4.16). Their contribution has been recognized by the The Royal Swedish Academy of Sciences. They shared the Nobel Prize in Physics for 2008[19] "for the discovery of the origin of the broken symmetry which predicts the existence of at least three families of quarks in nature" [43].

[14] Charmless denote decays without a c quark in the final state. If one neglects a possibility of higher order processes, the only process leading to a charmless final state for a decaying b quark inside a B mesons is a $b \to u$ process.

[15] For explanations on how other unitarity triangle observables - sides and angles - are measured, the reader shold consult some advanced books and papers, e.g. [5, 46].

[16] A confidence region is determined for each measured variable. Assuming the measurement has a probability distribution function $w(o_i;\vec{p})$ (typically a Gaussian function, o_i is the observable under question, and $\vec{p}$ a vector of parameters on which the observable depends upon, e.g. ρ and η), the confidence region $\mathscr{S}$ is defined as $\int_{\mathscr{S}} w(o_i;\vec{p})d\vec{p} = \varepsilon$, where ε is the confidence level of the region - 95% in this case.

[17] Predecessor of the current LHC.

[18] A proton antiproton collider operating at Fermi National Accelerator Laboratory near Chicago until 2011. Top quarks were experimentally observed there for the first time.

[19] With Yoichiro Nambu.

The essence of experimental efforts is best described by the words of the two Nobel laureates in the foreword to [5]:
"[The book describes] *a decade long effort of physicists in the quest for the precise determination of asymmetry - broken symmetry - between particles and anti-particles. We now recognize that the matter we see around us is the residue - one part in a billion - of the matter and antimatter that existed in the early universe, most of which annihilated into the cosmic background radiation that bathes us.*"
"The B Factories have contributed a great deal to our understanding of particle physics, as documented in this book. [...] *Obviously we owe our Nobel Prize to this result.*"
Certainly the words that make any member of the experiments at *B* Factories proud.

Note: Overconstrained measurements of processes related to CKM matrix prove with an excellent accuracy the correctness of Kobayashi-Maskawa description of *CP* violation in the world of subatomic particles.

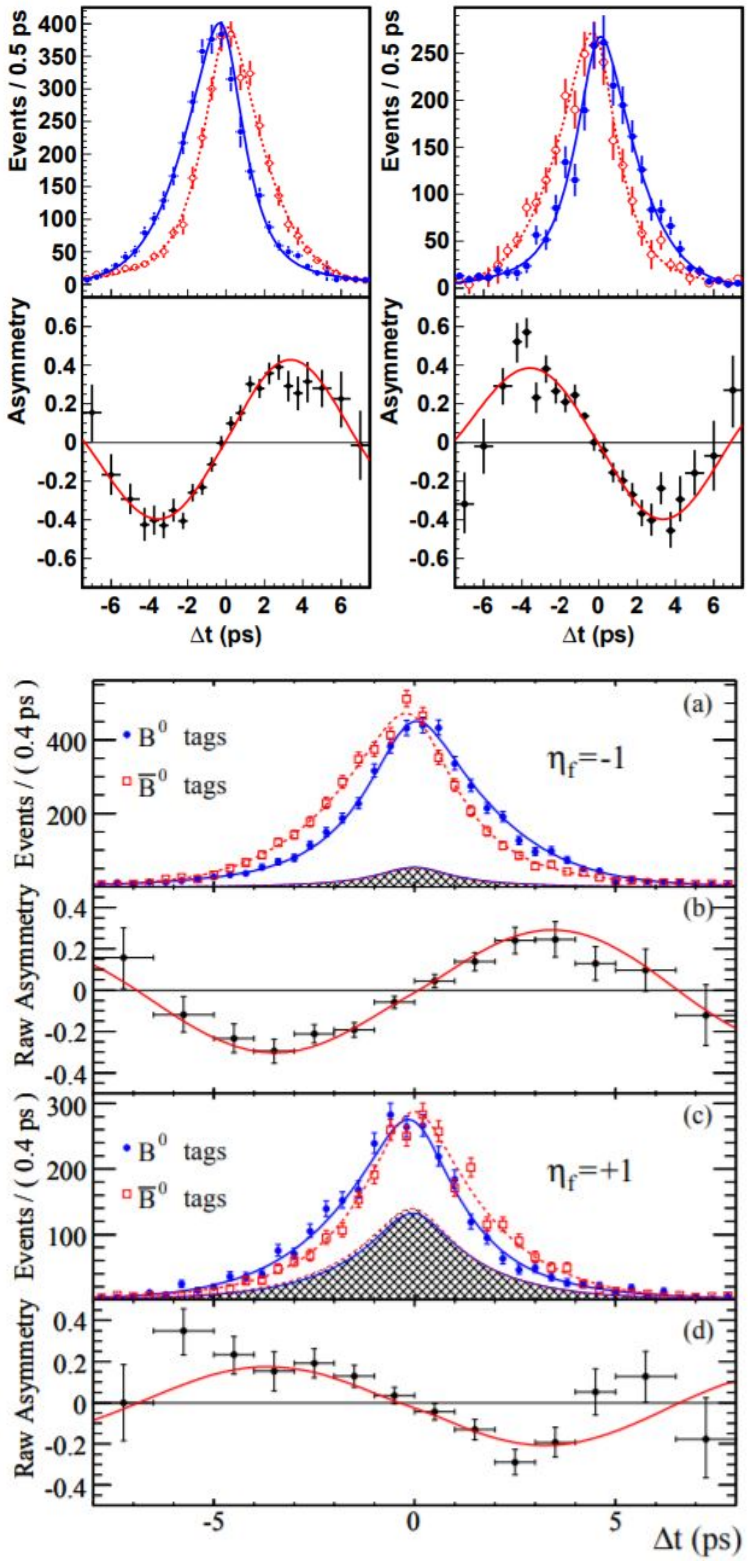

Figure 4.13: Top pannel: Mesurement of $\sin(2\varphi_1)$ by Belle [40]. Top plots show Δt distribution for $B_{tag} = \bar{B}^0$ (blue points) and $B_{tag} = B^0$ (red points). Left and right plots are for $CP = -1$ final states ($J/\psi K^0_S$, $\psi(2S)K^0_S$ and $\chi_{c1}K^0_S$) and $CP = +1$ final states ($J/\psi K^0_L$), respectively. The asymmetry $\mathscr{A}_{CP}$ is shown in the bottom plots. Bottom pannel: Analogous measurement by BaBar [41]. Top two plots are Δt distribution and $-\mathscr{A}_{CP}$ (with color legend opposite to the one in Belle plots) for $CP = -1$ final states and bottom two the same for $CP = +1$ final state.

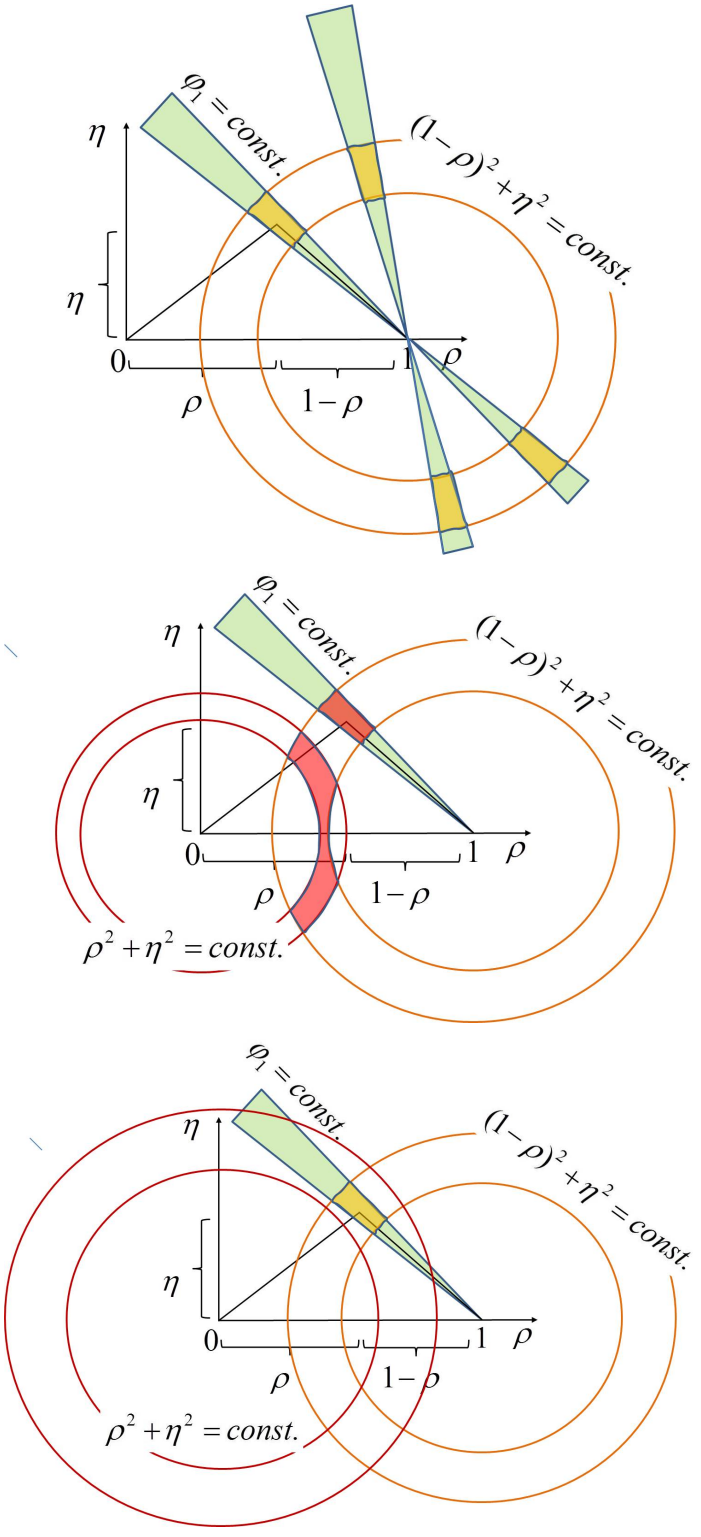

Figure 4.14: Top: Measurement of $\sin(2\varphi_1)$ schematically represented in the (ρ,η) plane (green area). Superimposed is a sketch of Δm measurement (between brown lines) and the overlap area of the two measurements (yellow). Middle: An addition of a third measurement, $|V_{ub}|^2$, may result in a non-overlapping region of three measurements (red). Bottom: If the description with CKM matrix is correct, all over-constrained measurements should overlap to yield the true values of (ρ,η) (yellow). Note that in middle and bottom plot only one solution for φ_1 is shown for simplicity.

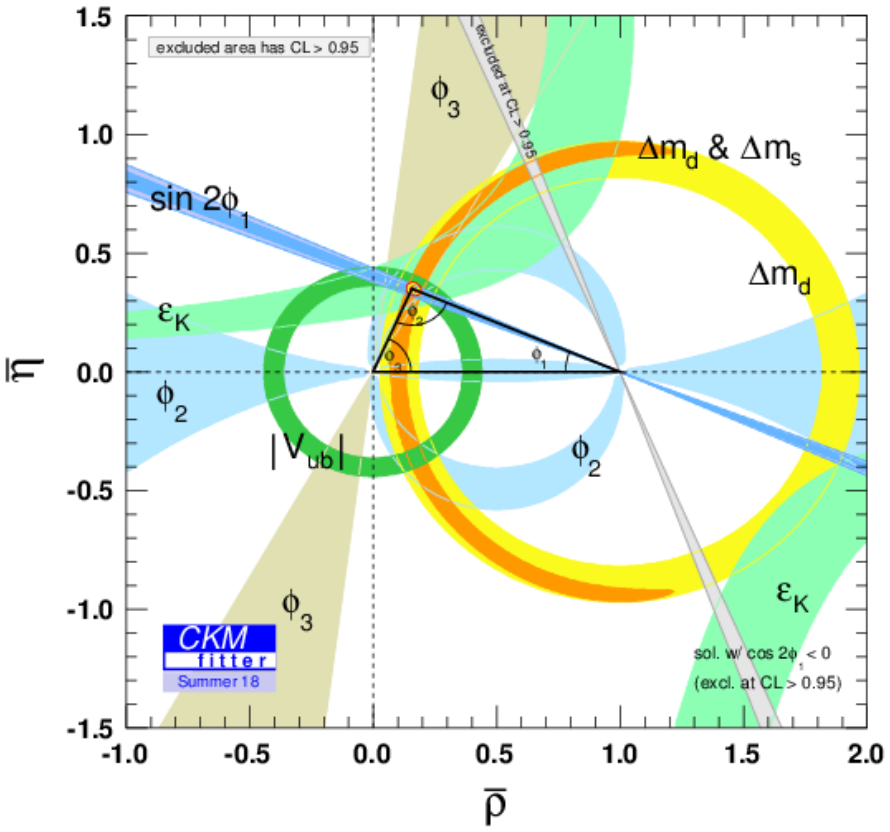

Figure 4.15: Current experimental situation regarding the unitarity triangle[42]. Measurement averages of various CKM matrix related variables are shown as coloured bands with 95 % confidence level intervals. All measurements have a common overlap region (red).

Figure 4.16: Makoto Kobayashi (left) and Toshihide Maskawa (right) [43].

Chapter 5

Into the New Era

5.1 The Heritage

It would be erroneous to think the measurement of *CP* violation was the most reboant result of the previous generation *B* Factories. It was indeed their main motivation, it is fair to say it was probably the most important one from the particle physics evolution perspective, and in a way a *fill rouge* throughout the operations. It is one of the most cited results; results by both experiments presented at the 2001 conferences were cited in various scientific publications slightly less than 1000 times each. Through the years, however, an emphasize shifted more and more to searches for processes beyond the Standard Model, as explained in Sect. 1.3. Ironically, to some extent, the very precise determinations of parameters describing *CP* violation within the SM raise a question of New Physics by themselves.

In Sect. 2.3.2 the constant J was introduced, arguing that $J \neq 0$ is the sign of *CP* violation, and that the value of J is one hand a measure of symmetry breaking and on the other that it can be related to the baryon asymmetry of the Universe. To do so, and without going into any detail we can constitute that the expression for J involves dimension of energy to the power of 12. It is to be compared to the appropriate power of the temperature (energy) at which the baryon violating processes in the course of Universe evolution appeared, $T_{BV} \sim \mathcal{O}(100\ GeV)$ [44]. One finds

$$\frac{J}{T_{BV}^{12}} \sim 10^{-20} \quad . \tag{5.1}$$

The current excess of baryons over anti-baryons in the Universe, repeated from Sect. 2.3.1, is

$$\left.\frac{n_{\text{bar}} - n_{\text{antibar}}}{n_\gamma}\right|_{\text{now}} = \left.\frac{n_{\text{bar}} - n_{\text{antibar}}}{n_{\text{bar}} + n_{\text{antibar}}}\right|_{\text{early}} \approx 10^{-10} \quad . \tag{5.2}$$

The value of J/T_{BV}^{12} falls 10 orders of magnitude below the observed baryon asymmetry of 10^{-10}! The *CP* violation as described within the SM and as measured with the contemporary experiments is many orders of magnitude too small to explain the nowadays state of Universe. One may say we were rather vague in estimating (5.1), however, a factor of 10,000,000,000 is hard to miss...

Despite an enormous success in description of *CP* violation as observed at the level of elementary particles, the complex phase of CKM matrix as the only source of *CP* violation

fails to explain the mystery of the asymmetric Universe. Hence results of B Factories tell us that there must exist further, so far unobserved sources of CP violation, New Physics.

Unknown sources of CP violation have been searched for by Belle and BaBar, especially in some extremely rare B meson decays. The reason for searching for deviations between the SM predictions and experimental results in extremely rare processes is trivial: if a process has a very low probability within the SM, then at least potentially a relative contribution of unknown processes, New Physics, may be relatively large with respect to the SM contribution. Hence, deviations from the SM may be easier to identify. If the process can be measured accurately enough, of course.

Especially interesting for NP searches are higher order processes; they are typically very rare and proceed through loop diagrams in which heavy unknown virtual particles may contribute. An example is shown in Fig. 5.1. In the figure a B meson decay is shown with a

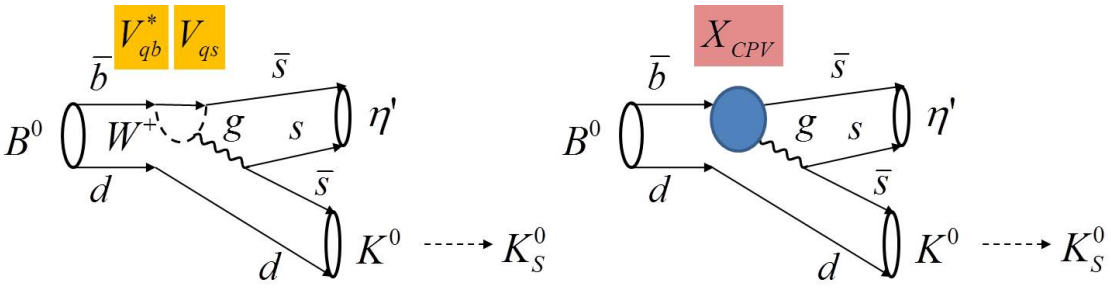

Figure 5.1: Left: Diagram of $B^0 \to \eta' K_S^0$ decay, an example of $b \to sq\bar{q}$ quark subprocess, with CKM factors entering the amplitude. Right: Beyond the SM unknown particles may be exchanged in the loop and contribute to CP violation.

quark process $\bar{b} \to \bar{s}q\bar{q}$ (in the specific case $q = s$). While within the SM such a process is possible through a loop diagram shown in Fig. 5.1 (left), there may exist unknown particles that can be exchanged as virtual ones in the loop (Fig. 5.1 (right)). If these particles have CP violating couplings (X_{CPV} , like $W^{\pm}$ bosons have in a form of CKM matrix elements) this may lead to CP violation different than the one expected from the SM calculations.

Several measurements of CP violation in $b \to sq\bar{q}$ process exist. The method of measurement is analogous to the one described in the previous chapter for $B^0 \to J/\psi K_S^0$, with the underlying $b \to c\bar{c}s$ quarks process; the parameter S measured in these rare decay modes is usually written as

$$S_{b\to sq\bar{q}} = -\eta_f \sin\varphi_1 + \Delta S \ . \tag{5.3}$$

ΔS parametrizes possible deviations from S as measured in $b \to c\bar{c}s$ process, arising from NP contribution. Due to corrections arising from strong interaction among quarks in specific hadrons, ΔS has a mild dependence on the specific hadron decay mode, but is in general within SM expected to be zero. The most accurate theoretical prediction as well as the current experimental knowledge exist for $B^0 \to \eta' K^0$ decays. ΔS in this decay mode is measured to be consistent with 0 within an accuracy of ± 0.06 [45]. On the other hand, the theory (SM) predicts ΔS to be null within ± 0.01 [46]. Hence the experimental accuracy must be improved, in order to seek for any deviations from the SM it should reach the level of around ± 0.01 or better. This is not possible using Belle and BaBar data (note that the

branching fraction of this specific decay is only around $7 \cdot 10^{-5}$). It is only one of examples where the next generation B Factory, SuperKEKB and Belle II (see Sect. 3.1.2) is needed.

With largely increased luminosity and significantly improved detector and measurement methods both, statistical and systematic uncertainties will be reduced at Belle II. For any decay-time dependent measurements, accuracy of decay vertex determination is crucial. At Belle II, semiconductor detectors (Fig. 3.24 (left)) are expected to provide a significantly better precision than available in the previous generation B Factories. This precision influences also the accuracy of ΔS measurement in $B^0 \to \eta' K^0_S$; the latter is shown as a function of integrated luminosity in Fig. 5.2 (left; adopted from [46]). The statistical part of the uncertainty

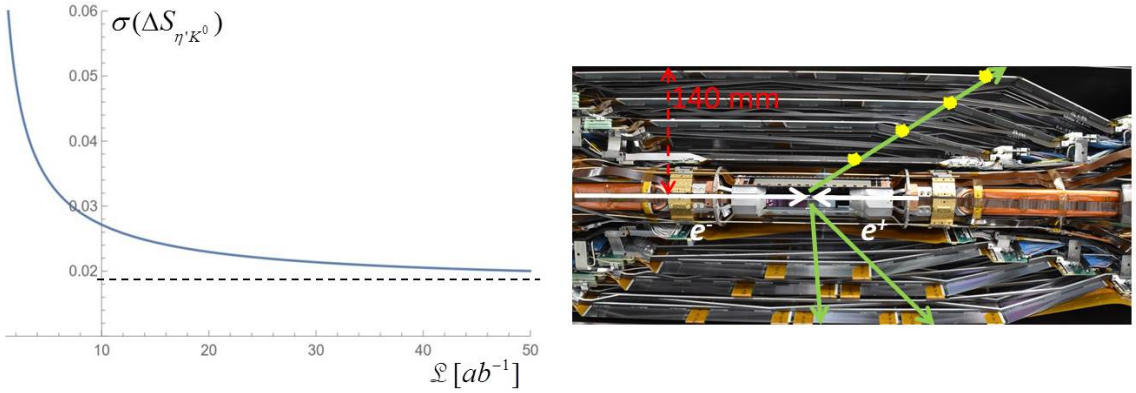

Figure 5.2: Left: Expected accuracy on ΔS in $B^0 \to \eta' K^0_S$ measurement with Belle II as a function of integrated luminosity (adopted from [46]). Dashed line marks the expected amount of irreducible systematic uncertainty. Right: close up of Belle II semiconductor vertex detector, consisting of two inner layers of pixel detectors, and four layers of double-sided silicon strip detectors. Schematically some tracks with illustrated hits in the four outer layers of silicon strip detectors are also plotted. The outermost layer has a radius of 140 mm [27].

decreases inversely proportional to integrated luminosity (see (3.3)). The systematic part may or may not decrease with luminosity. For example, if a part of systematic uncertainty arises from a finite knowledge of a given parameter which can be determined using some data, that part of systematic uncertainty will decrease with integrated luminosity. On the other hand there are sources of systematic uncertainty that do not decrease with an increased data sample size, and are hence called irreducible[1]. By performing studies of simulated data one can estimate the expected accuracy of a given measurement with a specific detector. With the final dataset of Belle II (50 ab^{-1}) one expects a measurement of S in $B^0 \to \eta' K^0_S$ with an accuracy of around 0.02.

Note: B Factories of previous generation provided for accurate measurements of CP violation in elementary particle processes, unveiling the fact that the level of observed symmetry breaking is many orders of magnitude too low to explain the observed matter

[1] Irreducible in this context should not be taken too literally. It usually happens that bright new ideas for measurement methods can additionally reduce the systematic uncertainty.

anti-matter asymmetry of the Universe. The present B Factory will search for possible new sources of CP violation and by that for evidences of New Physics in extremely rare processes, which were beyond the reach of experiments so far.

5.2 Strong and Weak

As a guideline in importance of individual results one can consider the number of citations of a given scientific paper[2]. Interestingly enough, despite the general aim of searching for NP in high energy physics experiments, some of most cited Belle and BaBar results are actually the ones dealing with some unknown properties and their consequences of known interaction, the strong one. By far the most cited article by Belle collaboration, and perhaps also the most unexpected finding is the one from 2003. In studies of decays of B mesons, $B^+ \to K^+ J/\psi\pi^+\pi^-$, an unknown type of hadron has been discovered, shown in Fig. 5.3 [47]. The $X(3872)$ state decays into $J/\psi\pi^+\pi^-$ and consequently appeared as a narrow peak in the invariant mass distribution of these final state particles (note that J/ψ decays into an $\ell^+\ell^-$ pair, $\ell = e$ or μ; in the figure a difference of invariant masses, $\Delta M = M(\pi^+\pi^-\ell^+\ell^-) - M(\ell^+\ell^-)$, for which the resolution is better than directly for $M(\pi^+\pi^-\ell^+\ell^-)$, is shown). While produced in a similar manner as some other charmonium states in decays of a B mesons (Fig. 5.3 (bottom), compare to Fig. 3.29), the state $X(3872)$ has some peculiar properties (mass, decay width, decay modes) preventing to systematize it into the spectrum of known charmonium states[3]. Numerous further studies showed that $X(3872)$ - the name of which reflects its unknown nature, and approximate mass, expressed in MeV - is a state composed of four quarks[4]. As such it represents a so far unknown form of hadrons (only conventional mesons and baryons were experimentally known until then).

Beside $X(3872)$ several other hadrons experimentally observed for the first time at B Factories, either conventional or exotic [5], enabled further studies of strong interaction. Needles to say, Belle II will enable further precise studies of these states, with one to two orders of magnitude larger samples of their decays. The sample size will increase because of the larger expected integrated luminosity, as well as due to the improved reconstruction efficiency. In reconstruction of various hadronic states, particle identification is of utmost importance. Beside the detector module briefly described in Sect. 3.2.2, at Belle II also Cherenkov radiation in aerogel radiator is used for this purpose. Fig. 5.4 shows a view of an array of semiconductor sensors at Belle II, capable of single photon detection.

Among the processes mediated by weak interaction, another result cited widely in the follow-up studies by various groups is the discovery of D^0 oscillations. As presented graphically in Fig. 3.27 and numerically in Tab. 3.2, values of mixing parameters in the system of neutral D mesons result in a tiny probability for a D^0 meson to mix into its anti-particle before it decays. A direct search for oscillations in a manner similar to that for B_s^0 mesons, for example, did not produce a positive result. A different method was devised.

[2] The author does not promote usage of the mentioned indicator in general to evaluate importance of specific results and/or the quality of a research.

[3] Bound states of $c\bar{c}$ are well known both theoretically and experimentally.

[4] Either in a form of a di-meson molecule, or perhaps as four independent quarks - a tetraquark.

[5] Exotic means not a conventional meson or a baryon.

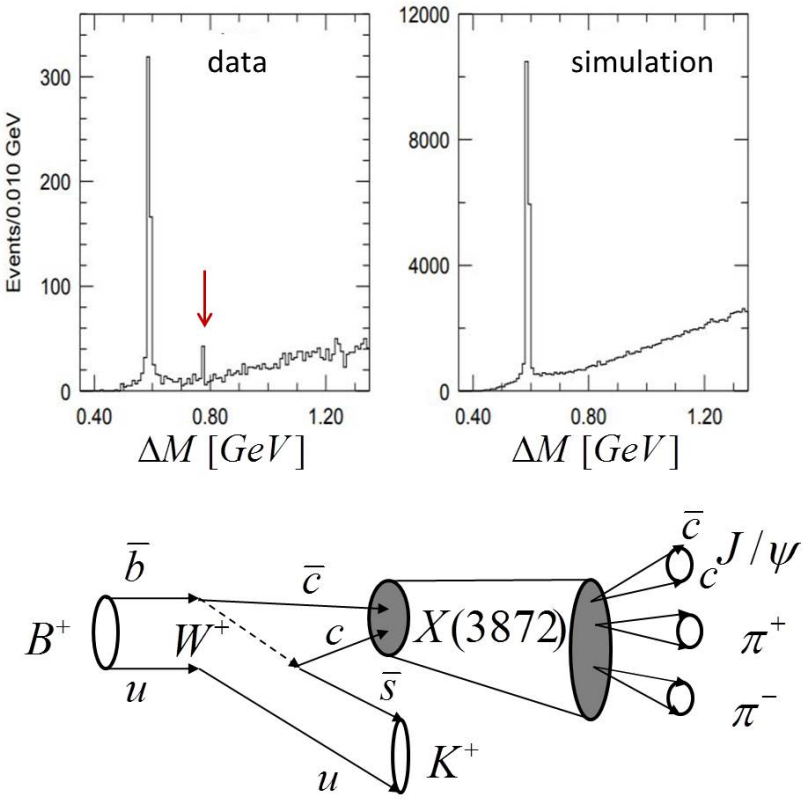

Figure 5.3: Top: Difference of invariant masses $\Delta M = M(\pi^+\pi^-\ell^+\ell^-) - M(\ell^+\ell^-)$ in selected $B^+ \to K^+ J/\psi\pi^+\pi^-$ decays (J/ψ decays to a pair of light leptons, $\ell^+\ell^-$). Adopted from [47]. Red arrow marks a peak in the invariant mass distribution corresponding to $X(3872)$ (left), not present in the simulation (right). Bottom: A diagram of $X(3872)$ production in B decays.

In the absence of CP violation ($q = p = 1$) states $|P_{1,2}\rangle$ defined in (3.22) are eigenstates of $\hat{CP}$ operator. If CP asymmetry would be conserved - or if its violation is small enough to be neglected - $|P_1\rangle$ decays into CP-even and $|P_2\rangle$ into CP-odd final states. As it turns out CP violation in processes with charm quarks is indeed tiny. The reason is that CKM matrix elements related to the first two generations of quarks are almost real. Consider, as an example, $D^0 \to \pi^+\pi^-$ decay. Comparing this decay and its charge-conjugated version, $\bar{D}^0 \to \pi^-\pi^+$, it is easy to see that the phase of CKM elements entering the ratio of amplitudes is

$$\mathrm{Arg}\left[\frac{\langle\pi^-\pi^+|\bar{D}^0\rangle}{\langle\pi^+\pi^-|D^0\rangle}\right] = 2\,\mathrm{Arg}\left[V_{cd}V_{ud}^*\right] \quad . \tag{5.4}$$

Wolfenstein parametrization as given in (2.22) is not sufficient to estimate the above expression. One needs further terms in Taylor expansion, to find $\mathrm{Arg}\left[V_{cd}V_{ud}^*\right] \sim A^2\lambda^4\eta \sim 10^{-3}$. CP asymmetries in charm processes are of the order of 10^{-3}, and can be neglected in the following.

A produced D^0 or $\bar{D}^0$ is a linear superposition of CP eigenstates D_1 and D_2, which are

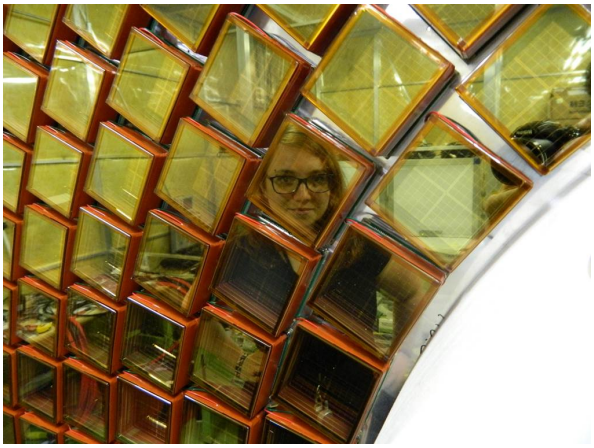

Figure 5.4: Array of Hybride Avalanche Photo Diodes (HAPD), placed in one of the endcaps of Belle II and designed to detect photons from Cherenkov light being emitted by charged particles in an aerogel. Photo: R. Pestotnik.

the states with a well defined mass and decay width. If a D^0 or its anti-particle decays into a final state f_{CP}, an eigenstate of CP as well, then only a D_1 or D_2 component contributes to such a decay. Consequently, decay-time dependence of neutral D meson into a CP-even (CP-odd) final state exhibits a simple exponential form with a decay time of D_1 (D_2). On the other hand, decays into non-CP eigenstate (i.e. a final state which is a mixture of two CP components) follow a decay-time distribution with a lifetime which is an average of D_1 and D_2 lifetimes. A difference of lifetimes in specific types of final states is an evidence of $D_{1,2}$ components and by that evidence of oscillations.

Belle [48] measured decay-time distribution of neutral D mesons in decays to K^+K^- and $\pi^+\pi^-$ (both CP even final states) and compared those to the distribution of decays into $K^-\pi^+$ (a mixture of CP eigenstates). Result is presented in Fig. 5.5 (left). In the figure a deficit of decays to $K^+K^-, \pi^+\pi^-$ compared to decays to $K^-\pi^+$ is clearly evident at high decay-times. Hence the lifetime in former decays is shorter than the lifetime in the latter decays. With some algebra of decay rates the measured lifetimes in both groups of decays can be translated into a mixing parameter $\Delta\Gamma/2\Gamma = (1.11 \pm 0.22 \pm 0.11)\%$.

BaBar [49] used a different method, exploiting decays to so called wrong-sign decays, $D^0 \to K^+\pi^-$ and $\bar{D}^0 \to K^-\pi^+$. Such a final state is accessible to D^0 through two ways: either a direct decay (with amplitude proportional to $V_{cd}V_{us}^*$, Cabibbo suppressed; see Fig. 5.6) or through mixing, $D^0 \to \bar{D}^0$, followed by a $\bar{D}^0$ decay (with amplitude proportional to $V_{cs}V_{ud}^*$, Cabibbo allowed). Interference of the two amplitudes, neglecting CP violating effects, leads to an exponential decay-time dependent rate, modulated by additional decay-time t dependent terms. Coefficients in front of the latter terms are proportional to mixing parameters. Assuming the parameters to be small it suffices to take into account only the first two terms in Taylor series expansion, proportional to t and t^2. The decay-time distribution of wrong-sign decays is compared to distribution of right-sign decays, $D^0 \to K^-\pi^+$ and $\bar{D}^0 \to K^+\pi^-$, to which mainly a single amplitude for direct decay (proportional to $V_{cs}V_{ud}^*$, Cabibbo allowed) contributes. Their distribution is a simple exponential. The ratio of wrong- and right-sign

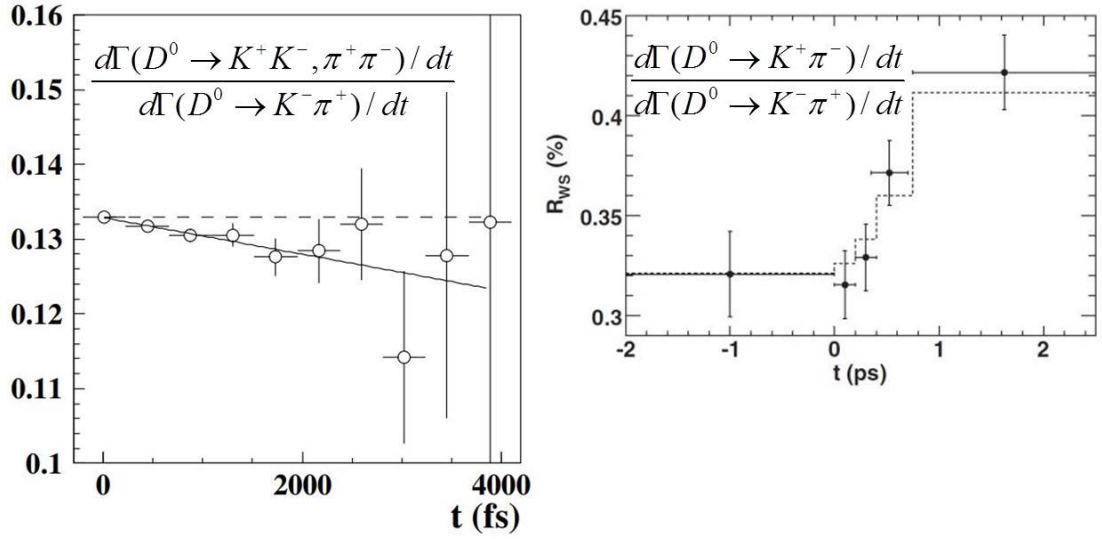

Figure 5.5: Left: Ratio of decay-time distributions for $D^0 \to K^+K^-$ or $D^0 \to \pi^+\pi^-$ and $D^0 \to K^-\pi^+$ decays [48]. Right: Ratio of decay-time distributions for $D^0 \to K^+\pi^-$ and $D^0 \to K^-\pi^+$ decays [49].

decay-time distributions is hence approximately parabolic, as seen in Fig. 5.5 (right). Coefficients of the parabola depend on the D^0 mixing parameters; however another apriori unknown strong phase enters the expressions[6]. Hence a direct determination of the mixing parameters using only this measurement is not possible. Nevertheless a non-zero mixing parameters and hence a presence of oscillations can be unambiguously proved.

The two collaborations presented their results, measurement of the oscillations in the last neutral meson system, where the phenomena was not yet observed, at one of the conferences in the winter of 2007. Scientific papers on the subject were published back-to-back in an international scientific journal the same year.

An important piece of information is - despite large efforts - still missing among the results of B Factories related to charm quark physics. As explained above, CP violation in processes with hadrons composed of c quarks is small. Both collaborations performed various measurements of CP violation in charm sector. Time integrated asymmetries, $[\Gamma(D \to f) - \Gamma(\bar{D} \to \bar{f}]/[\Gamma(D \to f) + \Gamma(\bar{D} \to \bar{f}]$, have been measured for more than 10 different final states f. Performing a measurement of CP violation in D^0 decays requires the initial meson flavour tagging. In most cases this is achieved by using mesons produced in a decay of an excited D meson, $D^{*+} \to D^0\pi^+$. Charge of the pion accompanying the neutral D meson tags its flavour.

Considering the expected amount of symmetry breaking the accuracy of measurements must be at the per-mill (i.e. 10^{-3}) level. This requires an excellent control of experimental method in order to keep the systematic uncertainty at low enough level. There are many effects which may cause asymmetries between original and charge conjugated decays at this

[6]It is a phase between the amplitude of Cabibbo allowed and Cabibbo suppressed decay, not arising from the CKM matrix elements. This phase does not change sign in conjugated decays.

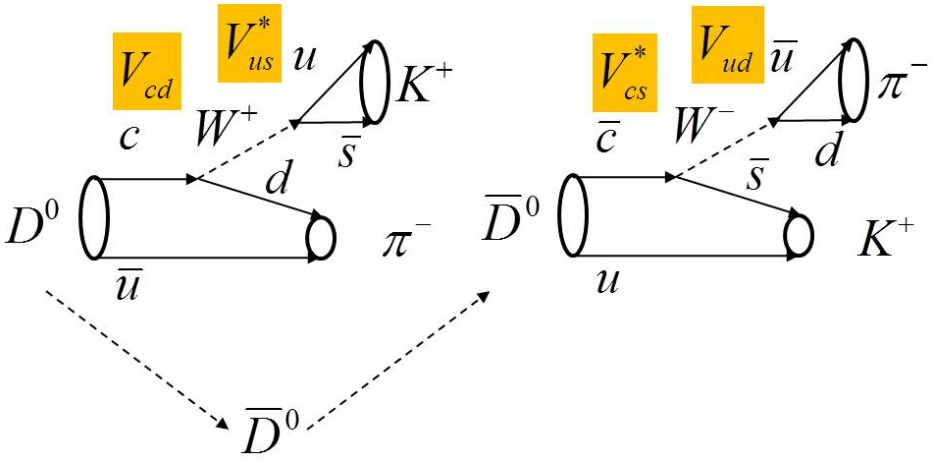

Figure 5.6: Two possible amplitudes leading to wrong-sign D^0 decays: through a Cabibbo suppressed decay of a D^0 (left), or through a mixing, followed by a Cabibbo allowed $\bar{D}^0$ decay (right).

level. For example, reconstruction efficiencies of positively and negatively charged particles tracks in detector may differ by this amount. Such effects must be taken into account in order to be subtracted from the observed asymmetries. Simulated data, typically used to determine efficiencies, are not precise enough to determine such small details. One must rely on real data - control data - selected specifically for that purpose. In order to determine detector induced asymmetries, control data sample must be free of *CP* violation. In *D* meson decays, usually such samples include Cabibbo allowed decays, like the example in Fig. 5.6 (right). For such decays only a single amplitude is dominant and hence no significant *CP* violation is expected. On the other hand Cabbibo suppressed decays like the example in Fig. 5.7 receive contribution from more underlying processes and in principle may exhibit *CP* violation. An alternative in determination of detector induced asymmetries is a measurement of *CP*

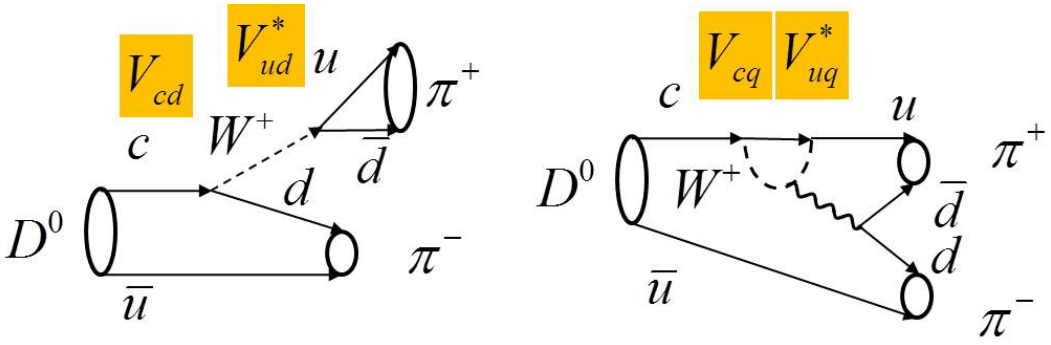

Figure 5.7: Cabibbo suppressed decay $D^0 \to \pi^+\pi^-$. It proceeds through a lowest order process (left) or higher order process (right).

asymmetry difference between two final states. In the difference unwanted contributions cancel, if the two final states are suitably chosen. A non-vanishing difference of asymmetries

would be a sign of *CP* violation (at least in one of decay modes the asymmetry must be different than 0), however the interpretation of results in terms of *CP* violating parameters is in this case more complicated, of course.

Further examination and possible discovery of *CP* violation in charm sector remains a task for the current generation *B* Factory, Belle II.

Among more than 500 journal papers published by each, Belle and BaBar collaboration (and still publishing since analyses of data are still in progress), several hints of discrepancies between the Standard Model predictions and measurement results appeared. We say hints, as opposed to observations. The reader is by now for sure familiar with a statistical nature of measurements in high energy physics. A measurement of a given significance can only be interpreted probabilistically, i.e. quoting a probability that the true value of an observable lies in an interval around the measured value[7]. If the measurement accuracy is such that the deviation from the SM prediction is not so highly probable to dismiss any practical doubt of discrepancy, one can not talk about observation[8].

Perhaps the most intriguing among hints of discrepancies arises from tests of lepton flavour universality. Before shortly discussing those we need to take a look at an important experimental method, possible at *B* Factories. In an electron positron collision a pair of *B* mesons is produced through an $\Upsilon(4S)$. Since no other particles can be produced, conservation of energy and momentum requires

$$p_{ee} = p_{sig} + p_{tag} \quad , \tag{5.5}$$

where p denotes a four-momentum, and indices stand for the electron-positron system, the signal and the tagging *B* meson, respectively. Energy and momentum of the initial electron-positron system is known, but momenta of the produced mesons are not. If one, however, is able to reconstruct momentum of the tagging *B* meson, the momentum of the signal *B* meson can be obtained from the above equation, even if the decay products of B_{sig} are not reconstructed. This is of extreme importance in decays where all or some of the signal *B* meson decay products are not detected in the detector. This is the case with neutrinos in the final state. Neutrinos capable of only weak interaction have a low probability of an interaction with material of the detector, and hence a low (negligible, actually) probability of leaving any signal in it[9]. If B_{sig} undergoes a semileptonic decay, $B_{sig} \to \ell \nu_\ell X$, neutrino is not detected and hence it is impossible to reconstruct the decaying *B* meson from its decay products. If the tagging *B* meson is reconstructed, momentum of neutrino can nevertheless be recovered, assuming the charged lepton ℓ and the produced hadronic system in the final state, X, are detected:

$$p_\nu = p_{ee} - p_{tag} - p_\ell - p_X \quad . \tag{5.6}$$

An example of the method at work is shown in Fig. 5.8. In the figure a computer reconstruction of a *B* meson pair decay, as detected by the Belle detector, is shown. In the example

[7] Intentionally we do not dwell into more precise statistical interpretations, as it would lead to discussions regarding Bayesian and/or Frequentists approach to statistical issues, and these are far beyond the scope of the book.

[8] A commonly accepted definition by several scientific journals is that a significance of 3 σ (in units of measurement uncertainty σ) is considered as an evidence and 5 σ as an observation.

[9] A 1 MeV neutrino has roughly a probability of 10^{-11} to undergo an interaction when passing through the Earth.

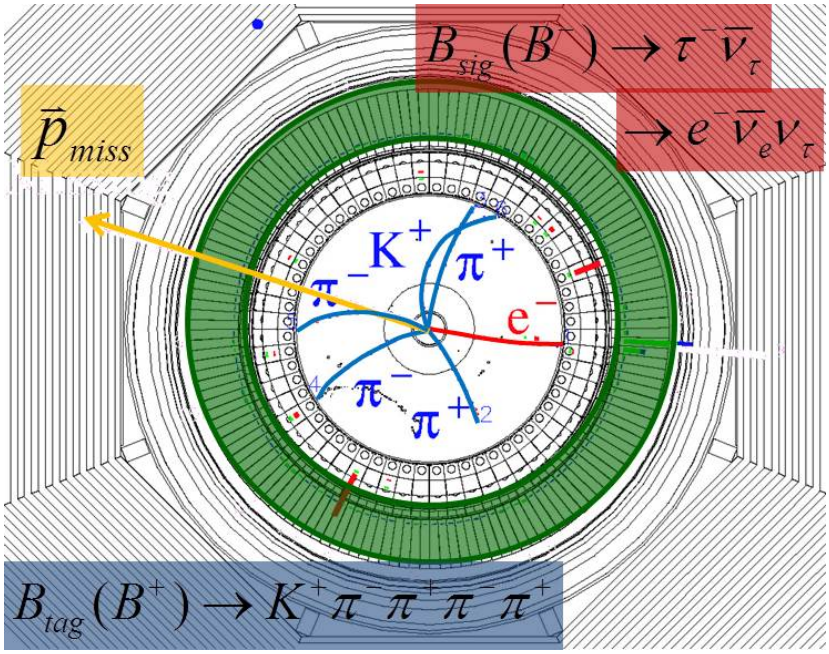

Figure 5.8: Reconstruction of a B meson pair decay in Belle detector. B_{tag} decays into a charged kaon and four charged pions, all being reconstructed in the detector (blue). B_{sig} decays into $\tau^-(\to e^- \bar{\nu}_e \nu_\tau)\bar{\nu}_\tau$. Of B_{sig} decay products only the e^- is detected (red). Using energy and momentum conservation the missing momentum (yellow), taken by neutrinos, can also be determined. Energy detected in the electromagnetic calorimeter (green) and not associated to reconstructed charged particles E_{ECL} should be zero.

shown the tagging B meson (a charged B^+ meson) decayed into a charged kaon and four charged pions in the final state, the tracks of which are reconstructed in the detector. The signal B meson (B^-) most probably decayed into a τ lepton and a corresponding neutrino. τ, in turn, seemed to decay through $\tau^- \to e^- \bar{\nu}_e \nu_\tau$. Of the decay products of B_{sig} only the electron is reconstructed. Using Eq. (5.6) momentum, taken by neutrinos (missing momentum, $\vec{p}_{miss}$) can be reconstructed. Moreover, after accounting for the energy deposits in the electromagnetic calorimeter (coloured in green in the figure) produced by the detected charged particles, any possible extra energy (E_{ECL}) detected may be only due to the final state neutrinos. Since they don't interact in the material this extra energy is expected to be null. Decays like this can thus be identified by the extra energy $E_{ECL} \sim 0$.

The described method represents an extremely powerful method for measurement of B meson decays in which (for detector) invisible particles are produced. These may be arising from Standard Model processes (neutrinos) or could be some yet unknown potential particles (e.g. candidates of dark matter particles, not interacting with the ordinary matter). The method thus enables measurements of leptonic (e.g. $B^+ \to \tau^+ \nu_\tau$) and semileptonic (e.g. $B^+ \to \bar{D}^0 \tau^+ \nu_\tau$) decays of B mesons, as well as searches for New Physics particles potentially produced in e^+e^- collisions. A drawback is the need for full reconstruction of a B_{tag} from its decay products. Since B mesons have a large number of possible decay modes, each with a relatively low branching fraction, the efficiency of such full B_{tag} reconstruction is low,

typically around 0.5%.

An example of measurement using the method described is presented in Fig. 5.9. The method is used to measure the branching fraction $B^+ \to \tau^+ \nu_t au$ [50], where the signal decays are identified as those with $E_{ECL} \approx 0$. It is clear from the figure that the number of selected

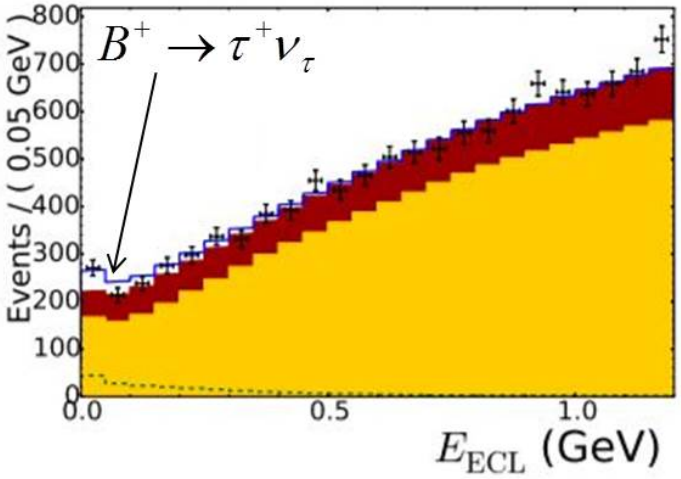

Figure 5.9: Distribution of extra energy E_{ECL} for B meson decays selected as $B^+ \to \tau^+ \nu_\tau$ candidates. Points with error bars represent the data, coloured histrograms are estimated contributions of backgrounds. Signal decays contribute the excess of events at small values of E_{ECL} [50].

$B^+ \to \tau^+ \nu_\tau$ candidates is low (actually in the measurement around 200 candidate events from $770 \cdot 10^6$ $B\bar{B}$ pairs were isolated). Accuracy of this decay branching fraction will be significantly improved using the data collected by Belle II detector.

After briefly explaining the method of measurements of B decays with undetected particles in the final state, we can return to the question of lepton flavour universality. The term describes the fact that the amplitude for the quark level process $q \to q' \ell^- \bar{\nu}_\ell$ is the same, regardless of the flavour of the charged lepton ℓ, i.e. the same for $\ell = \tau, \mu, e$. To be precise, the coupling constant of weak interaction mediating the process is the same - Fermi coupling constant G_F - regardless of the lepton flavour. In expressing a probability of semileptonic decays also masses of leptons - very different for various leptons - as well as some properties of hadrons in which quarks are bound play a role. The differential semileptonic decay width for a B meson decay into D^* (process of Fig. 5.10) is written as [51]

$$\frac{d\Gamma(B \to D^* \ell \nu_\ell)}{dq^2} \propto G_F^2 |V_{cb}|^2 \frac{q^2}{m_B^2} \left(1 - \frac{m_\ell^2}{q^2}\right) \left[H_L^2(q^2) \left(1 + \frac{m_\ell^2}{2q^2}\right) + \frac{3}{2} \frac{m_\ell^2}{q^2} H_T^2(q^2)\right] \quad . \quad (5.7)$$

The expression includes a variable q^2 - square of the invariant mass of the $\ell \nu_\ell$ pair (or, alternatively, square of the momentum transferred by W^+). It depends also on the lepton mass m_ℓ. Our ignorance of quantum chromodynamics (binding quarks inside the hadrons, schematically denoted by red gluon lines in the plot) is parametrized by phenomenological

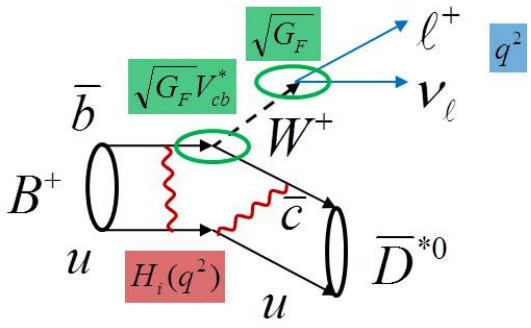

Figure 5.10: Diagram of B meson semileptonic decay, with marked some of the factors entering the differential decay rate (see text for description).

functions $H_{L,T}(q^2)$. They are calculated using models or lattice QCD[10] and are subject to theoretical uncertainty.

Taking into account different masses of leptons (in reality only mass of the τ lepton, 1.78 GeV, which is much larger than masses of muons and electrons, 0.106 GeV and 0.0005 GeV, respectively, must be considered) ratios of decay rates can be calculated:

$$R(D^{(*)}) \equiv \frac{\Gamma(B \to D^{(*)}\tau\nu_\tau)}{\Gamma(B \to D^{(*)}\ell\nu_\ell)} \quad . \tag{5.8}$$

In the above equation ℓ denotes only an electron or a muon, while the τ lepton is excluded from the notation. Uncertainties related to calculations of functions $H_{L,T}(q^2)$ are significantly reduced in the ratios $R(D^{(*)})$ (because they cancel in the ratio). Hence the ratios can be predicted rather precisely in the framework of SM:

$$\begin{aligned} R(D)^{SM} &= 0.300 \pm 0.008 \text{ [52]} \\ R(D^*)^{SM} &= 0.252 \pm 0.003 \text{ [53]} \quad . \end{aligned} \tag{5.9}$$

Measurement of the ratios represent a test of universality between τ leptons on one hand, and light leptons - e and μ - on the other. And the reconstruction of tagging B mesons, described above, enables such measurements. Both B Factories performed measurement with D and D^* mesons in the final state. The average[11] of measurements, presented in Fig. 5.11 (left) [45], is somewhat surprising. The current average of measurements is around four standard deviations away from the SM prediction. This suggest that τ leptons couple to weak interaction slightly differently than electrons and muons.

In exploiting the above mentioned measurement method at Belle II, improvements to the electromagnetic calorimeter will be important. The Belle II electromagnetic calorimeter is a detector module composed of CsI(Tl) crystals (Cesium Iodide dopped with Thallium, crystals similar to the one shown in Fig. 5.11 (right)). This material is a scintillator, part

[10] Lattice quantum chromodynamics is a method of calculation of strong interaction processes on a discrete lattice of space-time points.

[11] Also LHCb experiment at LHC contributed with their measurements.

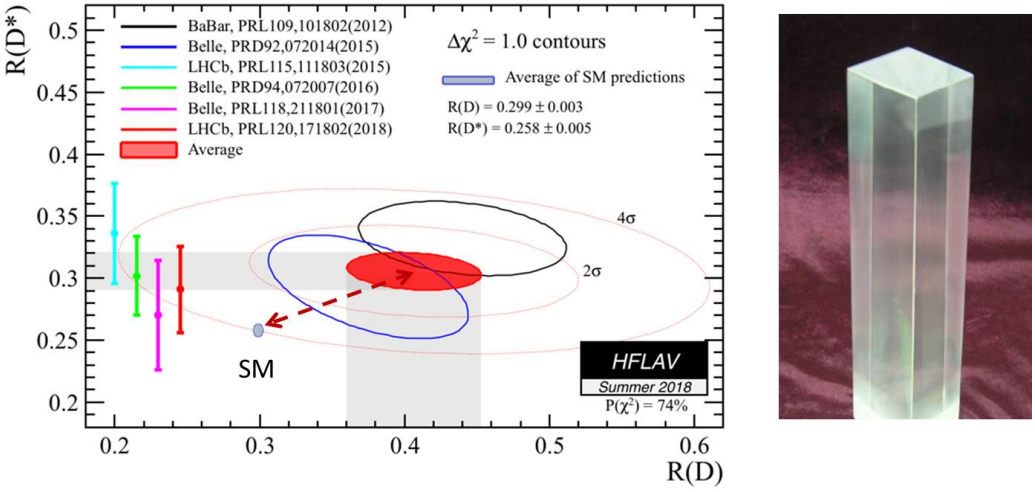

Figure 5.11: Left: Average of $R(D)$ and $R(D^*)$ measurements, in comparison to the SM prediction (adopted from [45]). The central value of measurements is around four standard deviations away from the prediction. Right: A CsI crystall (adopted from [54]), similar as those building up Belle II electromagnetic calorimeter.

of the energy deposited in it by charged and neutral particles is emitted in a form of light that is detected by an array of light sensors. By that the energy of the traversing particles can be determined (hence the term calorimeter). At Belle II new electronics will be used for reading out the signals, resulting in a better separation among energy deposits of various particles and noise.

The precision of the measurements presented in Fig. 5.11 (left) is currently not sufficient to judge on a possible shortcomings of Standard Model. In case the discrepancy proves to be genuine it would be a smoking gun of New Physics. To achieve a more precise results on $R(D)$ and $R(D^*)$, and to reach conclusions regarding the universality of leptons in Nature, one will have to rely on the data recorded by Belle II, as well as expected updated measurements from LHCb experiment at LHC.

Note: Previous generation B Factories initiated several experimental methods and reveal few hints of discrepancies between measurement results and predictions of the Standard Model. Present B Factory, Belle II, will be able to upgrade the measurement accuracy and search deeper into particle world for signs of New Physics.

Bibliography

[1] Particle Data Group, http://www.particleadventure.org/scale.html

[2] C. Patrignani *et al.* (Particle Data Group), Chin. Phys. C, 40, 100001 (2016) and 2017 update.

[3] J. Beringer *et al.* (Particle Data Group), Phys. Rev. D86, 010001 (2012).

[4] https://workspace.imperial.ac.uk/theoreticalphysics/public/MSc/PartSymm/SU%283%29Notes.pdf (October 2014).

[5] The Physics of the B Factories, ed. A.J. Bevan, B. Golob, Th. Mannel, S. Prell, and B.D. Yabsley, Springer-Verlag Berlin Heidelberg (2015), also as SLAC-PUB-15968, KEK Preprint 2014-3, Eur. Phys. J. C74, 3026 (2014)

[6] C. Jarlskog, Phys. Rev. Lett. 55, 1039 (1985).

[7] https://www.lhc-closer.es/taking_a_closer_look_at_lhc/0.rf_cavities

[8] Y. Ohnishi *et al.*, Prog. Theor. Exp. Phys., 03A011 (2013).

[9] M. Masuzawa *et al.*, Proceedings of IPAC2016, Busan, Korea.

[10] D. Besson, T. Skwarnicki, Annu. Rev. Nucl. Part. Sci. 43, 333 (1993), and references therein.

[11] http://www.hephy.at/en/research/belle-experiment-at-kek/

[12] https://www.flickr.com/photos/slaclab/31163869706/in/photostream/

[13] J. H. Christenson et al., Phys. Rev. 140, B74 (1965).

[14] V. Fitch, Nobel Lecture, https://www.nobelprize.org/prizes/physics/1980/fitch/lecture/ .

[15] J. H. Christenson, J. W. Cronin, V. L. Fitch, R. Turlay, Phys. Rev. Lett. 13, 138 (1964).

[16] J. Alcaraz *et al.* (AMS Coll.), Phys. Lett. B461, 387 (1999).

[17]] O. Adriani *et al.* (PAMELA Coll.), Phys. Rev. Lett. 105, 121101 (2010).

[18] Vivian Poulin *et al.*, arXiv:1808.08961 (2018), https://arxiv.org/abs/1808.08961

[19] L. Canetti, M. Drewes, M. Shaposnikov, New J. Phys. 14, 095012 (2012).

[20] A.D. Sakharov, J. Exp. Theor. Phys. Lett. 5, 24 (1967).

[21] L.-L. Chau, W.-Y. Keung, Phys. Rev. Lett. 53, 1802 (1984).

[22] L. Wolfenstein, Phys. Rev. Lett. 51, 1945 (1983).

[23] T. Matsumoto *et al.* (Belle Coll.), presentation at IX Int. Workshop on Advanced Comp. and Anal. Techniques in Phys. Research, December 2003, Tsukuba, Japan, https://www-conf.kek.jp/past/acat03/

[24] J. Schwiening it et al. (BaBar Coll.), Nucl. Instr. Meth. A553, 317 (2005).

[25] I. Adam it et al. (BaBar Coll.), Nucl. Instr. Meth. A538, 281 (2005).

[26] D.A. Baylor, T.D. Lamb, K.W. Yau, J. of Physiology 288, 613 (1979).

[27] Belle II experiment on Twitter.

[28] R. Abe *et al.*, Nucl. Instr. Meth. A535, 379 (2004).

[29] A. Einstein, B. Podolsky, N. Rosen, Phys. Rev. 47, 777 (1935).

[30] A. Go *et al.* (Belle Coll.), Phys. Rev. Lett. 99, 131802 (2007).

[31] R. Aaij *et al.* (LHCb Coll.), New J. Phys. 15, 053021 (2013).

[32] B. Aubert *et al.* (BaBar Coll.), Phys. Rev. Lett. 88, 221803 (2002).

[33] A. Poluektov *et al.* (Belle Coll.), Phys. Rev. D81, 112002 (2010).

[34] H. Albrecht *et al.* (Argus Coll.), Z. Phys. C46, 15 (1990).

[35] B. Aubert *et al.* (BaBar Coll.), Phys. Rev. D66, 032003 (2002).

[36] D.G. Hitlin *et al.* (BaBar Coll.), arXiv:hep-ex/0011024 (2001), https://arxiv.org/pdf/hep-ex/0011024.pdf

[37] H. Aihara *et al.* (Belle Coll.), arXiv:hep-ex/0010008 (2001), https://arxiv.org/pdf/hep-ex/0010008.pdf

[38] C. Touramanis *al.* (BaBar Coll.), arXiv:hep-ex/0110064 (2001), https://arxiv.org/pdf/hep-ex/0110064.pdf

[39] S. Schrenk *et al.* (Belle Coll.), in proceedings of "Int. Europhysics Conf. on High Energy Phys. 2001". Proc. Sci., https://pos.sissa.it/007/068/pdf

[40] I. Adachi *et al.* (Belle Coll.), Phys. Rev. Lett. 108, 171802 (2012).

[41] B. Aubert *et al.* (BaBar Coll.), Phys. Rev. D79, 072009 (2009).

[42] J. Charles *et al.* (CKMfitter Group), Eur. Phys. J. C41, 1-131 (2005), updated results and plots available at: http://ckmfitter.in2p3.fr

[43] https://www.nobelprize.org/prizes/physics/2008/press-release/

[44] V.A. Kuzmin *et al.*, Phys. Lett. 155B, 36 (1985).

[45] Y. Amhis *et al.*, Eur. Phys. J. C77, 895 (2017), and updates at https://hflav.web.cern.ch/

[46] E. Kou *et al.*, arXiv:1808.10567 (2018), https://arxiv.org/ftp/arxiv/papers/1808/1808.10567.pdf

[47] S.-K. Choi *et al.* (Belle Coll.), Phys. Rev. Lett. 91, 262001 (2003).

[48] M. Staric *et al.* (Belle Coll.), Phys. Rev. Lett. 98, 211803 (2007).

[49] B. Aubert *et al.* (BaBar Coll.), Phys. Rev. Lett. 98, 211802 (2007).

[50] B. Kronenbitter *et al.* (Belle Coll.), Phys. Rev. D92, 051102 (2015).

[51] J.G. Korner, G.A. Schuler, Z. Phys., C46, 93 (1990).

[52] H. Na *et al.*, Phys. Rev. D92, 054410 (2015).

[53] S. Fajfer *et al.*, Phys. Rev. D85, 094025 (2012).

[54] A. Boyarintsev *et al.*, J. of Instr. 11, P03013 (2016).